Title
Suicidal Cells and Lipid Storms: Mechanisms and Consequences of Cytokine–independent Inflammasome Activation

Author
von Moltke, Jakob Helmuth

Publication Date
2012

Peer reviewed|Thesis/dissertation

Suicidal Cells and Lipid Storms

Mechanisms and Consequences of Cytokine-independent Inflammasome Activation

By

Jakob Helmuth von Moltke

A dissertation submitted in partial satisfaction of the

requirements for the degree of

Doctor of Philosophy

in

Molecular and Cell Biology

in the

Graduate Division

of the

University of California, Berkeley

Committee in Charge:
Professor Russell E. Vance, Chair
Professor David Raulet
Professor Laurent Coscoy
Professor Brian Staskawicz

Spring 2012

Suicidal Cells and Lipid Storms

Mechanisms and Consequences of
Cytokine-independent Inflammasome Activation

By Jakob Helmuth von Moltke

Abstract

Suicidal Cells and Lipid Storms:
Mechanisms and Consequences of Cytokine-independent Inflammasome Activation

By Jakob Helmuth von Moltke

Doctor of Philosophy in Molecular and Cell Biology
University of California, Berkeley

Russell E. Vance, Chair

To protect against infectious disease, the innate immune system must mount a rapid response that distinguishes between self and non-self, and between pathogen and harmless commensal. Invasion of the host cell cytosol, either directly or through the injection of effector proteins, is a uniquely pathogen-associated event. Therefore, the innate immune system includes numerous cytosolic sensors to detect foreign molecules or the disruption of intracellular homeostasis. Among these sensors is the NBD-LRR family of proteins, which oligomerize into large complexes called "inflammasomes", and serve as a molecular platform for the activation of the protease CASPASE-1.

The outcome of innate sensing in the cytosol is determined by the downstream effector functions of each pathway. In most cases, this occurs through the transcriptional induction of effector proteins, such as inflammatory and chemotactic cytokines. In contrast, inflammasome effector functions are carried out by CASPASE-1 in the absence of *de novo* transcription or translation, making inflammasome activation one of the most rapid innate signaling responses.

Experiments in mice deficient for CASPASE-1 or other inflammasome components, have revealed the importance of inflammasome activation in restricting bacterial pathogens *in vivo*. Bacterial restriction is achieved by the effector functions of CASPASE-1, the best characterized of which are the processing and secretion of the inflammatory cytokines IL-1β and IL-18, and the induction of a lytic cell death called pyroptosis. The relative contribution of CASPASE-1 effector functions to immunity varies depending on the disease model; however, in several cases inflammasome-dependent protection is completely retained in *IL-1β/IL-18*$^{-/-}$ mice, suggesting cytokine-independent inflammasome functions. In this dissertation I explore the molecular mechanisms that regulate cytokine-independent inflammasome activity, and describe a novel CASPASE-1 effector function *in vivo*.

The dissertation begins with an overview of inflammasome activation and function, highlighting some of the important areas for future research. Next, I describe a full-genome siRNA screen we undertook to identify novel proteins required for inflammasome signaling, and in particular for pyroptosis. Although the screen led to the unbiased identification of *known* inflammasome components, all novel candidate genes failed to validate after further analysis. Perhaps this negative result indicates a functional redundancy among the CASPASE-1 substrates required for pyroptosis.

In chapter 3, we examine how autoproteolysis determines the effector functions of CASPASE-1. We show that a non-cleavable allele of CASPASE-1 retains the ability to initiate pyroptosis, but fails to process IL-1β/IL-18. This finding explains the previous observation that in the absence of the inflammasome adaptor protein ASC, inflammasome activation leads to cell death without release of cytokines. Furthermore, we show that pyroptosis and cytokine processing can be initiated from spatially and structurally distinct inflammasome complexes, suggesting a mechanism for tuning the outcome of CASPASE-1 activation.

In chapter 4, we identify a novel CASPASE-1 effector function using an *in vivo* model of inflammasome activation. We show that systemic cytosolic delivery of flagellin, a potent inflammasome agonist, leads to massive vascular fluid loss and can kill mice in less than 30 minutes. This unexpected response is dependent on CASPASE-1, but independent of IL-1β and IL-18. Instead, CASPASE-1 activation leads to a cellular calcium influx that triggers the biosynthesis of eicosanoids – a family of inflammatory lipids that includes the prostaglandins and leukotrienes. Mice deficient in COX-1, an enzyme required for synthesis of prostaglandins, are resistant to the rapid pathology caused by inflammasome activation.

Our findings therefore link the rapid sensing capacity of inflammasomes to the potent activity of eicosanoids. Activated within minutes, this pathway represents one of the most rapid cellular innate immune responses described to date, and suggests a model for the initiation of inflammation at the site of infection. In the 5th and final chapter, I discuss this model and other emerging themes in inflammasome research, highlighting several mouse models I have developed to uncover additional inflammasome functions *in vivo*. Although to date the emphasis has been on IL-1β and IL-18, the findings reported in this dissertation highlight how much there is to learn about the cytokine-independent functions of inflammasomes.

For

Mary Francesca Fontana,
with whom I set sail

and for

My family (parents, siblings, cousin),
who helped me build the boat

In memory of Konrad and Freya von Moltke

Acknowledgements

These acknowledgments can only begin with an enormous thank you to Russell for recognizing potential when I barely knew how to operate a centrifuge. I consider myself enormously lucky to have been a part of the Vance Lab these last five (exciting) years. Thank you Russell for keeping the faith when I lost it, and for a healthy dose of pessimism when I got ahead of myself. I am glad to know that I will have you as a mentor, colleague, and friend for years to come.

To members of the Vance Lab past, thanks for taking me in, serving me non-alcoholic beer, and teaching me to put basil *under* the other pizza toppings. Oh, and you're all amazing scientists too. To Vance Lab present, it's been wonderful to work with such a dedicated, professional (most of the time), and talented group of scientists. Thank you for expanding my musical horizons and for muscle-T Tuesdays; keep the piñata tradition alive when we're gone. Thank you also to Barton Lab past and present for setting the work and play bars above even *my* 6'7" head. And especially to Greg Barton for his insights and questions that always push me to think more deeply, and for his sense of humor and advice. Thank you also to Laurent Coscoy, Matt Welch, and their labs for training me in the early days of my rotations.

Science is a wonderfully collaborative effort, and I've been lucky to work with many other talented scientists outside the Vance and Barton labs. The *Cell Host and Microbe* paper included as chapter 3 was a close collaboration with Petr Broz in Denise Monack's lab at Stanford University. The 4-5 months spent completing that paper stand as the most productive time in my graduate career, and I am grateful to Petr and Denise for the opportunity to contribute to the story.

The data in chapter 4 represent the real core of my graduate work, and it has been an exciting sleuthing expedition since I first stumbled upon the rapid lethality of FlaTox. Thank you to all the mice that contributed to the cause, and to the dedicated OLAC technicians, particularly Luis, who take care of them. Thanks to Alex Kintzer for a bottomless supply of recombinant protein, to Mahtab Moayeri for an engaging collaboration, and to Norver "tail vein" Trinidad for hours and hours of skilled assistance with *in vivo* experiments. I'd let him operate on me if he decides to become a surgeon. Finally, the FlaTox mystery may have landed in the "cold cases" file without Karsten Gronert. Karsten's eicosanoid expertise has been crucial, and I am grateful to him for allowing me to use his LC/MS/MS setup.

More broadly, I have benefited enormously from the communities of the 4th floor immunology labs in LSA (particularly Paul Herzmark's microscopy expertise), the Barton/Vance/Portnoy Tri-lab, and the monthly Bay Area bacterial pathogenesis P01 group. Special thanks to Dan Portnoy for anchoring and organizing the P01. Dan is a brilliant scientist and an inspiring mentor. To my dissertation committee – David Raulet, Laurent Coscoy, and Brian Staskawicz – thank you for your support and guidance, and for timely responses to all emails (not to be underestimated).

Although it seems most scientists live to work, rather than the other way around, the time in lab is only bearable if you can get away. Thank you to John Young and Brandon Bunker for rescuing me from a cramped and noisy apartment by inviting me to live with them. The house on Carberry (goat-head, rat, dartboard and all) was a true refuge. Also, Rickey F-ing Henderson!

The Friday morning basketball game and MCB intramural team restored my sanity on a weekly basis. It's been a pleasure playing with a group of guys who try hard without all the silly posturing. Finally I can say "Why yes, I do play basketball". Thank you also to Alex Engel for his friendship, the many games of squash in the bowels of RSF and the bike rides on the East Bay ridges, to Kwan Chow (my lunch, movie, and concert-buddy), and to my Bay Area Dartmouth friends for science-free diversion.

To my mother, who told me I should become a truck driver if it made me happy, my siblings, their partners, and my six nieces and nephews: thank you for supporting my leap across the country. I wish I could see all of you more often. A special thank you to Alexej Steinhardt for repeatedly bridging the gap, and for getting me through that first summer. I love you all.

And finally, to my wife Mary Fontana: thank you for listening to my science rants at all hours of the day, for your sage advice, for your humor (and appreciation of mine), and for making these last four years the happiest of my life. We should work together sometime!

Table of Contents

List of Figures & Tables

Chapter 2

Chapter 3

Chapter 4

Chapter 5

Chapter 1: Inflammasome Overview

1.1 Introduction

Detection of bacterial invasion by the innate immune system is critical for host immunity and survival, but also presents several challenges. First, unlike the adaptive immune system, which requires days to respond, innate immune sensing must be rapid. This problem is solved by germline-encoded invariant sensors, such as the toll-like receptors (TLR), that are widely expressed at barrier surfaces and other sites of host-pathogen interaction. However, by binding to ligands such as bacterial flagellin or lipoproteins in the extracellular and endosomal spaces, TLRs often fail to distinguish between pathogenic and non-pathogenic microbes. Therefore, it is also important for the innate immune response to identify microbial activities associated exclusively with pathogenicity[1]. One such activity is the bacterial invasion of the host cell cytosol, either directly or through the injection of effector proteins. Although they often recognize the same ligands as TLRs, activated innate sensors in the cell cytosol encode additional information simply by virtue of their localization. It stands to reason, therefore, that these pathways might be licensed to trigger rapid, potent, and potentially dangerous responses to an infection that has already breached several lines of innate defense, including antimicrobial peptides and epithelial barriers.

The most rapid cytosolic sensing pathway identified to date requires the formation of large molecular complexes termed "inflammasomes", and proceeds without *de novo* transcription or translation. Inflammasome formation is coordinated in macrophages and dendritic cells (and probably in other cells as well, as discussed in Chapter 5) by members of the NBD-LRR protein family (e.g., NLRP1B, NLRP3, NLRC4 and the NAIPs) or the PYHIN protein family (e.g., AIM2) that function as sensors of a variety of pathogens and other inflammatory stimuli[2]. Upon detection of their stimulus, NBD-LRR and PYHIN proteins oligomerize to form a platform for the recruitment and activation of the protease CASPASE-1 (CASP1). The mechanisms of inflammasome sensing, oligomerization, and downstream effector functions are discussed in detail below.

1.2 Inflammasome Activation

1.2.1 Inflammasome Protein Domains

The inflammasome proteins share several conserved protein domains that determine their function. Although not yet proven directly, the leucine rich repeat (LRR) domains are generally thought to control the ligand/agonist specificity of the NBD-LRR. Structurally, these domains are believed to resemble the LRR folds of toll-like receptors (TLR), which in several cases have been crystallized together with their cognate ligand[3,4]. The nucleotide binding domain (NBD) is believed to bind ATP (and perhaps other nucleotides[5]), and is required for oligomerization[6], and the caspase activation and recruitment domain (CARD) can bind the CARD of pro-CASP1[7]. Some NBD-LRR proteins have a pyrin domain (PYD) in place of the CARD and therefore require the adaptor ASC (a CARD-PYD protein discussed in more detail below) for recruitment of CASP1[8]. The NAIP proteins have neither a CARD nor a PYD and instead contain three baculovirus inhibitory repeats (BIR), the function of which is not yet clear[9].

1.2.2 The NAIP/NLRC4 Inflammasomes

Best characterized at the molecular level, are the inflammasomes containing members of the NAIP protein family, which respond to bacterial proteins secreted into the host cytosol. *Salmonella* spp., *Pseudomonas aeruginosa*, *Listeria monocytogenes, Shigella* and *Legionella pneumophila* infections all activate NAIP inflammasomes[10-17].

In mice, the cluster of NAIP genes on chromosome 13 appear to have arisen from genetic duplication events and share about 85% sequence homology[18]. There are several pseudogenes in the locus, and only *Naip1*, *Naip2*, *Naip5*, and *Naip6* are thought to be functionally expressed[18]. The NAIP5 inflammasome responds to bacterial flagellin, and NAIP2 is activated by the inner rod protein of the type III bacterial secretion system[19-22]. NAIP6, which shares ~95% sequence homology with NAIP5[23], also oligomerizes in response to flagellin in a non-heterologous system, but this has not been confirmed for the endogenous protein[19,22]. An agonist for NAIP1 inflammasomes has not yet been reported.

For a long time, the mechanism of flagellin and rod protein detection by the NAIP inflammasomes was unclear. Recent data has shown, however, that these proteins are complexed with the inflammasome, suggesting a simple ligand-receptor model for NAIP inflammasome activation, although a direct interaction has not yet been conclusively demonstrated[19,22].

As mentioned, the NAIP proteins contain neither a CARD nor a PYD, and therefore require NLRC4, a CARD-containing member of the NBD-LRR family, for downstream signaling. NLRC4 is found in complex with all NAIP containing inflammasomes and NLRC4-deficient cells fail to respond to both flagellin and rod proteins[20-22]. Homotypic interaction of the NLRC4 and CASP1 CARD domains has been demonstrated[7], but the mechanism of NLRC4 and NAIP interaction remains unclear.

1.2.3 The NLRP1B Inflammasome

In mice, NLRP1B is the inflammasome sensor of anthrax lethal toxin[24], an AB toxin consisting of protective antigen (PA) B-subunit and the metalloprotease lethal factor (LF) A-subunit. At decreased pH, PA inserts into the endosomal membrane to form a pore for translocation of LF to the host cytosol[25], where LF cleaves and inactivates several mitogen activated protein kinase kinases (MEKs)[26]. Whether this MEK cleavage contributes to activation of the NLRP1B inflammasome is unknown. In fact, very little is known about how NLRP1B senses LF, although the protease activity of LF[27] and the host proteasome are required[28]. Two appealing models include (1) a direct activating cleavage of NLRP1B by LF, or (2) the LF-dependent cleavage and degradation of a host protein that normally inhibits LF oligomerization. This latter model is similar to the "guard" paradigm described for plant NBD-LRR proteins[29].

1.2.4 The NLRP3 Inflammasome

Unlike the NAIPs, NLRC4, and NLRP1B, which are constitutively expressed, NLRP3 requires transcriptional induction downstream of NFκB[30]. *In vitro* this is usually achieved by pre-treating cells with a TLR agonist such as LPS. Once NLRP3 expression has been primed, a remarkable array of stimuli are capable of inducing NLRP3 oligomerization in cell culture, including ATP, nigericin, alum, crystal-like structures (e.g. uric acid or cholesterol crystals and asbestos), whole pathogens (e.g. *C. albicans, L. monocytogenes, S.*

typhimurium, influenza*),* UVB irradiation, and skin irritants (e.g. dinitrofluorobenzene), to name just a few[6]. Given this diversity of agonists, the activation of NLRP3 is unlikely to occur via direct recognition of the initiating signal. Instead, NLRP3 must respond to a downstream signal shared by all of these stimuli, such as a change in cellular homeostasis for example. Several models have been proposed to explain the activation of NLRP3 by multiple agonists. It has been proposed that particulate agonists disrupt phagosome integrity leading to the release of cathepsin B, which somehow activates NLRP3[31]. For other agonists the production of reactive oxygen species appears crucial for NLRP3 oligomerization[32-34]. Unfortunately, none of the current models provide a unifying mechanism, and much work remains to be done on NLRP3 sensing.

It is difficult to assess the relevance of NLRP3 agonists identified *in vitro*, where almost any disruption in cell homeostasis appears to trigger the inflammasome once it has been transcriptionally primed. *In vivo* experiments in *Nlrp3*$^{-/-}$ mice have provided far more convincing evidence supporting the importance of NLRP3 in host immunity and disease. Although not the focus of this dissertation, NLRP3 has been associated with numerous diseases, including gout, artherosclerosis, a rare group of autoinflammatory diseases, and type II diabetes[6].

1.2.5 The AIM2 Inflammasome

The AIM2 inflammasome responds to the double-stranded cytosolic DNA of several viruses (e.g. MCMV and vaccinia) and also of lysed bacteria in the cytosol, as has been demonstrated for. *L. monocytogenes* and *F. tularensis*[14,35-42]. AIM2 is an unusual inflammasome sensor because it lacks both an NBD and LRR. Instead, AIM2 encodes a HIN200 domain, which directly binds DNA[42].

1.2.6 The Other NBD-LRRs

Many NBD-LRR proteins remain completely uncharacterized, and this will be an important area of future research. Data from *Nlrp6*$^{-/-}$ and *Nlrp12*$^{-/-}$ mice suggest that these proteins contribute to intestinal homeostasis. Both knockouts show increased susceptibility to colitis and gastrointestinal tumors using the dextran sodium sulfate (DSS) and DSS/azoxymethane models, respectively[43,44]. In the case of *Nlrp6*$^{-/-}$, this sensitivity appears to arise from a dysbiosis of intestinal commensals that also leaves the mice more susceptible to diet-induced liver disease and obesity[45,46]. Deletion of NLRP12 has also been linked to a migratory defect in mouse myeloid cells[47]. Whether NLRP6 and NLRP12 form functional inflammasomes and what the relevant agonists might be remains to be determined.

In humans, polymorphisms in NLRP7 are associated with reproductive disorders in women[48]. More recently, an NLRP7 inflammasome was shown to assemble in human macrophages in response to microbial acylated lipopeptides[49]. So far, it is unclear if there is any mechanistic link between these observations.

1.2.7 Apoptosis-associated Speck-like Protein Containing a Caspase Recruitment Domain (ASC)

In addition to NBD-LRR proteins, inflammasome complexes also include a bipartite adaptor protein called ASC that contains both a CARD and PYD[50]. For NBD-LRR proteins lacking a CARD, ASC serves as a linker between their PYD and the CARD of pro-CASP1[51].

Surprisingly, ASC is also found in NLRC4 and NLRP1B inflammasomes, even though these NBD-LRRs encode a CARD and can interact with CASP1 in the absence of ASC[7]. As described in Chapter 3, ASC is required in all inflammasomes for auto-proteolytic cleavage of CASP1 and processing of IL-1β/IL-18, but not for pyroptosis.

1.2.8 Oligomer Structure

Although several different inflammasomes have been described, the precise molecular architecture and composition of inflammasomes remains largely unknown. The apoptosome, a related structure that serves as a platform for activation of CASPASE-9, has been shown to be a 700-1400 kDa heptameric, wheel-shaped complex containing APAF-1 and CYTOCHROME-C[52]. Recently, it was shown that in response to NLRC4, NLRP3 or AIM2 stimuli, endogenous ASC can aggregate to form a single "ASC focus" in the cytoplasm with a diameter of 1-2 microns[39,53], vastly larger than the apoptosome. Similar ASC foci were previously observed when THP-1 cells overexpressing ASC-GFP activated NLRP3[54].

1.2.9 Inflammatory Effector Caspases

With the exception of a recently identified non-canonical inflammasome that activates CASPASE-11(see below), all other known inflammasomes converge on the recruitment and activation of CASP1, a member of the caspase family of cysteine proteases that share an exquisite specificity for cleaving target proteins at sites next to aspartic acid residues[55]. CASP1 is synthesized as an inactive, monomeric zymogen (pro-CASP-1) that is thought to be activated by dimerization and autoproteolytic processing[55]. Autoproteolysis of pro-CASP1 results in the generation of the characteristic large and small subunits (termed p20 and p10), as well as the removal of the N-terminal CARD, both of which occur following recruitment into the inflammasome[56,57]. Detection of the p20 and p10 subunits by Western blot is often used as a marker for CASP1 activity and inflammasome activation; however, as described in Chapter 3, inflammasome effector functions can also be mediated by uncleaved pro-CASP1.

The only functionally validated substrates of CASP1 are the cytokines IL-1β and IL-18. Several proteomic studies have been undertaken to identify novel CASP1 substrates, particularly those required for induction of pyroptosis[58-60]. Unfortunately, there is little overlap between the candidates identified in these studies and their functional significance remains unclear. IL-1β and IL-18 are both expressed as an inactive zymogen that lacks a classical secretion signal. CASP1 is required both for the activation of these cytokines – by cleaving off the pro-domain – and for their secretion. The mechanism of CASP1-dependent secretion is poorly understood but discussed in more detail below.

CASP1 is not the only inflammasome effector caspase. After confirming earlier reports that *Casp1*$^{-/-}$ mice are actually *Casp1/11*$^{-/-}$ double knockouts[61], Kayagaki et al generated *Casp11*$^{-/-}$ mice to show that pyroptosis induced by *E. coli* and *V. cholerae* is CASP11-dependent, although it is unclear how the protease is activated. Cytokine processing and secretion downstream of these pathogens requires both CASP1 and CASP11[62].

CASP1-independent IL-1β processing has also been reported[63,64]. In neutrophils, the serine proteases proteinase 3 (PR3) and neutrophil elastase have been shown to activate

IL-1β[64,65]. There is also evidence that a CASP8 inflammasome can process IL-1β in response to fungal pathogens or mycobacteria signaling through DECTIN-1 on dendritic cells[66].

1.3 Inflammasome Effector Functions

A protective *in vivo* role for the inflammasome has been reported using many models of bacterial pathogenesis, including *Salmonella typhimurium, Legionella pneumophila, Francisella tularensis, Shigella flexnerii, Pseudomonas aeruginosa, Burkholderia thailandensis,* and *Yersinia pseudotuberculosis* [11,13,53,67-74]. *In vitro*, deletion of inflammasome components from host cells or of inflammasome activators from pathogens leads to a dramatic increase in bacterial replication[10,12,13]. Similarly, bacterial replication is increased and host survival is decreased *in vivo* when inflammasome sensing is disrupted [see citations above], while aberrant inflammasome activation restricts bacterial pathogens[11,67,70,75].

For some bacterial pathogens, notably *L. monocytogenes* and mycobacteria, the nature of inflammasome detection remains controversial or poorly defined. *L. monocytogenes* has been shown to activate the AIM2, NLRP3, and NLRC4 inflammasomes *in vitro*[12,14,35,38,41,75], however the data are conflicting about the contribution of inflammasome activation to host immunity *in vivo*[35,75]. Similarly, there are reports of *in vitro* inflammasome activation by *M. tuberculosis*[76-78], but *in vivo* the role of inflammasomes, if any, is unclear[76]. Some of these discordant results may arise from bacterial inhibition or evasion of the inflammasome, as discussed below.

The control of bacterial infections by inflammasomes results primarily from the effector functions of CASP1, on which all canonical inflammasomes converge. To date, the best characterized CASP1 effector functions are the processing and secretion of pro-IL-1β/IL-18 and a lytic cell death called pyroptosis

1.3.1 Cytokines - IL1β & IL-18

Active IL-1*β* is a potent pyrogen, but is also critical for inflammation and helps to shape the adaptive immune response. Signaling through the widely-distributed IL-1 receptor (IL-1R) rapidly induces the expression of hundreds of genes, including IL-6, IL-8, IL-12, COX-2, numerous chemokines, anti-microbial peptides, and IL-1β transcript itself[79]. In the liver, Il-1β together with IL-6 drives the acute phase response, and on CD4+ T-cells, IL-1R engagement together with TGFβ and Il-6 promotes Th17 differentiation[80,81].

Of particular note in bacterial infections, IL-1R signaling in epithelial cells induces chemokines that recruit inflammatory cells such as neutrophils to sites of inflammation[82]. *Casp1*$^{-/-}$ or *IL-1R*$^{-/-}$ mice infected with the Ames 35 *B. anthracis* strain show decreased survival that can be phenocopied by neutrophil depletion[83]. Similarly, neutrophil recruitment is decreased and bacterial replication increased in *L. pneumophila* infected *IL-1R*$^{-/-}$ mice[82].

The recruitment of neutrophils carries with it the risk of significant damage to host tissues. Therefore, in circumstances where neutrophils fail to restrict the microbe, their recruitment is associated with severe pathology and even increased bacterial dissemination[68,70,84,85]. Accordingly, *Il-1R*$^{-/-}$ mice infected with *B. pseudomallei*, which can replicate in neutrophils, are *protected* compared to wild-type mice[84].

Signaling through the IL-18 receptor (IL-18R) induces pro-inflammatory cytokines and, depending on the cytokine context, can drive $CD4^+$ T-cells to Th1 and perhaps even Th2 and Th17 phenotypes[86]. However, IL-18 was first identified as interferon-gamma-inducing factor (IFN-γ), and this remains its primary contribution to innate restriction of bacterial pathogens. For example, restriction of *B. pseudomallei* is lost in *IL-18*$^{-/-}$ mice, but can be restored by exogenous IFN-γ[84]. In the spleen, memory $CD4^+$ T-cells secrete IFN-γ in response to IL-18 produced by inflammasome activation in $CD8\alpha^+$ dendritic cells[87].

1.3.2 Caspase-dependent Lytic Cell Death (Pyroptosis)

CASP1-dependent cell death has been reported for many years, but was first given the name "pyroptosis" in 2001[88]. The key morphological changes associated with pyroptosis include the formation of 1.1-2.4 nm membrane pores followed by rapid Ca^{2+} influx, osmotic swelling, cell lysis, and release of cytoplasmic contents[89,90]. Pyroptosis is also associated with nuclear condensation and fragmentation of genomic DNA[90]. In contrast to apoptosis, however, this DNA fragmentation appears to proceed independently of poly(ADP-ribose) polymerase (PARP) activity[90]. The kinetics of pyroptosis vary depending on the inducing inflammasome, but pore formation and lysis can occur within minutes of CASP1 activation (JvM unpublished data). Pyroptosis has been described in macrophages and dendritic cells, but may also occur in other cell types. In some cases, particularly downstream of NLRP3 oligomerization, CASP1 activation does not result in pyroptosis, although the mechanism for this remains unclear (JvM & REV unpublished data). To date, the CASP1 substrate(s) required for pyroptosis has proven elusive. The contribution of pyroptosis and/or other cytokine-independent CASP1 effector functions to host immunity is a central theme of this work and is discussed in more detail below.

1.3.3 Other Effector Functions

As already noted for IL-1β and IL-18, the release of proteins lacking canonical secretion signals is an important CASP1 effector function. The underlying mechanism for this pathway, which is calcium-dependent and begins prior to the passive release of cytosolic proteins associated with pyroptosis, remains uncertain[89,91,92]. Current models include microvesicle shedding and lysosome exocytosis, the relative contributions of which may vary by cell type[89,91,93]. Substrates of the CASP1-dependent secretion pathway (even though they are not cleaved by CASP1) include proteins such as fibroblast growth factor (FGF)-2 that are associated with tissue remodeling and repair, and inflammatory mediators such as macrophage migration inhibitory factor (MIF) and high-mobility group B1 protein (HMGB1)[94,95].

Additional effector functions of CASP1 include the promotion of *L. pneumophila*-containing phagosome maturation through its processing of CASPASE-7[96], and the induction of nitric oxide synthase in macrophages[97] and of lipogenic genes that might counteract cell death pathways in non-hematopoietic cells[98]. The *in vivo* contribution of these effector functions is as yet undetermined, and it is likely that novel effector functions remain to be identified.

1.4 Bacterial Inflammasome Inhibition

Bacterial evasion or inhibition of host innate immunity is a common theme, and the inflammasome is no exception. *L. monocytogenes* and *S. typhimurium*, for example, down regulate flagellin expression inside cells in order to evade detection by NAIP5/NLRC4[99,100]. Examples of bacteria-encoded inflammasome inhibitors include *zmp1*, a metalloprotease secreted by *M. tuberculosis*[101], the *P. aeruginosa* secreted phospholipase ExoU[102], and the *Yersinia* effectors YopE and YopK[67]. *Y. pseudotuberculosis* and *P. aeruginosa* lacking their inhibitory effectors are attenuated *in vivo,* unless host inflammasome sensing is also disrupted, further demonstrating the importance of inflammasome responses to bacterial pathogens[11,67].

1.5 Inflammasomes in Humans

The summary above describes our current understanding of inflammasomes in mice. Although the recruitment of CASP1 and its downstream effector functions appear much the same in humans and mice, it should be noted that there are important differences upstream of inflammasome oligomerization. Most notably, humans express only one NAIP protein and it does not respond to flagellin or rod proteins[19]. Instead, human NAIP has been reported to activate CASP1 in response to the needle protein of the *C. violaceum* type three secretion system[19]. Human cells also express only one NLRP1 protein[6]. The NLRP1 activating signal remains controversial, but it is not lethal toxin.

1.6 Dissertation Overview

CASPASE-1 was originally identified by its cytokine processing activity and first named interleukin-1 beta converting enzyme (ICE). Since then, CASP1 and inflammasome research has focused overwhelmingly on cytokine processing and its role in host immunity and disease. It has become clear however, that CASP1 has additional effector functions, as discussed above, and that these are important in the downstream consequences of inflammasome activation. For example, the replication of *L. pneumophila* in *Asc*$^{-/-}$ macrophages, which fail to process and secrete IL-1β/IL-18 but still undergo pyroptosis downstream of NLRC4, is indistinguishable from wild-type (JvM & REV unpublished data). Similarly, *L. pneumophila, B. thialandensis,* and *S. typhimurium* or *L. monocytogenes* overexpressing flagellin are all restricted by the inflammasome *in vivo* without IL-1β/IL-18[70,71,75].

A commonly employed *in vivo* model of sepsis provides another interesting example. Wild-type and *Il-1β/IL-18*$^{-/-}$ mice succumb to systemic delivery of endotoxin, but *Nlrp3*$^{-/-}$ and *Caspase-11*$^{-/-}$ mice are protected, suggesting inflammasome-dependent but IL-1β/IL-18-independent pathology[8,62]. Recent studies have suggested that pyroptosis is the critical inflammasome effector function for cytokine-independent bacterial restriction[70,75]. The model proposes that cell death eliminates the replicative niche of intracellular pathogens like *S. typhimurium* and *L. pneumophila* and perhaps delivers the bacteria to neutrophils for killing. During endotoxemia, CASP1-dependent release of HMGB1 contributes to pathology and lethality[94]. Therefore, it is important to expand our understanding of the mechanisms that underlie pyroptosis and its regulation. In addition, we cannot rule out the contribution of as yet unidentified inflammasome effector functions.

In this dissertation I present our work to characterize and expand on the cytokine-independent effector functions of CASP1 and the inflammasome. In Chapter 2 I describe a genome-wide siRNA screen to identify novel substrates of CASP1 and additional components of the inflammasome pathway. Chapter 3 examines the molecular mechanisms that regulate selection between cytokine processing and pyroptosis downstream of CASP1. We show that autoproteolysis of CASP1 is required for cytokine processing but not pyroptosis, and suggest that recruitment of ASC determines the character of inflammasome assembly, localization, and function. In Chapter 4 we identify the rapid biosynthesis of inflammatory lipids (eicosanoids) as a novel and cell-type specific effector function of the inflammasome with dramatic consequences *in vivo*. In the final chapter I discuss the outlook for inflammasome research, with particular emphasis on flagellin sensing in non-myeloid cells, a hypothesized adjuvant activity for pyroptosis, and the possible importance of inflammasome-dependent eicosanoid biosynthesis in immune recruitment and activation.

Chapter 2: Full Genome siRNA Screen to Identify Novel CASPASE-1 Substrates and Components of the NLRP1B Inflammasome

2.1 Introduction

Given the importance of inflammasomes in host immunity and disease, the identification of novel proteins required for inflammasome signaling has been an area of great interest. Unfortunately, the biochemical purification of inflammasome complexes has proven challenging, perhaps due to their 700-1400 kDa size, and proteomic approaches to identify novel CASPASE-1 (CASP1) substrates have been equally fruitless. To date, three proteomic studies have reported on the identification of novel CASP1 substrates, however there is almost no overlap in the substrates identified in the three studies, and it has proven difficult to validate any of the substrates in a physiologically relevant context[58-60].

Therefore, in an attempt to identify novel CASP1 substrates, I decided to take a forward genetic approach, pairing small interfering RNA (siRNA) mediated expression knockdown with the powerful negative selection of pyroptosis in mouse macrophages. In this chapter I report the development and results of a full genome siRNA screen of the NLRP1B inflammasome in immortalized bone marrow derived macrophages using anthrax lethal toxin (LT) for negative selection.

Gene silencing by small RNA is achieved by delivering ~20 bp RNA duplexes with sequences complimentary to the target mRNA to the cell cytosol. These oligos are loaded into the RNA-inducing silencing complex (RISC), where they bind their complementary mRNA sequence, targeting it for cleavage and degradation. Full genome siRNA screens have been a popular approach for uncovering novel host proteins required for immunity or pathogen replication[103-107]. Unfortunately, these screens have generated few validated candidates. It is particularly concerning that complementary screens have generated highly divergent lists of candidates, suggesting an abundance of false positives.

For the screen described in this chapter, I selected lethal toxin as the inflammasome agonist for its technical advantages over bacterial infection. Lethal toxin is a classic AB toxin consisting of protective antigen (PA) and the metalloprotease lethal factor (LF). Protective antigen binds one of two cell surface receptors (ANTXR1 and 2) and is taken up following binding of lethal factor (Figure 2.1). In the lower pH of the endosome, the PA molecules insert into the membrane to form a pore for the directed translocation of LF into the host cytosol. Functional PA and LF can be readily expressed in *E. coli* and purified in large quantities. Compared to a live infection, this recombinant protein toxin is easy to titrate and scale, yields more consistent results between experiments, and activates the inflammasome more selectively. When treated with LT, more than 95% of bone marrow macrophages expressing a functional allele of *Nlrp1b* undergo pyroptosis.

I also selected lethal toxin for the screen because activation of the NLRP1B inflammasome presents some intriguing biological mysteries. It is known that upon reaching the cell cytosol, LF cleaves numerous host mitogen-activated protein kinase kinases[26], although the contribution of this processing to inflammasome activation remains uncertain. Indeed, the mechanism of NLRP1B oligomerization in response to LF is largely mysterious. Previous studies have demonstrated a requirement for K^+ efflux and proteasome activity upstream of NLRP1B oligomerization, however neither the K^+ permissive pore nor the relevant proteasome substrate are known[28]. Our current

understanding of the NLRP1B inflammasome and important outstanding questions are summarized in Figure 2.1.

By using a forward genetic screen, I hoped to identify novel components of the NLRP1B inflammasome, positive regulators of this pathway, and CASP1 substrates required for induction of pyroptosis. Although the screen led to the unbiased identification of known pathway components, including *Casp1* and *Antxr2*, all novel candidates from the screen have failed to validate in secondary screens.

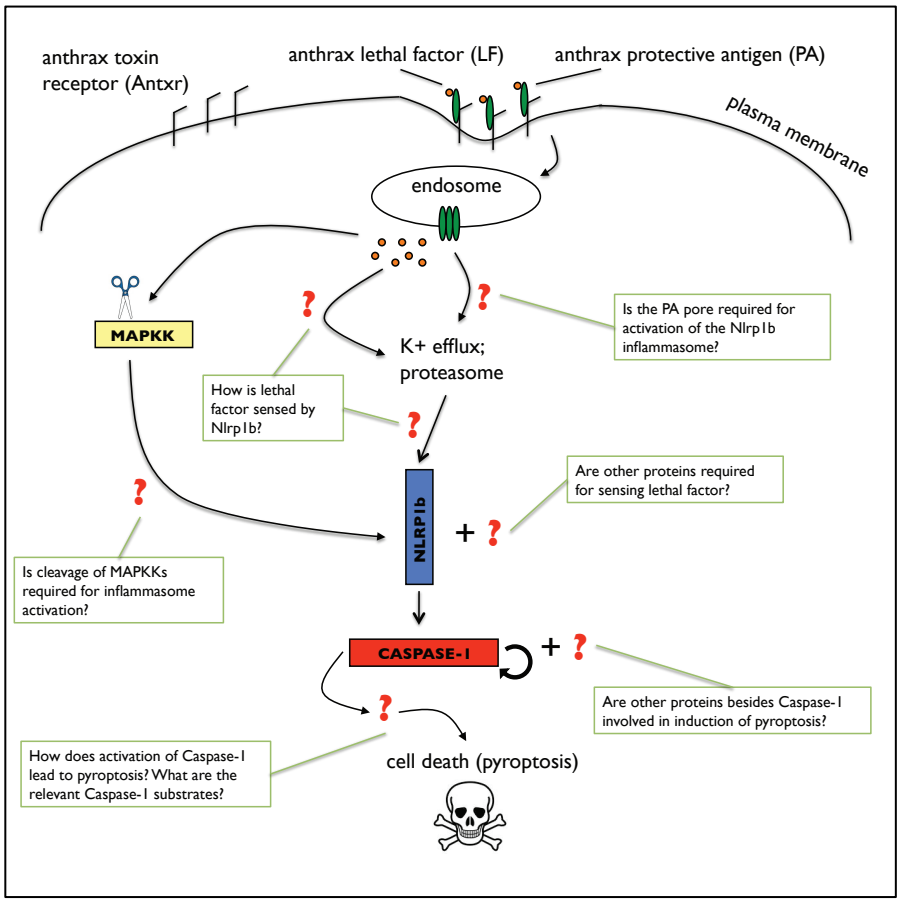

Figure 2.1 Current model of the NLRP1B inflammasome

2.2 Development of Tools for Screening

The NLRP1B protein required for inflammasome oligomerization in response to LT is highly polymorphic between in-bred mouse strains[24]. For example, the *Nlrp1b* allele expressed in the widely-used C57BL/6J mice is non functional, whereas 129/SvJ macrophages are fully responsive to LT. In order to establish a clonal, optimized cell line for screening, we chose to immortalize 129/SvJ macrophages by transformation with the v-myc/v-raf expressing J2 virus[108]. Although immortalized, these macrophages were recently derived from fresh bone marrow and therefore present an advantage over RAW 264.7 macrophages and other cell lines that have accumulated genotypic and phenotypic changes through long-term culturing. For example, RAW 264.7 cells do not express the ASC protein associated with many inflammasomes[109].

As expected, the immortalized 129 macrophages (i129) underwent pyroptosis in response to LT, but not the individual components PA and LF (Fig 2.2a). To establish a homogenous cell line with maximal responsiveness to LT, I generated clonal cell lines from i129 cells by limiting dilution. Visual analysis of viable cells using neutral red staining after LT treatment allowed me to track subtle differences in responsiveness that are masked in the less sensitive lactate dehydrogenase release assay often used to quantify pyroptosis. The responsiveness between cell lines was heterogeneous, but stable within a given line over multiple experiments (Fig 2.2b). Based on this LT responsiveness and general characteristics of cell viability and growth, I selected clone #22 for further analysis.

Macrophages undergoing pyroptosis release cytosolic proteins within a matter of minutes; therefore I hypothesized that labeling cells with cytosolic GFP would facilitate rapid and quantitative measurement of cell lysis in response to LT. I stably transduced i129 Clone #22 with MSCV virus expressing GFP, and isolated GFP+ cells with robust responsiveness to LT. The resulting clone (i129-22.3) underwent pyroptosis with >95% efficiency at saturating doses of LT (Fig 2.2c). Timelapse microscopy of i129-22.3 cells demonstrated the complete release of GFP within 2 hours of LT treatment (Fig 2.2d).

Although siRNA gene targeting in macrophages can present technical challenges due to low transfection efficiency, I was able to achieve robust (~50%) knockdown of GFP, a highly stable protein, in immortalized GFP^+ macrophages (Fig 2.2e). This result suggested that these cells were viable for functional screening using LT and NLRP1B-dependent pyroptosis as a negative selection.

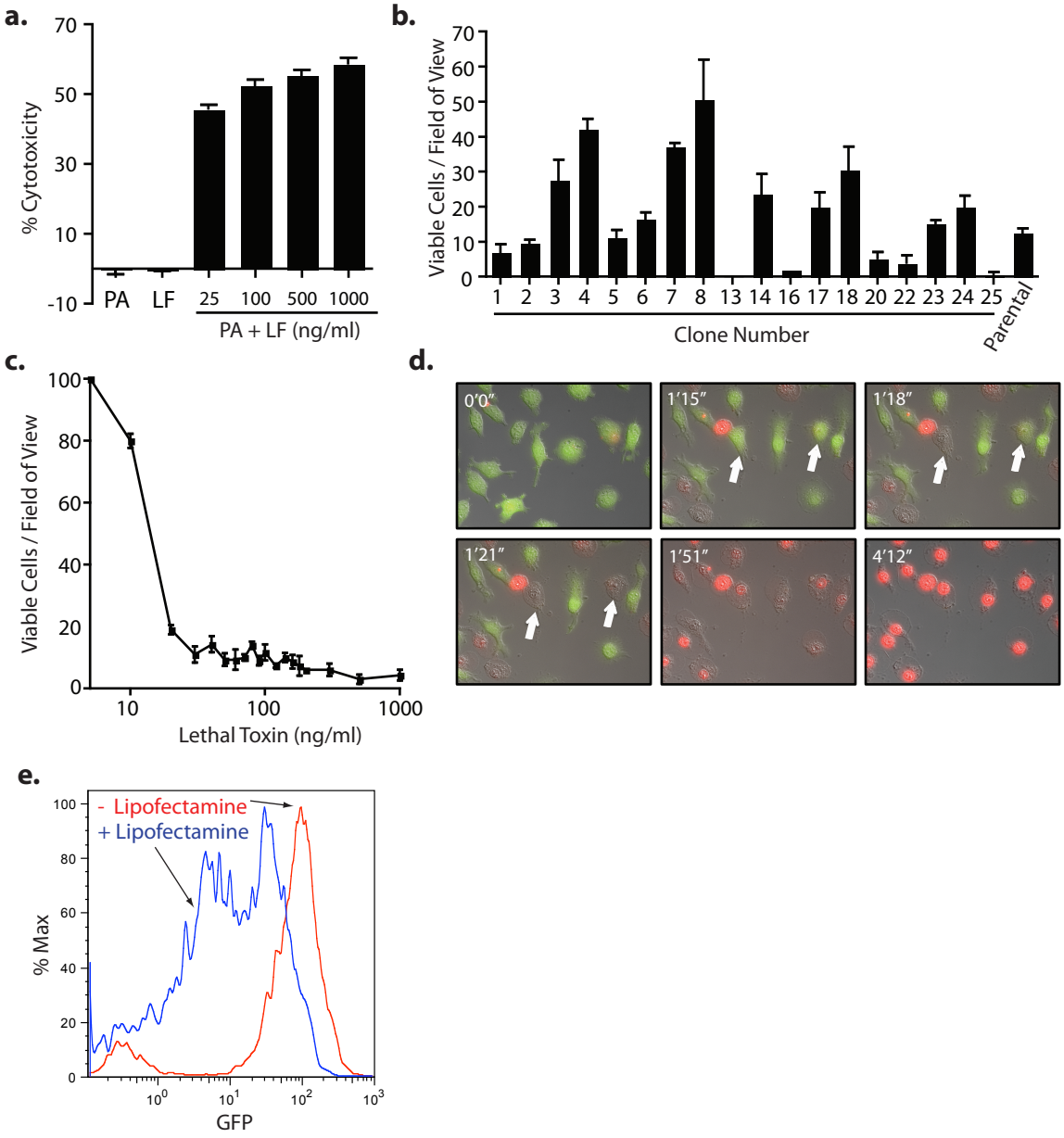

Figure 2.2 siRNA screening tools

(a) Immortalized bone marrow derived macrophages from the 129 mouse background (i129) were treated with PA alone (1 μg/ml), LF alone (1 μg/ml), or the indicated doses of lethal toxin (PA + LF). After 4 h, cell lysis was quantified by lactate dehydrogenase release assay. (b) Clonal i129 cells or the parental mixed population were treated with LT (1 μg/ml). After 5 h, live cells were quantified by neutral red assay. (c) i129 Clone #22.3 cells were treated with indicated LT doses (PA constant at 2 μg/ml). After 4 h, live cells were quantified by neutral red assay. (d) i129 Clone #22.3 (GFP+) cells were treated with LT (1 μg/ml) and imaged by time-lapse microscopy for 4 h. Red dye (1 μM $EtBr_2$) marks permeabilized cells. Arrows mark individual cells over time. (e) iB6 GFP+ (MSCV-GFP-FlaC20) cells were transfected with GFP-targeting siRNA or mock trasnfected. After 52 h GFP fluorescence was quantified by flow cytometry. Data shown (± s.e.m.) are representative of at least two experiments.

2.3 High-throughput Optimization of Screening Protocol

Given the preliminary results using GFP-targeted siRNA, I predicted that transfection with siRNA oligos targeting components of the NLRP1B inflammasome would protect i129-22.3 cells from LT-induced pyroptosis. Indeed, knockdown of CASP1 with 4 of 4 oligos and knockdown of NLRP1B with 2 of 4 oligos provided protection (Fig. 2.3a). Pooling of the oligos was also effective. Non-targeting 'scramble' oligos or GFP-targeted oligos provided no benefit and demonstrated the low background survival of i129-22.3 cells, with >99% of cells releasing GFP. Therefore, even if transfection and knock-down was effective in only a low percentage of cells (e.g. 20-25%), the surviving cells remain readily distinguishable from background due to the powerful negative selection of non-targeted cells by LT.

Next, I undertook a series of experiments to automate the assay from Fig 2.3a in 384-well format for high-throughput screening. After optimizing cell seeding density, transfection lipid and concentration, transfection time, and oligo concentration, I developed the protocol provided in detail as Appendix A. In brief, RNAiMax (0.1 µl/well) was mixed with siRNA oligo (50 nanomoles) and 1.8x10^3 cells were plated on top of these complexes for 'reverse' transfection. Following a 72-hour incubation, cells were treated for 3.5 h with 1 µg/ml PA + 0.75 µg/ml LF. This toxin concentration was selected based on titration experiments (Fig 2.2c) as a minimal saturating dose. Although lower concentrations also provided robust killing, I selected this higher concentration to minimize background survival, as this was a critical parameter for the success of the screen. Following toxin treatment, the cells were fixed and washed twice before analysis.

As an assay endpoint I compared analysis by microscopy with quantification of GFP fluorescence on a plate reader. I selected the plate reader because it gave the same results as microscopy but offered dramatic time and cost savings. Representative results from one optimization assay are shown in Fig 2.3b.

The Z-factor, which is derived from the difference between positive and negative controls and the variability between replicates, is a common metric used to assess the quality of a high-throughput screen. Given the large number of data points in a full-genome screen, the Z-factor must be evaluated very stringently. A score of 0-0.5 is considered a marginal assay, while scores above 0.5 indicate an excellent assay. Using CASP1 as the positive control, the Z-factor from Fig 2.3b is 0.79. Using NLRP1B as the positive control the score is 0.16. This means that the ability of the screen to detect genes that affect susceptibility to LT may be variable (see Discussion (2.6)).

2.4 Pilot Screening

To further test the screening protocol, I performed a small-scale pilot screen using a customized set of siRNA oligos targeting all NBD-LRR family members and any proteins encoding known or putative caspase activation and recruitment domains (CARD). Four oligos targeting each gene were included in separate wells. The complete list is provided in Appendix B. I repeated the pilot screen three times and a representative list of the top hits ranked relative to a pooled CASP1 positive control are listed in Table 2.1. I was pleased to note that all four oligos targeting *Casp1* and one of the oligos targeting *Nlrp1b* comprised the top hits. Interestingly, one oligo targeting *Nlrp1a* also scored highly, however further analysis revealed that while this oligo does not target the C57BL/6J allele of *Nlrp1b* used to design the library, it is a perfect match for the 129 allele of *Nlrp1b*. Furthermore,

Asc/Pycard, which is required for cytokine processing but not pyroptosis downstream of the NLRP1B inflammasome[110], did not appear among the top hits, as expected. It is also worth noting that none of the genes closely related in sequence to *Caspase-1* and *Nlrp1b*, but known not to be required for responsiveness to LT, appeared as false-positives. Based on the results of this screen, there is also no evidence for involvement of previously uncharacterized NBD-LRR or CARD proteins in the sensing of LT.

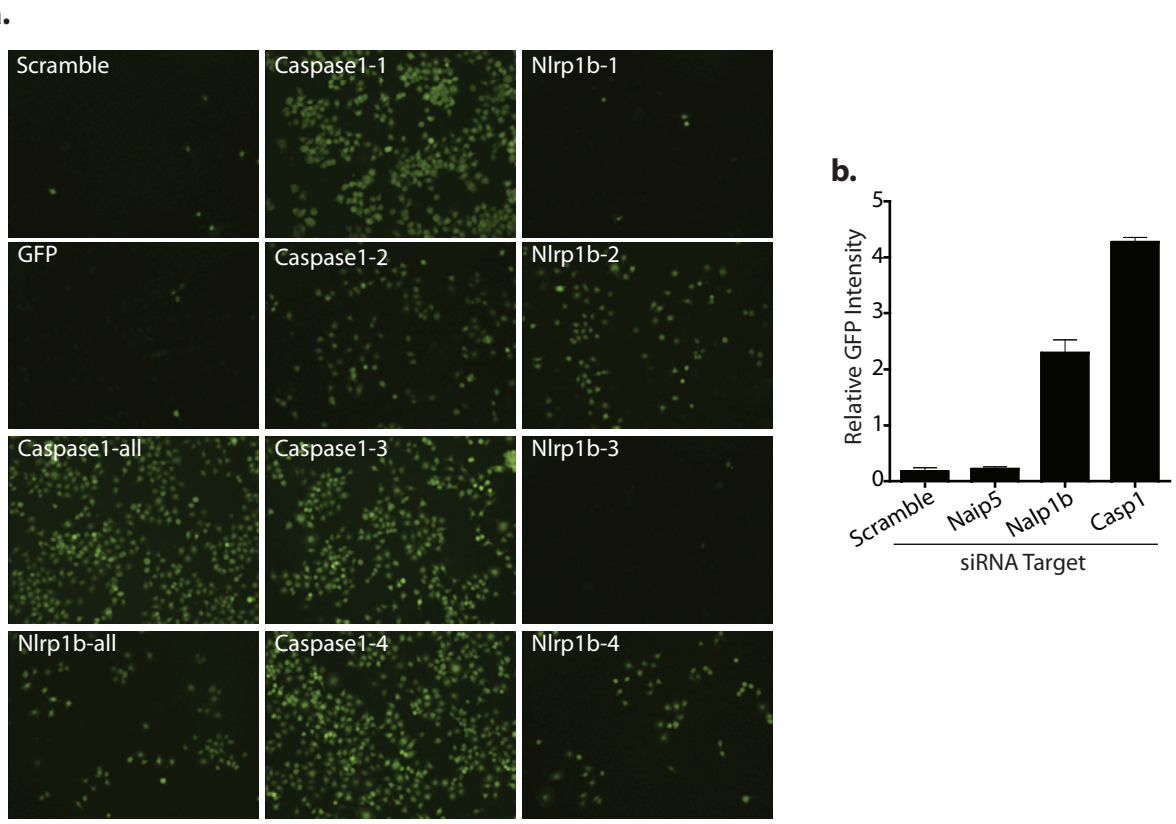

Figure 2.3 High-throughput optimization
(a) i129 Clone #22.3 cells were transfected with the indicated siRNA oligos (96-well format; 1x10^4 cells/well, 6 picomoles siRNA, 0.3 µl RNAiMax Lipofectamine). After 72 hours, cells were treated 4 h with lethal toxin, washed, and imaged for GFP. (b) Indicated siRNA oligos were tested using the optimized high-throughput screening protocol (Appendix A)

Table 2.1 Top hits from inflammasome pilot screen

Gene ID	Gene	Description	% Pos Control
12362	Casp1	caspase 1	131.98%
12362	Casp1	caspase 1	84.68%
195046	Nlrp1a	NLR family, pyrin domain containing 1A	49.26%
12362	Casp1	caspase 1	48.19%
637515	Nlrp1b	NLR family, pyrin domain containing 1B	47.81%
12362	Casp1	caspase 1	36.26%

Next I scaled up the pilot screen to include a commercially available multi-plate library targeting kinase-related genes (Qiagen). As was perhaps expected, since there is no known contribution of kinases to inflammasome signaling, knockdown of these genes

provided little protection from LT compared to the *Caspase1* positive control (Table 2.2). I performed this kinase screen twice, and four genes (*Hipk1, 2610207I05Rik, Trib1*, and *Skp2*) appeared among the top 30 hits both times. Although there is no obvious connection between these genes and the NLRP1B inflammasome based on a literature search, they may warrant future analysis. Global gene expression analyses suggest that *Hipk1* and *Trib1* are highly expressed in myeloid cells (biogps.org).

Table 2.2 Top hits from kinase library pilot screen

Gene ID	Gene	Description	% Control
56504	Srpk3	serine/arginine-rich protein specific kinase 3	42.45%
18715	Pim2	proviral integration site 2	38.87%
211770	Trib1	tribbles homolog 1 (Drosophila)	38.55%
19184	Psmc5	protease 26S subunit, ATPase 5	38.24%
80914	Uck2	uridine-cytidine kinase 2	37.59%
237459	Pctk2	PCTAIRE-motif protein kinase 2	37.41%
58231	Stk4	serine/threonine kinase 4	37.25%
15257	Hipk1	homeodomain interacting protein kinase 1	36.99%
328329	Mast4	microtubule associ serine/threonine kinase fam 4	36.54%
21915	Dtymk	deoxythymidylate kinase	36.50%
108097	Prkab2	prot kinase, AMP-act, beta 2 non-catalytic subunit	36.44%
26407	Map3k4	mitogen-activated prot kinase kinase kinase 4	36.32%
60597	Mapk8ip2	mitogen-activated prot kinase 8 interacting protein 2	36.21%
73086	Rps6ka5	ribosomal protein S6 kinase, polypeptide 5	36.09%
17347	Mknk2	MAP kinase-interacting serine/threonine kinase 2	36.08%
17346	Mknk1	MAP kinase-interacting serine/threonine kinase 1	35.75%
94093	Trim33	tripartite motif-containing 33	35.47%
22612	Yes1	Yamaguchi sarcoma viral oncogene homolog 1	35.04%
71743	Coasy	Coenzyme A synthase	35.01%

2.5 Results of the Full Genome Screen

Having optimized the protocol and completed two pilot screens that suggested reasonable false-positive and false-negative rates, I proceeded with a full genome screen using the mouse-targeted siRNA library from Qiagen. This library targets about 17,000 genes with an average of four pooled oligos for each gene. The resulting GFP signal in each well (correlated to cell survival) was expressed as the standard deviations above the mean GFP signal in wells transfected with non-targeting scramble oligo on the same plate. Based on these criteria, about 450 oligos gave a signal >2 standard deviations above the mean.

During the full-genome screen, several wells showed significant position effects due to equipment bias and were highly over-represented among the top hits. In particular, wells that failed to get sufficient siRNA oligo consistently gave an elevated GFP signal. This was likely due to enhanced cell growth in the absence of transfection-induced toxicity. An attempt to re-array the oligos from these false-positive wells and from the top 450 hits for secondary screening failed completely (data not shown). Most likely the RNA-based oligos were degraded during the long room temperature processing times required by the liquid-handling robotics used for the re-arraying.

For further analysis, I ordered fresh oligos targeting the top 140 hits (>3.5 standard deviations above the mean) (Table 2.3). These oligos were provided in deconvoluted

format, with each distinct oligo in a separate well. These oligos were screened twice in reverse plating orientation to eliminate position effects. Representative data for each individual oligo of the top 5 hits are shown in Figure 2.4a, and the top 15 hits based on aggregated results from the primary screen and re-screens are listed in Table 2.4.

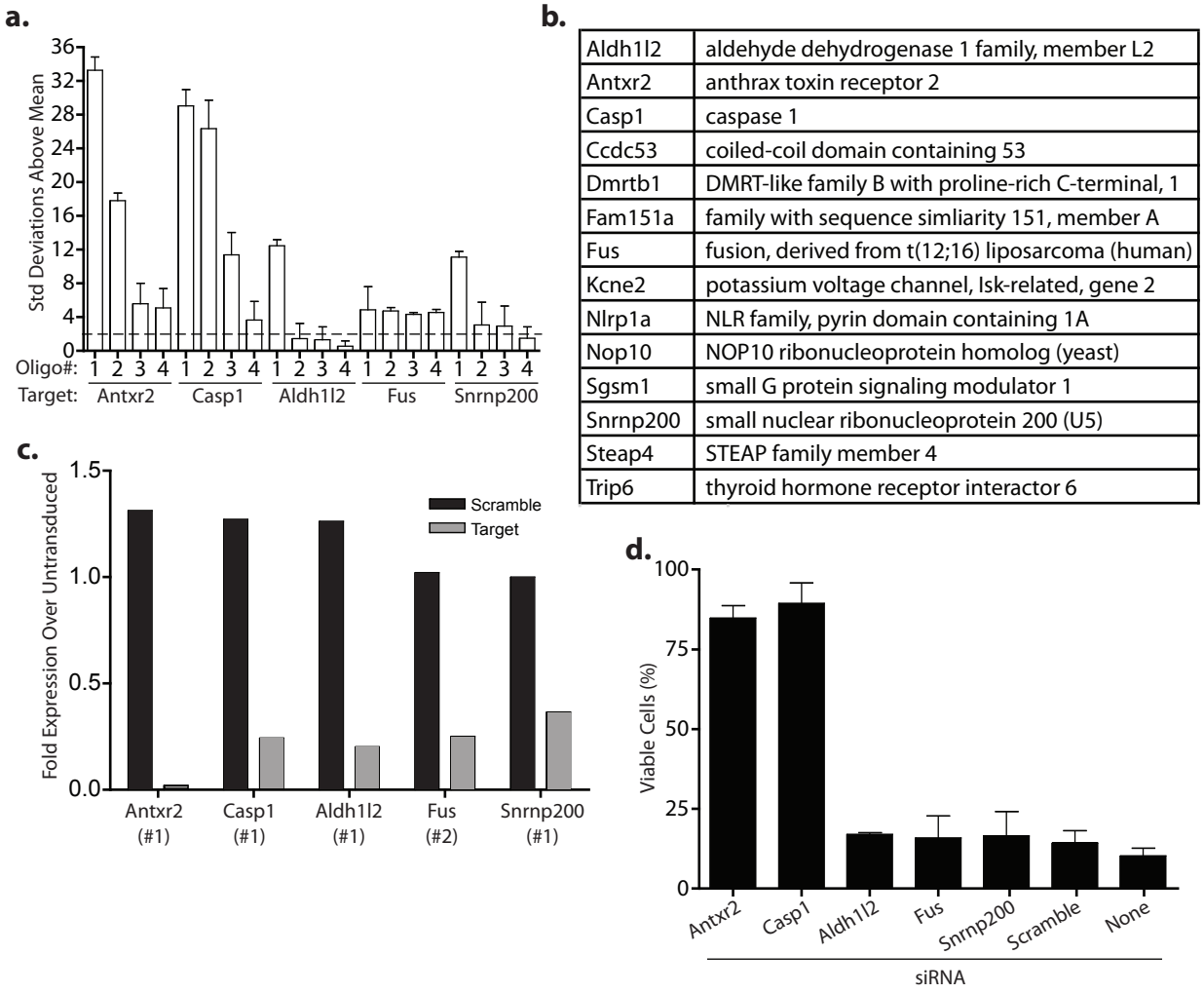

Aldh1l2	aldehyde dehydrogenase 1 family, member L2
Antxr2	anthrax toxin receptor 2
Casp1	caspase 1
Ccdc53	coiled-coil domain containing 53
Dmrtb1	DMRT-like family B with proline-rich C-terminal, 1
Fam151a	family with sequence simliarity 151, member A
Fus	fusion, derived from t(12;16) liposarcoma (human)
Kcne2	potassium voltage channel, Isk-related, gene 2
Nlrp1a	NLR family, pyrin domain containing 1A
Nop10	NOP10 ribonucleoprotein homolog (yeast)
Sgsm1	small G protein signaling modulator 1
Snrnp200	small nuclear ribonucleoprotein 200 (U5)
Steap4	STEAP family member 4
Trip6	thyroid hormone receptor interactor 6

Figure 2.4 Full genome screen and validation
(a) Deconvoluted results from top five re-screen hits. See Appendix A for protocol. (b) List of candidates for which stable shRNA cell lines were generated in i129-#22 cells. (c) qPCR quantification of candidate gene expression in shRNA cell lines. Numbers indicate oligo from (a) used for knockdown. (d) Viability (Guava assay) of stable shRNA knockdown cell lines following 3 h LT (1 μg/ml PA + 0.5 μg/ml LF) treatment.

Importantly, the two top genes identified in this non-biased screen were *Caspase-1* and *Antxr2*, which is the predominant receptor for LT expressed in macrophages[111]. This result strongly validates the screening assay. For both of these top hits, all four individual oligos scored >2 SD above the mean. Disappointingly, for most other top hits (e.g. *Aldh1l2* and *Snrnp200*) only one oligo scored well above the mean, and while all four oligos for *Fus* were >2 SD above the mean, none conferred robust survival.

Notably, *Nlrp1b* itself was not identified in this screen, likely due to the relatively poor targeting of this gene by the oligos included in the library (Fig 2.3). Nonetheless,

pooled *Nlrp1b* oligos were readily distinguishable from background in our optimization assays, suggesting a high false-positive rate in the full genome screen that masked the weak, but real, *Nlrp1b* result. This hypothesis is supported by the relatively low Z-factor calculated when using Nlrp1b as a control.

2.6 Novel Candidates Fail to Validate in shRNA Cell Lines

Eleven (Fig 2.4b and Appendix C) of the novel hits were selected for further analysis based on literature searches and predicted expression in macrophages. Stable shRNA knockdown lines were generated in i129-22 (GFP-) cells for these eleven genes plus positive and negative controls using the highest scoring 1-2 oligos for each gene (Appendix C). Knockdown of the target gene was confirmed by qPCR (Appendix D) and ranged from 64-98% (Fig 2.4c and data not shown). Protection against LT-induced pyroptosis was assessed in these knockdown lines using cell viability counting on a Guava Cell Analyzer. Surprisingly, only the *Caspase-1* and *Antxr2* positive controls showed any enhanced survival, even after testing a range of toxin doses and treatment times (Fig 2.4d and data not shown).

2.7 Discussion

Unfortunately, the full-genome siRNA screen described in this chapter failed to identify any validated novel components of the NLRP1B inflammasome. Although the unbiased identification of *Caspase-1* and *Antxr2* suggest a successful screening strategy, all novel candidates failed to validate using stable shRNA cell lines. This is surprising, because even if the results achieved with siRNA oligos represent off-target effects, these effects should be replicated when using the same targeting sequence in the shRNA constructs. Nonetheless, the contribution of off-target effects could be tested by complementing i129 cells with cDNA encoding non-targeted mRNA for candidate genes and repeating the siRNA analysis. Additionally, it would be interesting to test if candidate genes contribute to NAIP5/NLRC4 inflammasome activation by delivering flagellin in siRNA-targeted cells. Finally, it is possible that the knockdown achieved in shRNA cell lines is inefficient compared to siRNA. Indeed, it is widely recognized that shRNA-mediated knockdown is often less effective than siRNA-mediated knockdown and that knockdown phenotypes often exhibit a threshold effect, with small changes in knockdown giving rise to large phenotypic differences (Lin He, personal communication). Further analysis of candidate genes will likely require siRNA transfection, however this presents significant technical challenges unless the transfection efficiency in macrophages can be improved. Perhaps analysis in a reconstituted inflammasome system using more tractable cells, such as HEK-293T, will prove fruitful.

In the meantime, it is worth considering the possible causes for these disappointing results. First, the screen may have been limited by the quality of the siRNA library, although this is difficult to test empirically. In particular, because the library was designed using a C57BL/6J reference genome and our screen was necessarily carried out in 129 cells, gene targeting may have been inefficient. This effect is particularly amplified in highly polymorphic immune genes, as was demonstrated by the poor targeting of *Nlrp1b* and the off-target effect of the *Nlrp1a* oligo described in section 2.4. Furthermore, from analysis of knockdown efficiency in the shRNA cell lines, it appears that *Caspase-1* targeting achieved

above average results. Therefore, while the Z-factor calculated using *Caspase-1* as a positive control suggested a robust screen, this may not have been representative of the full library.

Next, it is of course possible that the screen was limited by the common technical challenges in high-throughput analysis and siRNA screening that give rise to false positives resulting from off-target effects, experimental error, highly stable protein products, and statistical chance. The challenge of siRNA screening is exemplified by the divergent results of previous screens mentioned in section 2.1.

If taken at face value, however, our results suggest some interesting conclusions about the underlying biology of the NLRP1B inflammasome. Perhaps inflammasome signaling and regulation are relatively simple, and there are no additional components to be discovered using a negative selection approach. It is also possible that CASP1 induces pyroptosis by processing multiple redundant substrates and/or that these substrates are required for cell survival and therefore not amenable to knockdown. A forward genetic ENU screen that is on-going in our lab could address this last concern. ENU induces point mutations and can therefore give rise to partial loss-of-function alleles that give are sub-lethal but sufficient to give a phenotype in our assays. Alternatively though, it is perhaps time, to return to non-genetic approaches for the identification of novel Caspase-1 substrates.

Table 2.3 Top hits selected for rescreening

Gene ID	Gene	Description	Standard Dev Above Mean
207778	Dnahc7l	dyne in, axonemal, heavy chain 7-like	32.41
319476	Lrtm1	leucine-rich repeats and transmembrane domains 1	12.36
56412	2610024G14	RIKEN cDNA 2610024G14 gene	11.93
67857	Ppp6c	protein phosphatase 6, catalytic subunit	11.36
246133	Kcne2	potassium voltage channel, Isk-related subfamily, gene 2	10.99
235067	Cypt4	cysteine-rich perinuclear theca 4	10.02
320632	Snrnp200	small nuclear ribonucleoprotein 200 (U5)	9.90
257978	Olfr1322	olfactory receptor 1322	9.28
67282	Ccdc53	coiled-coil domain containing 53	9.17
68480	1110007C09	RIKEN cDNA 1110007C09 gene	9.10
634882	Itih5l	inter-alpha (globulin) inhibitor H5-like	9.03
230579	Fam151a	family with sequence simliarity 151, member A	8.95
272381	Lrrc4b	leucine rich repeat containing 4B	8.86
12362	Casp1	caspase 1	8.59
19177	Psmb7	proteasome (prosome, macropain) subunit, beta type 7	8.38
74023	Rd3	retinal degeneration 3	8.29
93762	Smarca5	SWI/SNF related, actin dependent regulator of chromatin	8.28
67771	Arpc5	actin related protein 2/3 complex, subunit 5	8.25
67216	Mboat2	membrane bound O-acyltransferase domain containing 2	8.21
69288	Rhobtb1	Rho-related BTB domain containing 1	8.12
21337	Tacr2	tachykinin receptor 2	8.03
110616	Atxn3	ataxin 3	7.85
235956	Zfp825	zinc finger protein 825	7.58
259052	Olfr659	olfactory receptor 659	7.40

67399	Pdlim7	PDZ and LIM domain 7	7.29
217379	Ubxn2a	UBX domain protein 2A	7.23
74868	Tmem65	transmembrane protein 65	7.18
20658	Son	Son DNA binding protein	7.17
216188	Aldh1l2	aldehyde dehydrogenase 1 family, member L2	7.16
67057	Yaf2	YY1 associated factor 2	7.16
210035	Tmem194	transmembrane protein 194	6.98
66181	Nop10	NOP10 ribonucleoprotein homolog (yeast)	6.89
434378	7030419G21	RIKEN cDNA 7030419G21 gene	6.80
211652	Wwc1	WW, C2 and coiled-coil domain containing 1	6.71
66414	Ndufa12	NADH dehydrog (ubiquinone) 1 alpha subcomplex, 12	6.66
380702	Gm879	gene model 879, (NCBI)	6.60
22051	Trip6	thyroid hormone receptor interactor 6	6.56
634346	EG634346	predicted gene, EG634346	6.54
13079	Cyp21a1	cytochrome P450, family 21, subfamily a, polypeptide 1	6.54
18142	Npas1	neuronal PAS domain protein 1	6.42
19414	Rasa3	RAS p21 protein activator 3	6.42
234582	Ccdc102a	coiled-coil domain containing 102A	6.34
68728	Trp53inp2	transformation related p53 inducible nuclear protein 2	6.17
233908	Fus	fusion, derived from t(12;16) liposarcoma	6.12
22059	Trp53	transformation related protein 53	6.01
67534	Ttll4	tubulin tyrosine ligase-like family, member 4	5.89
630825	EG630825	predicted gene, EG630825	5.86
52850	Sgsm1	small G protein signaling modulator 1	5.59
230766	Fam167b	family with sequence similarity 167, member B	5.37
117167	Steap4	STEAP family member 4	5.35
71914	Antxr2	anthrax toxin receptor 2	5.31
209232	Wfdc5	WAP four-disulfide core domain 5	5.30
170644	Ubn1	ubinuclein 1	5.25
56016	Hebp2	heme binding protein 2	5.24
14219	Ctgf	connective tissue growth factor	5.23
84112	Sucnr1	succinate receptor 1	5.12
68240	Rpa3	replication protein A3	5.11
17355	Aff1	AF4/FMR2 family, member 1	5.11
102644	Oaf	OAF homolog (Drosophila)	5.09
258634	Olfr1164	olfactory receptor 1164	5.07
17158	Man2a1	mannosidase 2, alpha 1	5.00
259003	Olfr172	olfactory receptor 172	4.98
17079	Cd180	CD180 antigen	4.97
239827	Pigz	phosphatidylinositol glycan anchor biosynthesis, class Z	4.96
19052	Ppp2ca	protein phos 2, catalytic subunit, alpha isoform	4.95
56296	Dmrtb1	DMRT-like family B with proline-rich C-terminal, 1	4.90
233878	Sez6l2	seizure related 6 homolog like 2	4.78
237930	Ttll6	tubulin tyrosine ligase-like family, member 6	4.74

Table 2.4 Rank order hits after rescreen

			Standard Deviations Above Mean			# of oligos in top 35	
shRNA	**Gene ID**	**Gene Name**	**Genome Screen**	**Re-screen I**	**Re-screen II**	**Re-screen I**	**Re-screen II**
*	Antxr2	anthrax toxin receptor 2	5.3	31.7	34.8	4	4
*	Casp1	caspase 1	8.6	31.0	29.7	4	3
*	Snrnp200	small nuclear ribonucleoprotein 200 (U5)	9.9	11.8	10.5	3	1
*	Aldh1l2	aldehyde dehydrogenase 1 family, member L2	7.2	11.8	13.2	1	1
*	Fus	fusion, derived from t(12;16) liposarcoma	6.1	7.6	4.9	2	4
	Shisa6	shisa homolog 6 (Xenopus laevis)	6.6	5.9	8.9	2	1
	Ctgf	connective tissue growth factor	5.2	6.5	7.0	1	1
	Son	Son DNA binding protein	7.2	6.6	1.0	3	
	Rhobtb1	Rho-related BTB domain containing 1	8.1	1.7	5.5		1
	Cypt4	cysteine-rich perinuclear theca 4	10.0	4.6	1.3		
	Rd3	retinal degeneration 3	8.3	4.1	2.4		1
*	Kcne2	potassium voltage-gated channel	11.0	4.3			
*	Steap4	STEAP family member 4	5.4	5.8	2.1	1	1
	Rasa3	RAS p21 protein activator 3	6.4	5.1	1.7		2
	Psmb7	proteasome subunit, beta type 7	8.38	4.3	1.55	1	

Chapter 3: Differential Requirement for CASP1 Autoproteolysis in Pathogen-Induced Cell Death and Cytokine Processing

3.1 Introduction

As described in Chapter 1, recent work from our lab and others has shed light on the molecular mechanisms of inflammasome assembly in response to bacterial flagellin or rod proteins in the secretion apparatus. However, the role of the adaptor protein ASC in the inflammasome, and its regulation of CASP1 autoproteolysis and cytokine processing remain unclear. We and others have reported previously that ASC-deficient macrophages infected with pathogens that activate NLRC4 are severely impaired in their ability to process and release mature IL-1β/IL-18, but remarkably, are still able to undergo pyroptotic cell death[17,71,112]. Even more remarkably, this NLRC4-dependent/ASC-independent cell death occurs in the absence of any detectable CASP1 processing, but is nevertheless abolished in CASP1 knockout cells. It remains unclear how cells lacking processed CASP1 can undergo a CASP1-dependent death, since autoproteolytic processing is thought to activate CASP1. One possibility is that CASP11, a proposed regulator of CASP1[113], which is also absent from CASP1 knockout cells[61], might be critical for NLRC4-dependent cell death. Another possibility is that the catalytic activity of CASP1 is not required for pyroptosis, and instead, unprocessed CASP1 functions to recruit other downstream death effectors. Lastly, it is possible that NLRC4 activates CASP1 in a manner that does not require ASC or autoproteolysis.

In this chapter we investigate the molecular basis for CASP1-dependent cell death. We demonstrate that sensors containing a CARD (such as NLRC4, NLRP1B or even a synthetic CARD-AIM2 chimera) can promote ASC-independent cell death. We also show that the ASC-independent cell death that occurs in macrophages infected with *S. typhimurium*, *L. pneumophila* and *P. aeruginosa* depends on the catalytic activity of CASP1 and does not require CASP11.

To investigate the requirement for CASP1 autoproteolysis in activation of cell death, we reconstituted CASP1 deficient macrophages with CASP1 constructs unable to undergo autoproteolytic processing due to mutations in key aspartate residues. Surprisingly, signaling through both NLRC4 and AIM2 led to pyroptotic cell death in the absence of CASP1 autoproteolysis, while efficient cytokine processing required autoproteolysis. In addition, we used fluorescent microscopy to monitor CASP1 during ASC-independent cell death. In contrast to cytokine processing that correlates with the formation of a single, large ASC/CASP1 focus, we observed a punctate staining for CASP1 in *Asc*$^{-/-}$ macrophages.

Taken together, our results suggest that two spatially and functionally distinct inflammasome-complexes can be formed in pathogen-infected cells: a large ASC/CASP1 focus containing active, fully cleaved CASP1 that is critical for cytokine processing and release, and ASC-independent inflammasomes containing un-processed but active CASP1 that is able to initiate rapid cell death. The experiments reported in this chapter were undertaken in close collaboration with Petr Broz in Denise Monack's lab at Stanford University and were published in *Cell Host and Microbe* with Petr and myself as co-first authors[110].

3.2 NLRC4-dependent Macrophage Death Occurs in the Absence of Detectable CASP1 Processing in ASC-deficient Cells

The processing of pro-CASP1 into its p20 and p10 subunits is a hallmark of CASP1 activation. Detection of CASP1 processing is routinely carried out on culture supernatants, since active CASP1 is released via a secretion pathway that has yet to be characterized[95]. Consistent with this, we confirmed previous results that found that wild-type (WT) macrophages rapidly released large amounts of processed p10 and p20 into the culture supernatant when infected with bacterial pathogens activating the NLRC4 inflammasome, such as *S. typhimurium*, *P. aeruginosa* and *L. pneumophila* (refs 17,71,112; Fig. 3.1 A-C**,** first lane). In WT macrophages infected with these pathogens, CASP1 activation was accompanied by efficient secretion of mature IL-1β and pyroptotic cell death. In contrast, infections of *Casp1*$^{-/-}$ and *Nlrc4*$^{-/-}$ macrophages did not lead to IL-1β release or host cell death, indicating that cytokine maturation and release, and pyroptotic cell death were dependent on CASP1 and to a large part on NLRC4 (Fig. 3.1 A-C**,** second and forth lane). *Nlrc4*$^{-/-}$ macrophages infected with *P. aeruginosa* or *L. pneumophila* released a small amount of IL-1β, albeit significantly less than WT macrophages, indicating that these pathogens activate other receptors in addition to NLRC4 (refs 17,71,112; Fig. 3.1 B and C**,** fourth lane). To determine whether the adaptor protein ASC is important for cytokine maturation and pyroptotic cell death, we infected macrophages from ASC-deficient mice. Consistent with previous results, we found that *Asc*$^{-/-}$ macrophages infected with *S. typhimurium*, *P. aeruginosa* or *L. pneumophila* were severely impaired in their ability to process and secrete mature IL-1β, as shown by ELISA and western blotting. However, *Asc*$^{-/-}$ macrophages infected with these intracellular bacterial pathogens released LDH to the same extent as WT macrophages. As expected from previous reports[17,71,112], *Asc*$^{-/-}$ macrophages did not detectably process CASP1 (Fig. 3.1 A-C, third lane). Consistent with a defect in cytokine maturation, un-processed pro-IL-1β was detected in the supernatant of *Asc*$^{-/-}$ macrophages, which was probably released during pyroptotic lysis of the cells (Fig. 3.1 A-C**,** arrowheads).

To determine whether activation of the AIM2 inflammasome induces cell death in the absence of ASC and CASP1 cleavage, macrophages from ASC-deficient mice were infected with *F. novicida*, which stimulates the cytosolic DNA-sensor AIM2. In contrast to *S. typhimurium*, *P. aeruginosa* and *L. pneumophila*, *Asc*$^{-/-}$ macrophages infected with *F. novicida* did not process and release IL-1β and were defective for pyroptotic cell death, as previously shown (refs 17,71,112; Fig. 3.1 D). These data confirm, in our experimental system, that AIM2-dependent cell death and CASP1 processing requires the adaptor molecule ASC, whereas NLRC4-dependent cell death does not require ASC and does not appear to require CASP1 autoproteolysis.

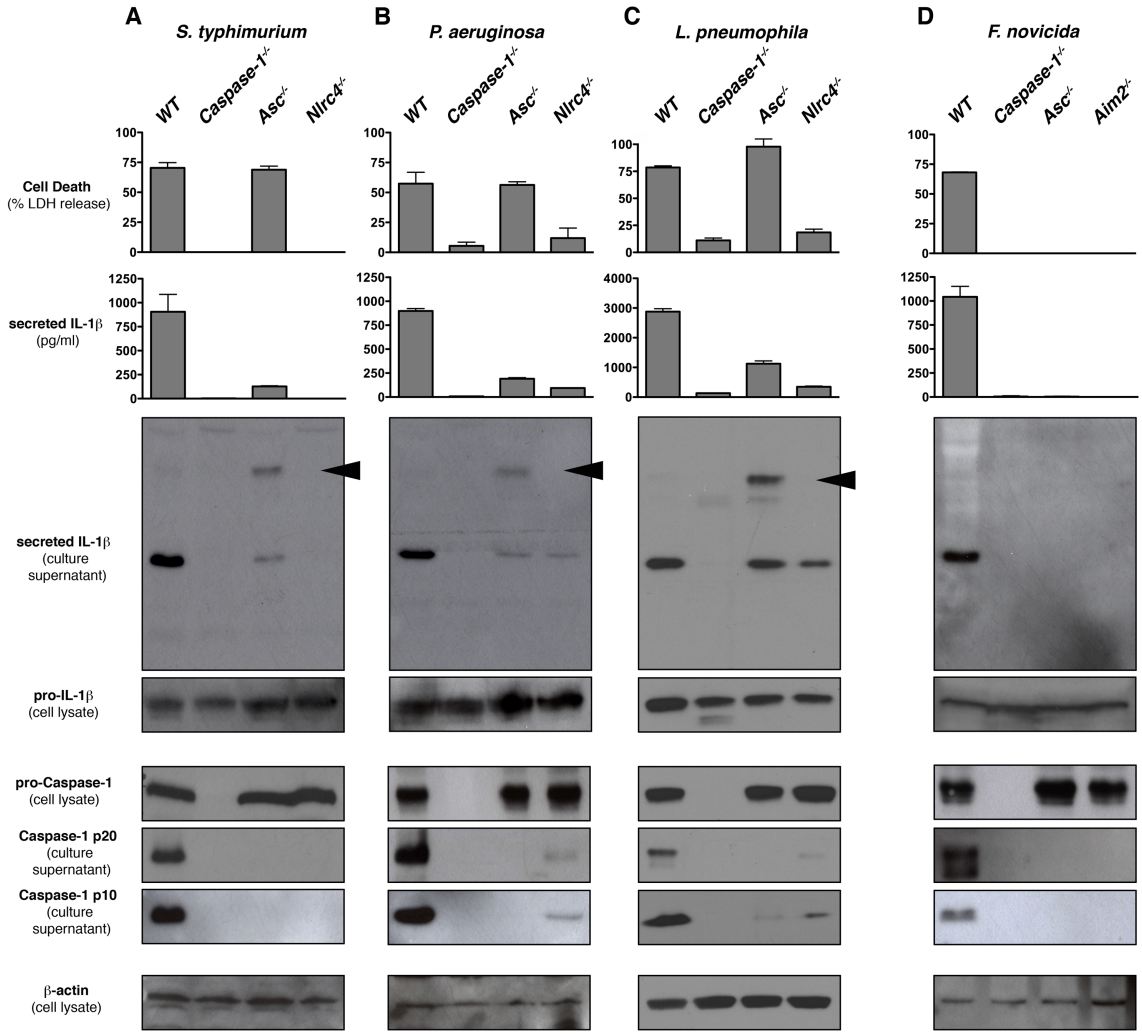

Figure 3.1 NLRC4-dependent macrophage death occurs in the absence of CASP1 cleavage in ASC-deficient cells

Bone marrow-derived macrophages of the genotypes indicated were infected with (a) *S. typhimurium* for 2h at an MOI of 20, (b) *P. aeruginosa* PAO1 for 2h at an MOI of 10, (c) *L. pneumophila* for 4h at an MOI of 1 and (d) *F. novicida* for 6h at an MOI of 100. Cell death was determined by measuring LDH release. Secretion of mature IL-1b into the culture supernatant was determined by ELISA and western blotting. Release of processed CASP1 p10 and p20 subunits into the culture supernatant was determined by western blotting. Corresponding cell lysates were probed for pro-IL-1β, pro-CASP1 and β-actin. Graphs show the mean ± standard deviation (SD) of triplicate wells and are representative of at least three independent experiments. Arrowhead indicates pro-IL-1β in the supernatant.

3.3 A CARD Domain is Required for ASC-independent Cell Death

In contrast to NLRC4, AIM2 contains only a PYRIN domain and no CARD domain, possibly rendering AIM2 incapable of recruiting CASP1 in the absence of ASC. We hypothesized that the presence of a CARD in NBD-LRR/PYHIN proteins would be sufficient to recruit and activate CASP1 and to promote cell death independently of ASC. To verify this hypothesis we first decided to test the only other known CARD-containing sensor, NLRP1B, which is activated by *Bacillus anthracis* lethal toxin (LT)[24]. As described in

Chapter 2, NLRP1B is extremely polymorphic in mice: macrophages derived from 129 mice express a functional allele and respond to LT by activating CASP1, while macrophages from C57BL/6 mice that have a non-functional allele do not respond to LT. Thus, we transduced immortalized C57BL/6 background WT and *Asc*$^{-/-}$ macrophages with the functional CARD-containing sensor *Nlrp1b* from 129 (Fig. 3.2A, 3.3A). WT macrophages expressing NLRP1B gained the ability to process IL-1β and to undergo cell death in response to LT. In contrast, *Asc*$^{-/-}$ macrophages expressing NLRP1B could only undergo pyroptosis, and did not efficiently process cytokines. Consistent with the NLRC4 data (Fig. 3.1), transduced *Asc*$^{-/-}$ macrophages were not able to process pro-CASP1 to its p20 and p10 subunits. All cell lines generated in this chapter, expressing functional inflammasome sensors or CASP1 (Appendix E), did not exhibit any spontaneous activation in the absence of inflammasome stimuli (Fig. 3.2C, D).

To further test our hypothesis that the CARD domain can activate CASP1-dependent death in the absence of ASC, we constructed a chimeric protein in which the NLRC4 CARD was fused to full-length AIM2 protein. Immortalized macrophages derived from AIM2- or ASC-deficient mice were transduced with WT AIM2 or the chimeric fusion construct and monitored for host cell death and cytokine processing in response to transfections of a synthetic AIM2 ligand, poly(dA-dT)•poly(dA-dT) [hereafter referred to as poly(dA:dT)] (Fig. 3.3B), and to *F. novicida* infection (Fig. 3.3C). *Aim2*$^{-/-}$ macrophages transduced with WT AIM2 or the CARD-AIM2 chimera constructs gained the ability to process and release IL-1β and to undergo cell death in response to transfection with poly(dA:dT) and infection with *F. novicida* (Fig. 3.3B, C). As expected, *Asc*$^{-/-}$ macrophages transduced with the WT AIM2 construct could not cleave IL-1β or induce cell death in response to both stimuli (Fig. 3.3B, C). The CARD-AIM2 fusion protein, however, restored the ability of *Asc*$^{-/-}$ macrophages to undergo cell death in response to *F. novicida* or poly(dA:dT) transfection, while only weakly restoring the ability of *Asc*$^{-/-}$ macrophages to process and release cytokine (Fig. 3.3B, C). Similar to the results obtained with *S. typhimurium*, *P. aeruginosa*, and *L. pneumophila* infections (Fig. 3.1), the ASC-independent cell death promoted by the CARD-AIM2 construct occurred in the absence of detectable CASP1 processing (Fig. 3.3B, C). Interestingly, expression of the CARD-AIM2 construct lead to the production of two proteins, one with the predicted size of the CARD-AIM2 fusion and a second one, with the same size as native AIM2 (Fig. 3.2B). The expression of the native-sized AIM2 is likely due to the presence of an alternative translation start codon at position 286, the native AIM2 start codon. Nevertheless, only the expression of the CARD-AIM2 fusion promoted the ability to cause ASC-independent cell death. Furthermore, expression of a CARD alone did not restore cell death or cytokine processing (data not shown). Taken together, these results demonstrate that in the context of an NBD-LRR/PYHIN protein, a CARD is sufficient to promote cell death in the absence of CASP1 processing and independently of ASC. We hypothesize that this cell death occurs following formation of complexes between CARD-containing NBD-LRR/PYHIN proteins and pro-CASP1.

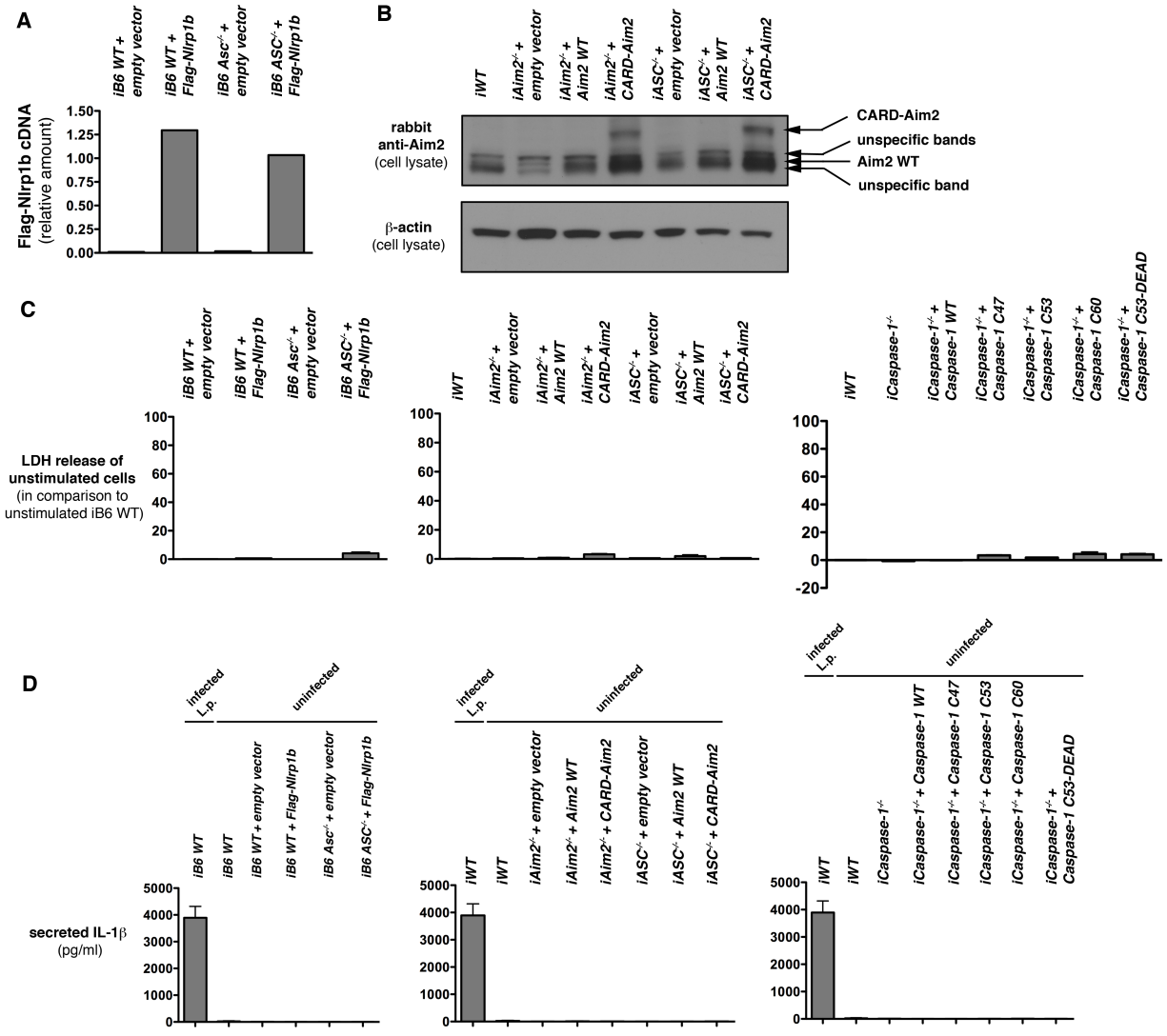

Figure 3.2 Cell Line Validation
(a) Quantitative RT-PCR analysis of Flag-*Nlrp1b* expression on RNA isolated from the indicated cell lines. Values are normalized to *Rps17* expression in each sample. (b) Cell lysates of immortalized WT, *Aim2*$^{-/-}$ or *ASC*$^{-/-}$ macrophages expressing an empty vector control, *Aim2* WT or a CARD-*Aim2* chimera were probed for AIM2 and β-actin. (c) Spontaneous LDH release from uninfected immortalized macrophages expressing an empty vector control or Flag-*Nlrp1b*, *Aim2* WT, CARD-*Aim2* or *Casp1* constructs. (d) IL-1β released by uninfected, immortalized macrophages expressing an empty vector control or Flag-*Nlrp1b*, *Aim2* WT, CARD-*Aim2* or the *Casp1* constructs. Infected immortalized WT macrophages are shown as comparison. Graphs show the mean ± SD of triplicate wells and are representative of two independent experiments.

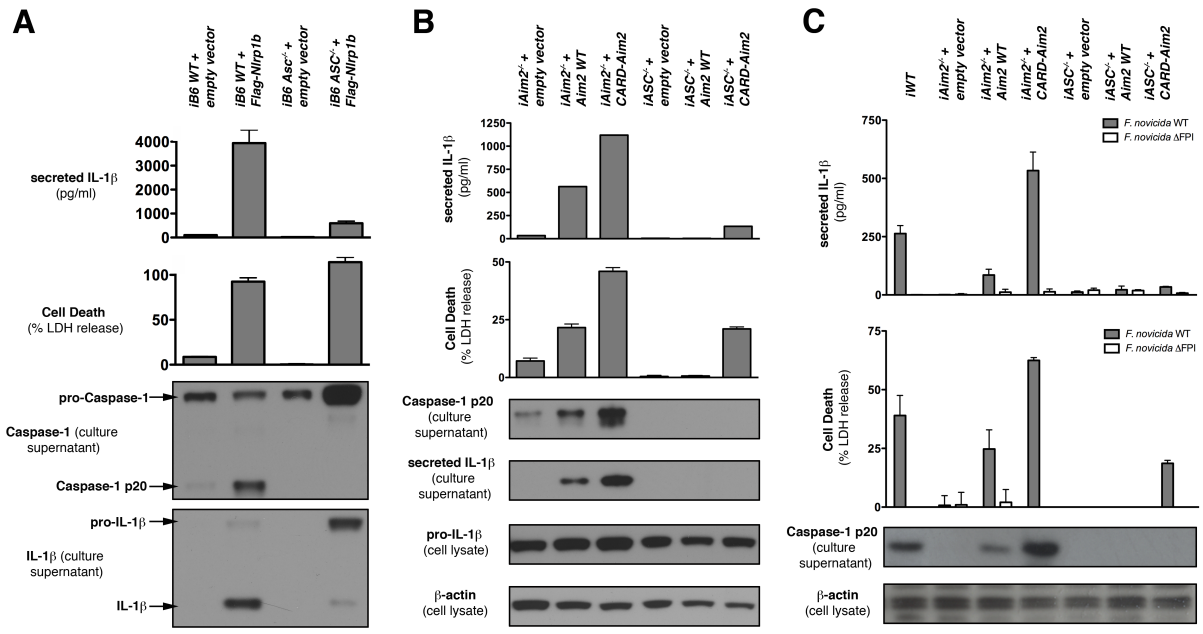

Figure 3.3 CARD-containing sensors promote ASC-independent cell death
(a) Immortalized WT and *Asc*$^{-/-}$ macrophages derived from C57BL/6 mice expressing an empty vector control or the functional *Nlrp1b* allele from 129S1 mice were stimulated for 4h with Anthrax lethal toxin. (b,c) Immortalized WT, *Aim2*$^{-/-}$ or *Asc*$^{-/-}$ macrophages expressing an empty vector control, *Aim2* WT or a CARD-*Aim2* chimera were transfected with poly(dA:dT) (b) or infected with *F. novicida* WT or a mutant that does not activate the inflammasome (ΔFPI) (c). Cell death was determined by measuring LDH release. Secretion of IL-1β into the culture supernatant was determined by ELISA and western blotting. Release of processed CASP1 p20 into the culture supernatant was determined by western blotting. Corresponding cell lysates were probed for pro-IL-1β and β-actin. Graphs show the mean ± SD of triplicate wells and are representative of two independent experiments.

3.4 Catalytic Activity of CASP1 is Required for ASC-independent Cell Death

To further investigate why processing of CASP1 is not required during ASC-independent cell death, we first considered the possibility that another caspase could be involved. Indeed previous reports proposed that CASP11 is critical for CASP1 activation[113] and demonstrated that CASP11 is absent in *Casp1*$^{-/-}$ mice[61]. Therefore the cell death observed in *Asc*$^{-/-}$ macrophages might be a result of CASP11 activity, independently of CASP1 and ASC. To address this, we compared WT, *Casp1*$^{-/-}$ and *Casp11*$^{-/-}$ macrophages infected with *S. typhimurium* (Fig. 3.4A). WT and *Casp11*$^{-/-}$ macrophages were killed to the same extent in response to infections with *S. typhimurium*. In contrast, *Casp1*$^{-/-}$ macrophages were not killed. Because CASP1 and CASP11 might act redundantly, we further validated our conclusions by stably transducing immortalized *Casp1*$^{-/-}$ macrophages (that lack both CASP1 and CASP11) with retroviral constructs expressing CASP1 or CASP11 (Fig. 3.4B). CASP1, but not CASP11, was able to complement the *Casp1*$^{-/-}$ macrophages.

Next we hypothesized that CASP1 might act as an adaptor to recruit other death effectors in the absence of its own cleavage or proteolytic activity. To test this model, we transduced BMDMs from *Casp1*$^{-/-}$ mice with retroviral constructs that contained either WT CASP1, or a catalytically inactive mutant CASP1 (CASP1 DEAD), in which we mutated the

active cysteine (C287A) to alanine (Fig. 3.5A). Both WT CASP1 and CASP1 DEAD were expressed to comparable levels, but only WT CASP1 restored the ability of *Casp1*$^{-/-}$ macrophages to secrete IL-1β and undergo cell death in response to *S. typhimurium*, and *L. pneumophila* infections.

We also sought to determine if the catalytic activity of CASP1 is necessary for ASC-independent cell death. Caspase inhibitors have been used previously to block the catalytically active enzyme by irreversibly binding to its active site. Thus, we infected WT and *Asc*$^{-/-}$ macrophages with *S. typhimurium*, and *L. pneumophila* in the presence of a CASP1 inhibitor (Z-YVAD-FMK) and monitored cell death and cytokine release (Fig. 3.5B). Inhibitor treatment completely abolished host cell death in *Asc*$^{-/-}$ macrophages in response to both pathogens, suggesting that ASC-independent cell death required CASP1 activity. Interestingly, inhibitor treatment only modestly reduced host cell death in WT macrophages (Fig. 3.5B). This was likely due to incomplete inhibition by Z-YVAD-FMK, as our results with the CASP1 DEAD mutant previously confirmed a complete dependence on CASP1 proteolytic activity in WT cells. Taken together, our results show that CASP1 does not act as an adaptor, but rather that its catalytic activity is required for cell death in WT and *Asc*$^{-/-}$ macrophages in response to stimuli that activate NLRC4.

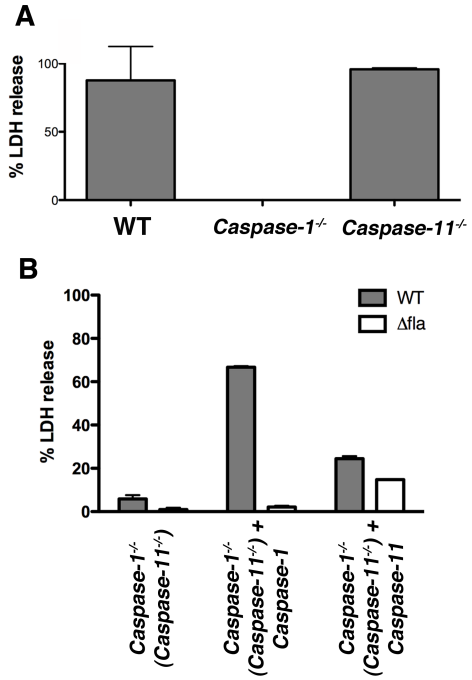

Figure 3.4 CASP11 does not promote cell death in *CASP1*$^{-/-}$ cells
(a) BMDMs derived from WT, *Casp1*$^{-/-}$ or *Casp11*$^{-/-}$ mice were infected with *S. typhimurium* for 2h at an MOI of 20. (b) Immortalized *Casp1*$^{-/-}$ macrophages were stably transduced with constructs expressing *Casp1* WT or *Casp11* WT. Cell death was determined by measuring LDH release. Graphs show the mean ± SD of triplicate wells and are representative of two independent experiments.

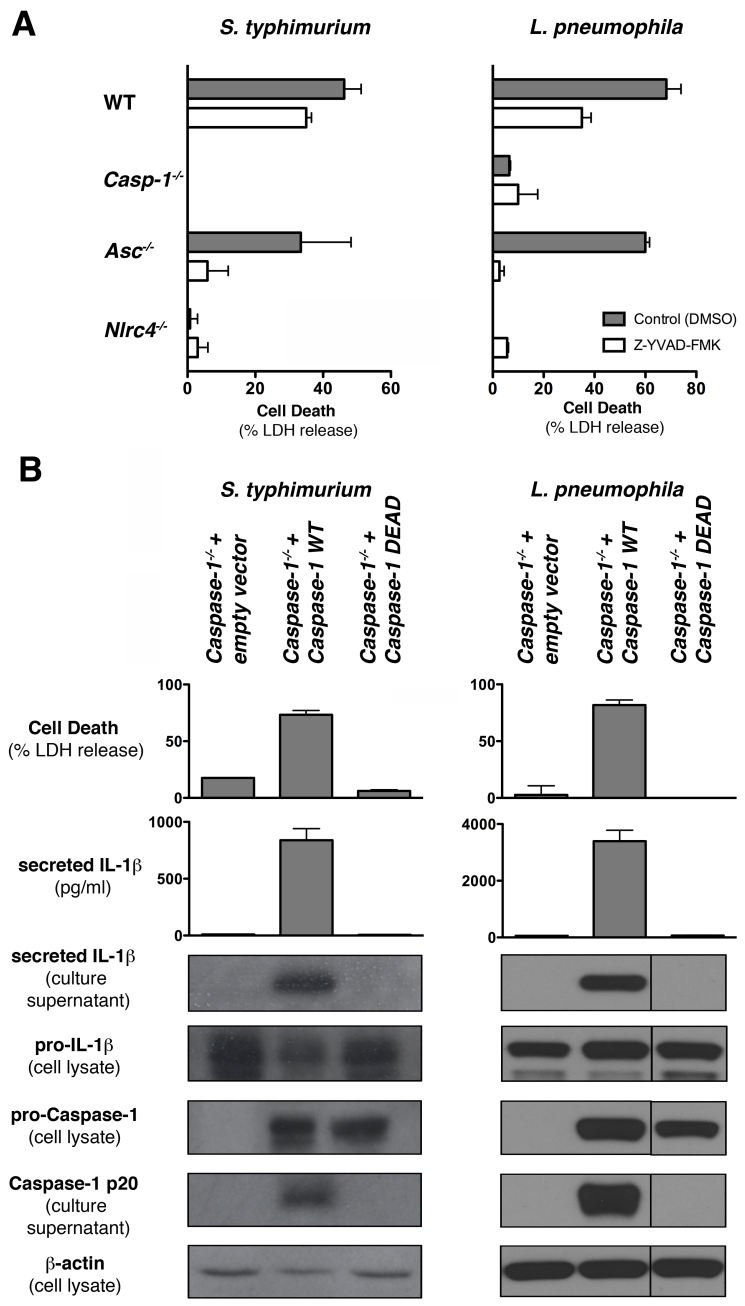

Figure 3.5 Catalytic activity of CASP1 is required for ASC-independent cell death
(a) *Casp1*$^{-/-}$ BMDMs expressing an empty vector control, WT *Casp1* or the catalytically inactive mutation C284A (CASP1 DEAD) were infected with *S. typhimurium* for 2h at an MOI of 20 or *L. pneumophila* for 4h at an MOI of 1. Cell death was determined by measuring LDH release. Secretion of IL-1β into the culture supernatant was determined by ELISA and western blotting. Secretion of processed CASP1 p20 into the culture supernatant was determined by western blotting. Corresponding cell lysates were probed for pro-IL-1β, pro-CASP1 and b-actin. (b) BMDMs of the genotypes indicated were infected with *S. typhimurium* for 1h at an MOI of 20 or *L. pneumophila* for 2.5h at an MOI of 1 in the presence of Z-YVAD-FMK or DMSO (vehicle control). Graphs show the mean ± SD of triplicate wells and are representative of at least two independent experiments.

3.5 Differential Subcellular Localization of CASP1

We showed previously that CASP1 is recruited to the ASC focus during *S. typhimurium* infection of WT macrophages[53]. In addition, we reported that staining with the fluorescent activity based probe FLICA (FAM-YVAD-FMK), detects active CASP1 at the site of the ASC focus. Since CASP1 activity is absolutely required for ASC-independent cell death in macrophages, we investigated whether FLICA could detect active CASP1 within cells in the absence of ASC. As expected, WT macrophages infected with *S. typhimurium*, formed an extremely bright focus of FLICA staining that co-localizes with the ASC focus; *Asc*$^{-/-}$ or *Casp1*$^{-/-}$ macrophages did not contain brightly stained foci (Fig. 3.6A, B asterisk; ref 53). However, we also detected a less intense speckled FLICA staining in the cytoplasm of infected cells. Intriguingly, this staining was observed in both WT and *Asc*$^{-/-}$ but not in *Casp1*$^{-/-}$ and *Nlrc4*$^{-/-}$ macrophages, indicating that it required inflammasome activation (Fig. 3.6C). Since the speckled staining correlated with cell death (Fig. 3.1, 3.6C), we speculated that these speckles could represent NLRC4-pro-CASP1 complexes that cause the ASC-independent cell death. To test the specificity of the FLICA-staining, we co-stained FLICA-labeled macrophages with an antibody that specifically recognizes the p20 subunit of murine CASP1, which contains the active site that is labeled by FLICA (Fig. 3.6A). To our surprise the CASP1 p20 staining and the speckled FLICA-pattern were non-overlapping, suggesting that the speckled FLICA pattern, although dependent on CASP1 activation, resulted from a non-specific FLICA labeling. Cells that could be stained with FLICA had lost almost all CASP1 p20 staining, except at the site of the ASC focus (Fig. 3.6A arrow). Indeed these cells were pyroptotic, since they clearly showed nuclear condensation, actin degradation and a loss of membrane integrity (Fig. 3.6A, B, D, unpublished data). We concluded that once pyroptosis is initiated, the cells rapidly release most of the active CASP1, except what is retained by the ASC focus. Pyroptotic cells may activate other proteases, which may explain the differential FLICA and CASP1 p20 staining pattern.

To prevent the rapid secretion of activated CASP1 and to determine whether CASP1 was recruited to structures other than the ASC focus, we repeated the experiments in the presence of Z-YVAD-FMK and in *Casp1*$^{-/-}$ macrophages expressing the CASP1 DEAD mutant (Fig. 3.6D, E). Under these conditions, WT macrophages and macrophages expressing the CASP1 DEAD mutant contained both the ASC/CASP1 focus as well as a punctate CASP1 p20 staining (Fig. 3.6D, E arrowheads). *Asc*$^{-/-}$ macrophages showed only the punctate staining, which was comparable to the CASP1 staining observed in both uninfected WT or *Asc*$^{-/-}$ macrophages (Fig. 3.6E). Altogether these data suggest that in the absence of ASC, CASP1 is not recruited into any large structure, comparable to the ASC focus, and thus might form smaller NLRC4-pro-CASP1 complexes.

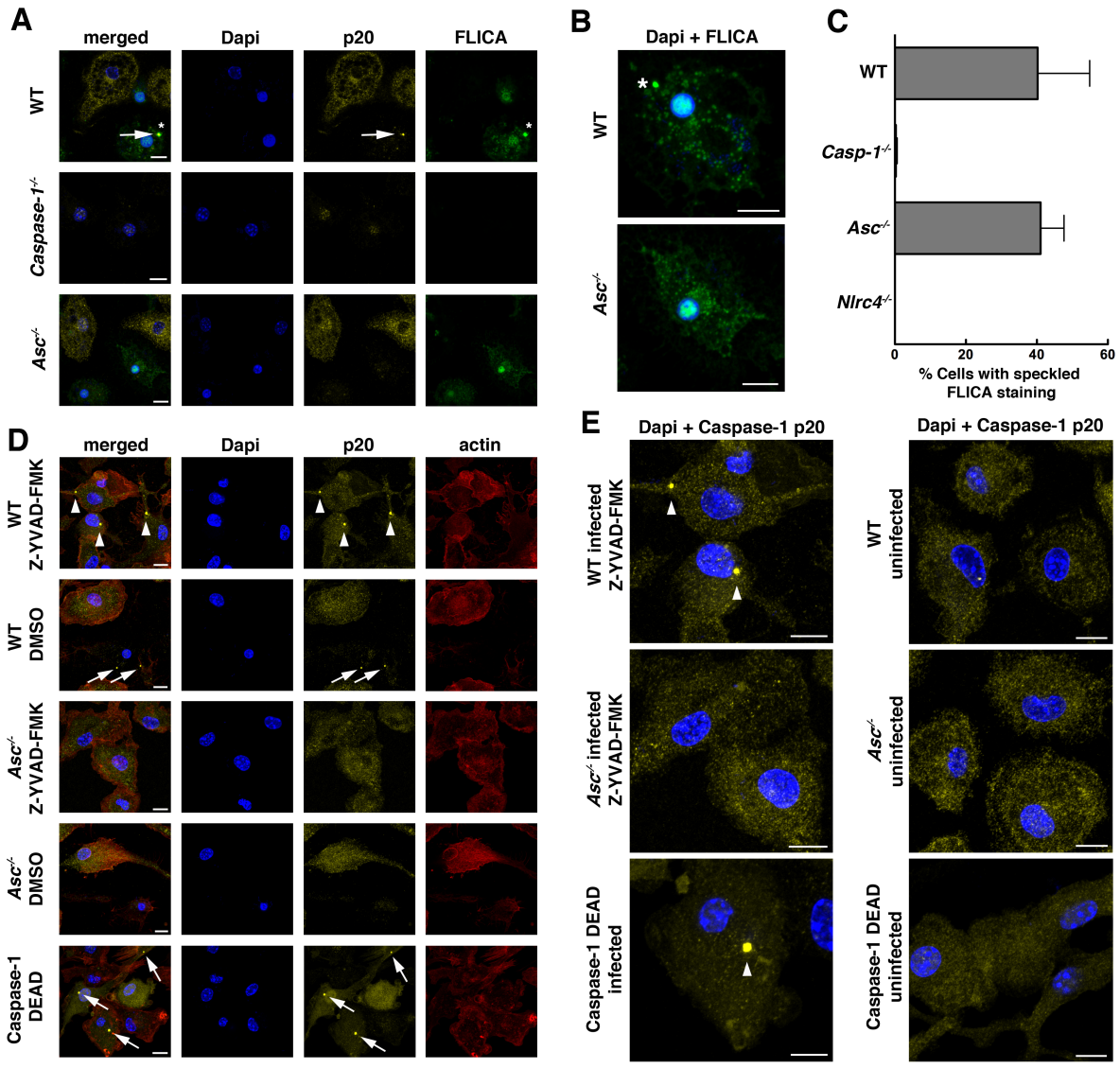

Figure 3.6 Differential subcellular localization of CASP1
(a) BMDMs of the genotypes indicated were infected with *S. typhimurium* for 2h at an MOI of 20, fixed and stained for DNA (Dapi), CASP1 p20 and with FLICA. Marked is an ASC focus stained by the CASP1 p20 antibody (arrow) or FLICA (asterisk). (b) Close up views of infected WT and *Asc*$^{-/-}$ macrophages stained for DNA (Dapi, blue) and with FLICA (green). (c) Percentage of cells with speckled, cytoplasmic FLICA staining. (d) WT and *Asc*$^{-/-}$ macrophages (treated with Z-YVAD-FMK or the vehicle control DMSO) or *Casp1*$^{-/-}$ macrophages expressing the catalytically inactive mutation C284A (CASP1 DEAD) were infected with *S. typhimurium* for 1h at an MOI of 20. Cells were fixed and stained for DNA (Dapi), CASP1 p20 and actin (Phalloidin). Indicated are ASC/CASP1 foci in the presence (arrowheads) or absence of the inhibitor (arrows). (e) Close up views of infected and uninfected WT and *Asc*$^{-/-}$ macrophages or *Casp1*$^{-/-}$ + CASP1 DEAD macrophages stained for DNA (Dapi, blue) and CASP1 p20 (yellow). Indicated are ASC/CASP1 foci (arrowheads). Cell counts in (c) were determined by counting twice 300 infected cells per sample. Images and cell counts are representative of at least two experiments. Scale bars in all images are 10 μm.

3.6 CASP1 Autoproteolysis is Necessary for Efficient Cytokine Processing, but not for Macrophage Cell Death

The above data suggest that rapid pathogen-induced cell death is mediated by NLRC4-pro-CASP1 complexes, which form through homotypic CARD domain interactions (Fig. 3.3). Interestingly, CASP1 is not detectably processed in these complexes (Fig. 3.1 and 3.3). However, our data imply that CASP1 must nevertheless be activated in these complexes, because a catalytically inactive mutant CASP1 does not mediate cell death in a CASP1-deficient background (Fig. 3.5). To investigate the importance of autoproteolytic processing of CASP1 into its p20 and p10 subunits, we decided to mutate putative cleavage sites in the linker domain between the p20 and p10 domains (Fig. 3.7A). Analysis of purified human pro-CASP1 suggests that the full-length zymogen (p45) is autoproteolytically processed at 4 Asp-Xaa bonds[56]. The first cleavage events at D297 and D316, remove the linker region between the p20 and p10 subunits, thus generating p10 and p35 subunits. The p35, which consists of the CARD and the p20, is then further cleaved at D122 and D103, releasing the mature p20 subunit from the CARD. The proteolytic separation of the CARD and p20 subunit, however, is not necessary for CASP1 activity, since mutating both D103 and D122 does not affect cell death and cytokine processing (unpublished data). Thus, for the sake of clarity, we refer to the proteolytic cleavage resulting in the separation of p20 and p10 subunits as CASP1 processing or autoproteolysis throughout the text. Interestingly, cleavage intermediates or alternative cleavage products like p24 and p14 subunits have been observed[56,114].

We first generated retroviral constructs, expressing murine pro-CASP1 mutated at cleavage sites defined previously in human CASP1. The constructs were tested by transducing immortalized *Casp1*$^{-/-}$ macrophage cell lines as well as bone-marrow derived *Casp1*$^{-/-}$ macrophages and infecting them with either *S. typhimurium* or *L. pneumophila* (Fig. 3.7, 3.8). In immortalized macrophages, the expression levels of the mutant CASP1 constructs were comparable, but lower than WT CASP1 (Fig. 3.7C). WT CASP1, as well as the mutant constructs, were expressed to similar levels when transduced into *Casp1*$^{-/-}$ bone-marrow derived macrophages (Fig. 3.7D, 3.8). However, the mutant constructs migrated at a slightly lower size than expected, likely due to the loss of charged residues. We first tested retroviral construct 47 (C47), expressing pro-CASP1 in which the aspartates D296, D313 and D314 were mutated to asparagines (Fig. 3.7B). To our surprise, the C47 mutant protein was still processed and restored the ability of *Casp1*$^{-/-}$ macrophages to cleave IL-1b and induce cell death in response to *S. typhimurium* or *L. pneumophila* infections (Fig. 3.7C, 3.8B, C). Although the C47 mutant construct was processed, the p20 and p33 (CARD-p20) subunits were slightly larger (Fig. 3.7C, 3.8B, C**,** asterisk), suggesting that the construct is processed at an alternative cleavage site. Alignment of pro-CASP1 from human and mouse revealed that murine CASP1 contained 3 additional aspartates between D296 and D314 (D297 and D316 in humans), of which at least two (D304, D308) could also serve as CASP1 cleavage sites based on the SVM algorithm (www.casbase.org; Fig. 3.7A). To define the cleavage sites between the p20 and p10 subunits, we constructed additional putative cleavage site mutations in the C47 mutant: C51, C52, C53 containing the D300N, D304N and D308N mutations, respectively (Appendix E, Fig. 3.7B). We then infected macrophages transduced with the different constructs with *S. typhimurium* or *L. pneumophila,* and analyzed CASP1 processing by western blotting for the p20 subunit in culture supernatants. Mutating D308 in addition to D296, D313 and D314 (construct C53)

completely abolished the generation of p20 and p10 subunits (Fig. 3.7C, D and 3.8B**,** C), while mutations in D300 and D304 had no effect (unpublished data). Instead, supernatants from macrophages transduced with the C53 construct contained two bands, labeled p32 and p34 that were detected by both the p20 and the p10 antibodies (arrowheads**,** unpublished data). We speculated that these cleavage products are the result of cleavage at residues D103 or D122 that leads to the removal of the CARD from the rest of the protein. This would be consistent with the observation that alternative cleavage at D103 and D119 can produce two different large subunits of human CASP1 (p20, p24) 56,114. The apparent size of these bands is slightly smaller than expected, presumably due to the change in charge of the mutated constructs. To prove that the p32/p34 subunits are a result of processing at residues D103 and D122, we mutated these residues in the C53 background, generating mutant construct C71 (Fig. 3.7B). Indeed, mutating D103, D122 in addition to D296, D308, D313 and D314 generated a completely uncleavable CASP1, since both the p34 and p32 bands disappeared and only full-length pro-CASP1 was released into the supernatant (Fig. 3.7D).

To analyze the importance of CASP1 processing for cytokine maturation and release, and host cell death, we infected the transduced macrophages with *S. typhimurium* or *L. pneumophila*. *Casp1*$^{-/-}$ macrophages transduced with WT CASP1 or C47 processed and released IL-1β and mediated cell death (Fig. 3.7C, 3.8). In contrast, the unprocessed CASP1 construct C53 mediated very low levels of IL-1β secretion into the supernatant when infected with *S. typhimurium* or *L. pneumophila* (Fig. 3.7C, D and 3.8). Surprisingly, transduction of Casp*1*$^{-/-}$ macrophages with the C53 construct partially rescued the cell death deficiency, causing >50% of WT CASP1 cell death in response to both pathogens. Importantly, cell death of macrophages expressing the C53 construct was dependent on CASP1 catalytic activity, since a mutation of the active cysteine C284 in the C53 background completely abolished activity (Fig. 3.8D).

It is, however, possible that low levels of cleavage at residues D300 and D304 (undetectable by western blotting) might be enough to mediate cell death in C53-transduced macrophages. Thus, we examined macrophages transduced with constructs C59 and C60 that contain additional D300N and D300N, D304N mutations, respectively (Fig. 3.7C, 3.8). Both C59 and C60 constructs had similar processing patterns to each other and were indistinguishable from C53, with p32/p34 subunits. Importantly, the unprocessed C59 and C60 constructs did not restore the ability of CASP1-deficient macrophages to process and release IL-1b, but they did mediate host cell death in response to *S. typhimurium* and *L. pneumophila* infections (Fig. 3.8B, C). Importantly, cell death in these mutants and C53 did not depend on the formation of the p32/p34 subunits, since the completely uncleavable mutant C71 (Fig. 3.7D**,** fourth lane) promoted cell death and only inefficiently processed IL-1β. This result confirmed that even if CASP1 cannot be processed, due to mutations of cleavage sites (Fig. 3.7B) or due to the absence ASC (Fig. 3.1), it can nevertheless efficiently promote pyroptotic cell death in response to bacterial infections. Overall, these results demonstrate that while CASP1 processing is not required for NLRC4-dependent macrophage death in response to infection with *S. typhimurium* or *L. pneumophila* (refs 13,112; Fig. 3.1), it is important for efficient cytokine processing.

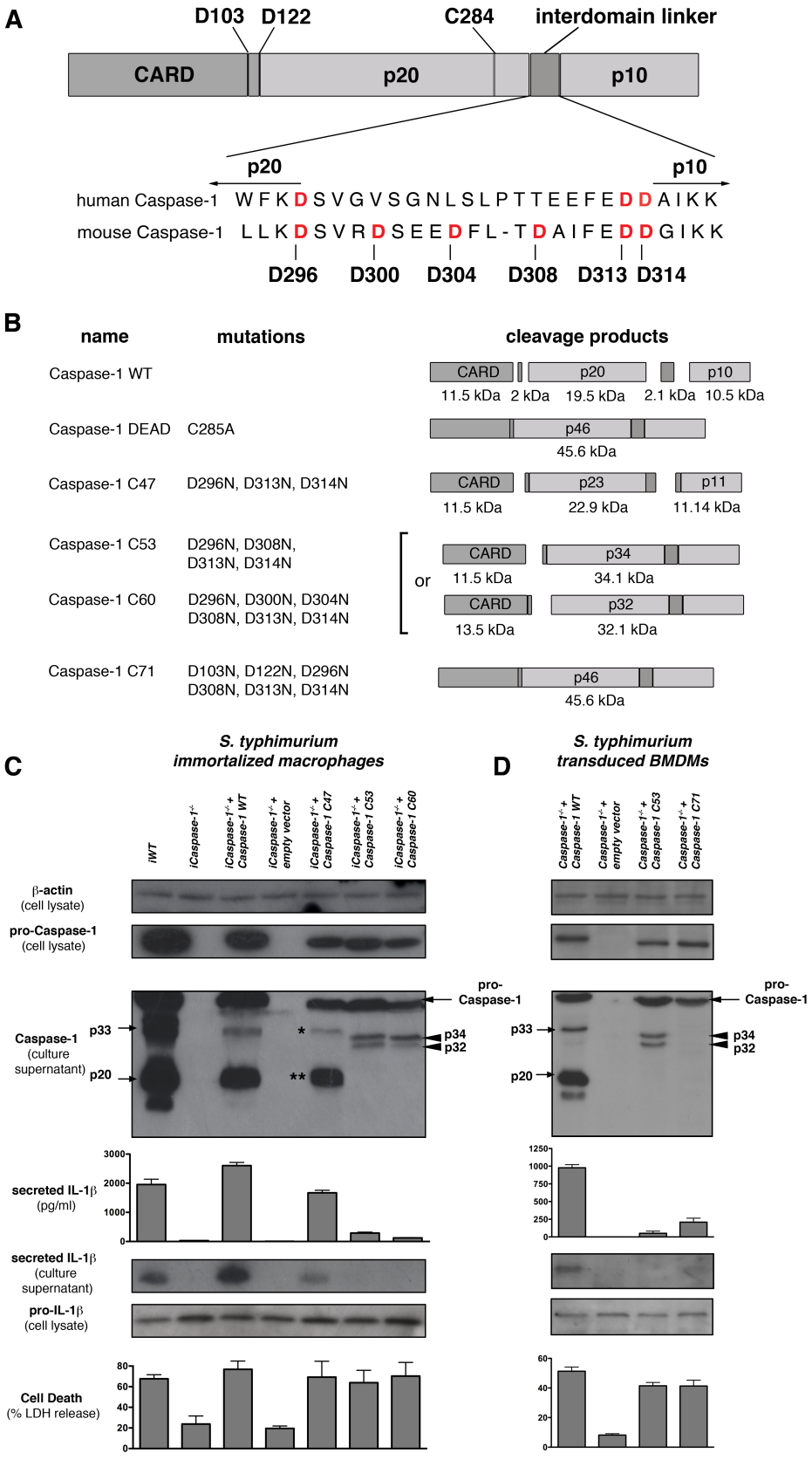
A
D103
D122
C284
interdomain linker
CARD
p20
p10
p20
p10
human Caspase-1 W F K D S V G V S G N L S L P T T E E F E D D A I K K
mouse Caspase-1 L L K D S V R D S E E D F L - T D A I F E D D G I K K
D296
D300
D304
D308
D313
D314
B
name
mutations
cleavage products
Caspase-1 WT
CARD
p20
p10
11.5 kDa
2 kDa
19.5 kDa
2.1 kDa
10.5 kDa
Caspase-1 DEAD
C285A
p46
45.6 kDa
Caspase-1 C47
D296N, D313N, D314N
CARD
p23
p11
11.5 kDa
22.9 kDa
11.14 kDa
Caspase-1 C53
D296N, D308N,
D313N, D314N
or
CARD
p34
11.5 kDa
34.1 kDa
Caspase-1 C60
D296N, D300N, D304N
D308N, D313N, D314N
CARD
p32
13.5 kDa
32.1 kDa
Caspase-1 C71
D103N, D122N, D296N
D308N, D313N, D314N
p46
45.6 kDa
C
S. typhimurium
immortalized macrophages
iWT
iCaspase-1-/-
iCaspase-1-/- + Caspase-1 WT
iCaspase-1-/- + empty vector
iCaspase-1-/- + Caspase-1 C47
iCaspase-1-/- + Caspase-1 C53
iCaspase-1-/- + Caspase-1 C60
β-actin
(cell lysate)
pro-Caspase-1
(cell lysate)
Caspase-1
(culture
supernatant)
p33
p20
pro-
Caspase-1
p34
p32
*
**
secreted IL-1β
(pg/ml)
3000
2000
1000
0
secreted IL-1β
(culture
supernatant)
pro-IL-1β
(cell lysate)
Cell Death
(% LDH release)
80
60
40
20
0
D
S. typhimurium
transduced BMDMs
Caspase-1-/- + Caspase-1 WT
Caspase-1-/- + empty vector
Caspase-1-/- + Caspase-1 C53
Caspase-1-/- + Caspase-1 C71
pro-
Caspase-1
p33
p20
p34
p32
1250
1000
750
500
250
0
60
40
20
0

Figure 3.7 CASP1 autoproteolysis is necessary for efficient cytokine processing, but not for macrophage cell death in response to *S. typhimurium* infections
(a) Schematic representation of the domain organization of murine pro-CASP1, showing an alignment of the interdomain linker of human and murine CASP1. Putative cleavage sites and the active cysteine are indicated. (b) Schematic representation of different mutated CASP1 constructs, showing mutations and expected cleavage products. (c-d) Immortalized or bone-marrow derived *Casp1*$^{-/-}$ macrophages expressing the indicated CASP1 constructs were infected with *S. typhimurium* for 2h at an MOI of 20. Cell death was determined by measuring LDH release. Secretion of IL-1β into the culture supernatant was determined by ELISA and western blotting. Release of CASP1 into the culture supernatant was determined by western blotting. Corresponding cell lysates were probed for pro-CASP1, pro-IL-1β and β-actin. Graphs show the mean ± SD of triplicate wells and are representative of at least two independent experiments.

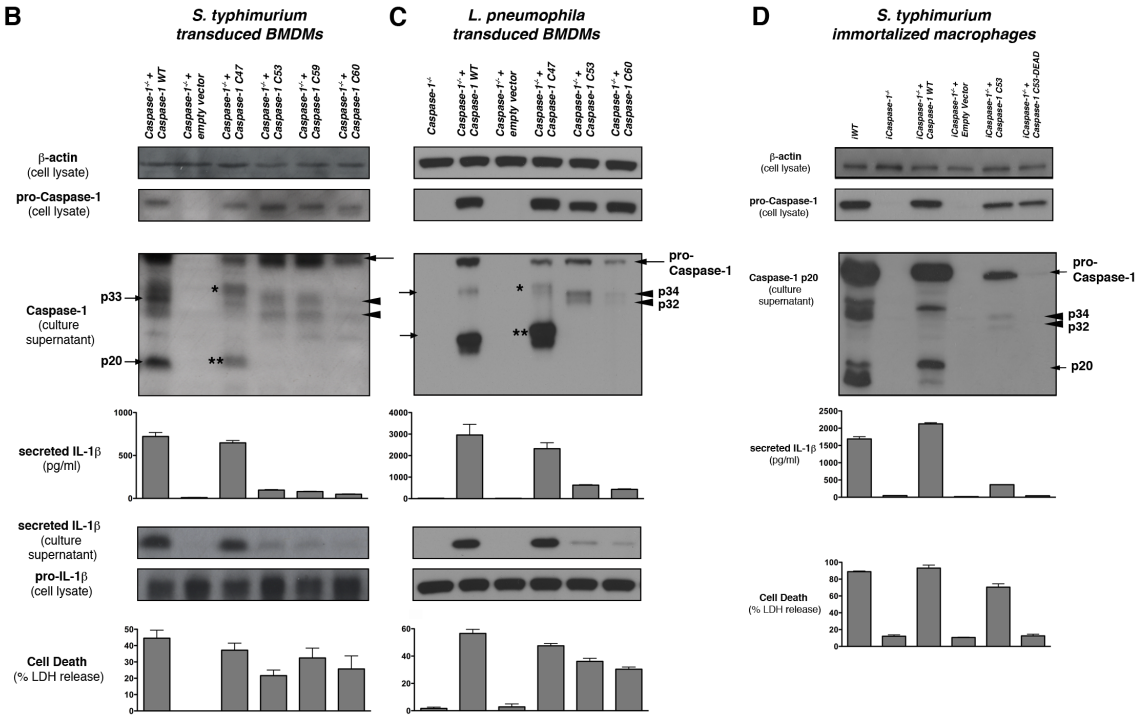

Figure 3.8 CASP1 autoproteolysis is necessary for efficient cytokine processing, but not for macrophage cell death in response to *S. typhimurium* and *L. pneumophila* infections
(b,c) Bone-marrow derived *Casp1*$^{-/-}$ macrophages, expressing the indicated CASP1 constructs, were infected with *S. typhimurium* for 2h at an MOI of 20 or *L. pneumophila* for 4h at an MOI of 1. Cell death was determined by measuring LDH release. Secretion of IL-1β into the culture supernatant was determined by ELISA. Secretion of processed CASP1 p20 into the culture supernatant was determined by western blotting. Corresponding cell lysates were probed for pro-CASP1, pro-IL-1β and β-actin. Graphs show the mean ± SD of triplicate wells and are representative of three independent experiments. (d) Bone-marrow derived *Casp1*$^{-/-}$ macrophages expressing the indicated CASP1 constructs were infected with *S. typhimurium* for 2h at an MOI of 20. Cell death was determined by measuring LDH release. Secretion of IL-1β into the culture supernatant was determined by ELISA and western blotting. Release of processed CASP1 p20 into the culture supernatant was determined by western blotting. Corresponding cell lysates were probed for pro-CASP1 and β-actin. Graphs show the mean ± SD of triplicate wells and are representative of two independent experiments.

3.7 CASP1 Processing is not Required for Macrophage Death in Response to AIM2 Stimuli

Our data suggest that NLRC4 can induce, through homotypic CARD domain interactions, CASP1-dependent cell death without a requirement for complete autoproteolytic processing of CASP1. We wondered, however, whether other receptors, such as AIM2, that require ASC for their interaction with CASP1, are capable of activating CASP1 autoproteolytic mutants. To test this, we infected immortalized *Casp1*$^{-/-}$ macrophages expressing the CASP1 mutant constructs described above (Fig. 3.7B) with *F. novicida*, which has been previously shown to activate AIM2 (refs 39-41, Fig 3.1D). Surprisingly, macrophages expressing CASP1 autoproteolytic mutants did not efficiently release IL-1β when infected with *F. novicida*, while they were killed to similar levels compared to WT macrophages (Fig. 3.9). Similarly, transfections of macrophages expressing CASP1 autoproteolytic mutant constructs with poly(dA:dT) or poly(dG:dC) did not result in cytokine processing but mediated levels of host cell death that were similar to those seen in WT macrophages (Fig. 3.10). Together our results demonstrate that CASP1 processing is not required for cell death in response to a variety of inflammasome stimuli that activate different inflammasome receptors.

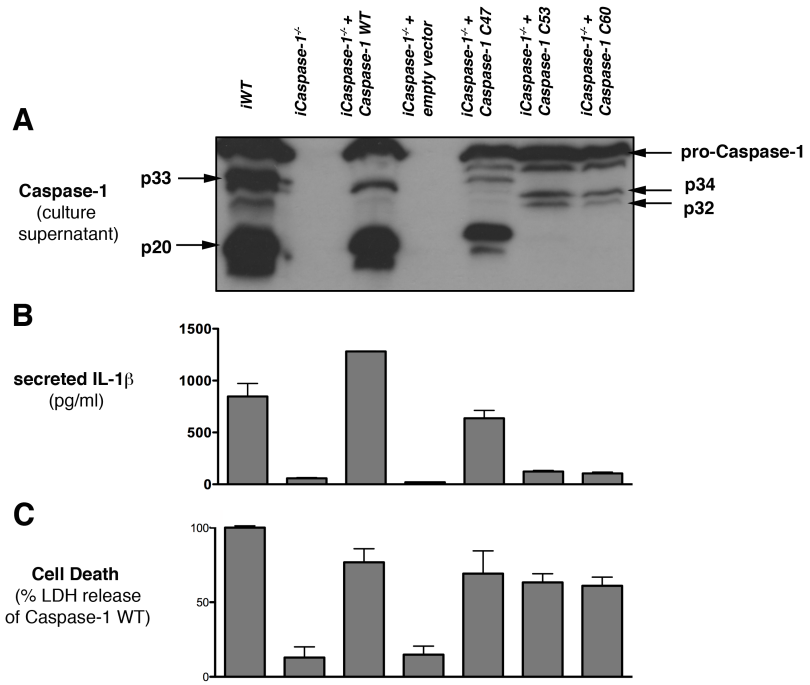

Figure 3.9 CASP1 processing is not required for macrophage death in response to *F. novicida* infections

Immortalized *Casp1*$^{-/-}$ macrophages expressing the indicated CASP1 constructs were infected with *F. novicida* for 9h at an MOI of 20. (a) Western blots for processed CASP1 p20 in culture supernatants. (b) ELISA for mature, secreted IL-1β in culture supernatants. (c) Cell death as determined by measuring LDH release. Arrows, arrowheads and asterisk indicate pro-CASP1 and different CASP1 auto-processing products. Results are representative of at least three independent experiments, error bars represent mean ± SD of triplicate wells.

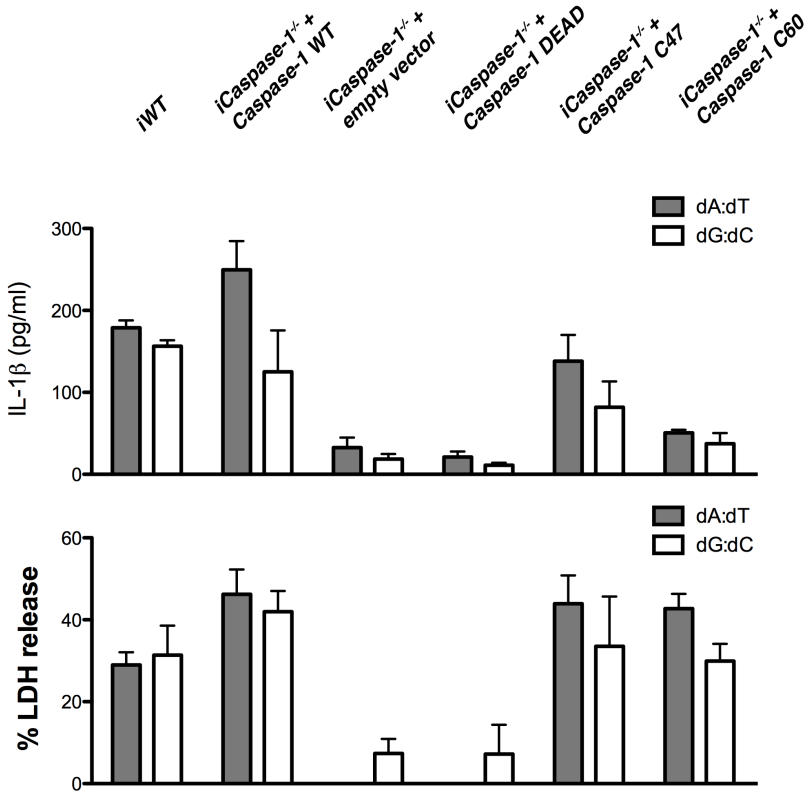

Figure 3.10 CASP1 processing is not required for macrophage death in response to DNA transfections
Immortalized *Casp1*$^{-/-}$ macrophages were transduced with retrovirus expressing the indicated CASP1 constructs and transfected with the synthetic DNA poly(dA:dT) or poly(dG:dC) for 5h. Secretion of mature IL-1β into the culture supernatant was determined by ELISA. Cell death was determined by measuring LDH release. Graphs show the mean ± SD of triplicate wells and are representative of three independent experiments.

3.8 Discussion

Mammalian genomes encode multiple NBD-LRR/PYHIN proteins, each with the potential to assemble inflammasomes and activate CASP1 independently in response to diverse signals. However, little is known about the molecular interaction of the assembled inflammasome with CASP1. A pivotal CASP1 activation step is thought to be the autoproteolytic separation of its p20 and p10 subunits. In addition to NBD-LRR/PYHIN proteins and CASP1, inflammasomes also contain ASC, an adaptor whose major function is believed to be to recruit CASP1 to PYRIN domain-containing proteins. NLRC4, however, lacks a PYRIN domain, but has a CARD that has been shown to interact directly with the CARD of CASP1 in the absence of ASC[7]. Since ASC is nevertheless required for some aspects of NLRC4-mediated CASP1 activation, the role of ASC remained unclear[17,71,112].

In this chapter, we have clarified the molecular mechanisms that lead to CASP1 activation and defined the role of ASC in CASP1 autoproteolysis, pro-inflammatory cytokine processing and host cell death. By using mutant CASP1 alleles defective for autoproteolytic processing, we were able to genetically and functionally distinguish two inflammasome

complexes (Fig. 3.11): (1) "death-inflammasomes", that do not require autoproteolysis of CASP1, and which mediate macrophage death but only inefficient cytokine release; and (2) one large ASC focus, which is formed when ASC aggregates with NBD-LRR/PYHIN proteins and CASP1, and which mediates very efficient processing and release of pro-inflammatory cytokines. Our data suggest that *Asc*$^{-/-}$ macrophages only assemble the "death-inflammasomes" in response to NLRC4 or NLRP1B stimuli. However, we can only speculate about the situation in WT macrophages. Both types of inflammasome complexes could be formed and remain spatially and functionally distinct. Alternatively, the "death-inflammasomes" might just be intermediates and serve as precursors or nuclei for the formation of the ASC focus. Future work investigating inflammasome assembly in single cells, using fluorescently-tagged components and time-lapse imaging, might provide more insight into the molecular dynamics and kinetics of inflammasome-complex formation.

Our results clarify the precise and essential molecular functions of ASC. Not only does ASC appear to function as a vital adaptor for the recruitment of CASP1 to PYRIN-containing receptors, such as AIM2, but our data indicate that ASC also seems to be crucial for induction of CASP1 processing. This processing, rather than merely ASC itself, in turn appears to be essential for efficient cytokine maturation. Indeed, although ASC is present in macrophages expressing completely uncleavable CASP1 (Fig. 3.7D**,** construct C71), and ASC foci are still formed in response to infection, cytokines are not efficiently processed. However, these cells release full-length pro-CASP1 and undergo cell death. This demonstrates that the pro-CASP1 zymogen can promote pyroptosis when activated, but requires ASC to be processed to its p20 and p10 subunits to promote cytokine maturation. It will be interesting to investigate the molecular mechanisms underlying the division of cell death and cytokine processing downstream of CASP1. Several non-exclusive models suggest themselves, including (1) auto-proteolytic processing of CASP1 alters substrate recruitment; (2) processing alters CASP1 substrate specificity; and (3) full length CASP1 has weak catalytic activity that is sufficient for inducing cell death, but insufficient for processing cytokines. This last model further suggest that CASP1 activity leading to cell death might activate an amplifying cascade that is absent in cytokine processing.

CASP1 processing has widely been used as the hallmark of CASP1 activation. However, our data imply that CASP1 can exist in two activation states, unprocessed and fully processed, depending on the composition of the inflammasome. How does this compare to other initiator caspases, such as CASPASE-2, -8, -9, *D. melanogaster* Dronc and *C. elegans* CED-3? Similar to CASP1, these other initiator caspases have been shown to require recruitment to multiprotein activation platforms, like the PIDDosome for CASPASE-2, the DISC-complex for CASPASE-8, the apoptosome for CASPASE-9, the DARK-apoptosome for DRONC, and the CED-4 tetramer for CED-3 [52]. All of these initiator caspases are expressed as inactive monomers, in contrast to effector caspases that are expressed as inactive dimers. According to the proximity-driven dimerization model, the activation step is the dimerization that is induced in the activation platform[115]. The importance of the autoproteolytic processing that occurs simultaneously with the dimerization is less clear. Experimental evidence using non-cleavable CASPASE-9 suggests that CASPASE-9 does not require processing for activity[116]. However, processing seems to be important to stabilize the dimers formed by CASPASE-2, -8 and DRONC, as auto-cleaved forms of these caspases preferentially form dimers and only these dimers have sufficient catalytic activity to induce cell death (for a review see ref 52). Consistent with previous studies of apoptotic caspases,

we suggest that CASP1 activation also proceeds by proximity-induced dimerization. However, our data suggest that CASP1 activation and autoproteolysis are distinct events and depend on the exact composition of the multiprotein activation platform. Human CASP1 has been crystallized in its processed forms as well as a zymogen[117], but the structure of CASP1 in complex with different receptors and/or ASC remains an exciting task for crystallographers to pursue.

Another distinguishing feature of inflammasome complexes compared to apoptosomes, is that the different inflammasome complexes seem to have distinct functions, i.e. cell death and cytokine processing, which are also spatially distinct. We propose that the "death-inflammasomes" could be a functional analog of the apoptosome complexes, since they are most probably small, do not localize in a large focus, and specialize in performing only one task, i.e. induction of cell death. The ASC focus, however, does not seem to have an equivalent in apoptotic signaling pathways. One could speculate that induction of host cell death might have been the primordial function of the inflammasome, providing the host with the vital features of eliminating the intracellular niche of the infected cell, and exposing intracellular pathogens to more robust extracellular immune defenses. Cytokine processing in the ASC focus could have developed as a secondary feature, enabling the infected cell to attract other immune cells like neutrophils to the site of the infection, where they would encounter the newly exposed intracellular pathogens. Most leukocytes have been shown to express both ASC and CARD-containing receptors, but variations in the expression levels could also allow some cell types to respond by either producing cytokines or inducing pyroptotic cell death. High expression levels of ASC might sequester CASP1, possibly preventing premature cell death and the resulting spread of pathogen, and allowing prolonged pro-inflammatory cytokine production. Intriguingly, several host- as well as pathogen-derived Pyrin-only proteins (cPOPs and vPOPs) have been shown to inhibit or regulate the inflammasome by sequestering ASC, which could also result in CASP1-dependent cell death in the absence of cytokine processing (for a review see ref 118). Thus, regulating the availability of ASC could be a mechanism to tip the balance between CASP1 mediated cell death and cytokine processing.

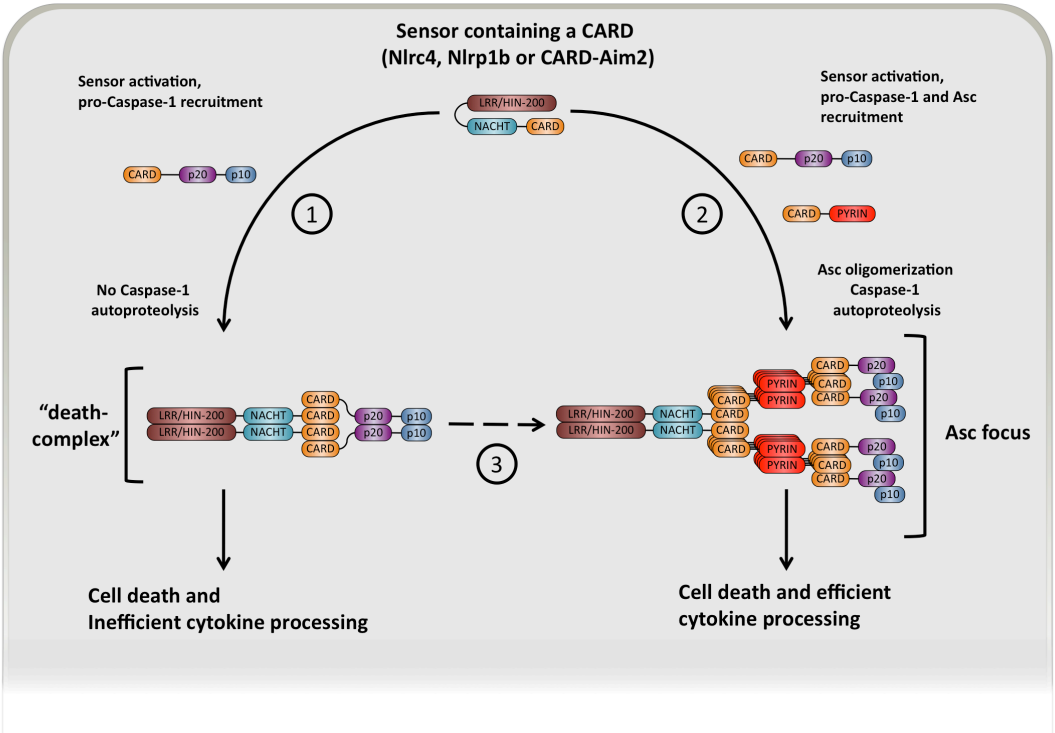

Figure 3.11 Formation of spatially and functionally specialized inflammasome-complexes by CARD-containing receptors
(1) Activation of CARD-containing sensors (NLRC4, NLRP1B or CARD-AIM2) by their respective stimuli induces dimerization of the sensor and recruitment of pro-CASP1 through CARD-CARD interactions. Proximity-driven dimerization in this "Death-complex" does not lead to autoproteolysis, however it activates pro-CASP1 sufficiently to promote cell death, but only inefficient cytokine processing. (2) ASC foci are formed when ASC is recruited in addition to pro-CASP1 to the activated sensor. Proximity driven dimerization of ASC promotes the recruitment of further ASC molecules by CARD-CARD and PYRIN-PYRIN interactions, leading to rapid oligomerization of ASC, thus forming the focus. In the ASC focus, conformational changes of the pro-CASP1 dimer allow for autoproteolytic processing into the p10 and p20 subunits. Only fully processed CASP1 is able to efficiently promote cytokine maturation. (3) Alternatively, the "Death-complexes" could serve as precursors or nuclei for ASC oligomerization and even be absorbed by the ASC focus once it has formed.

Chapter 4: Rapid Induction of Lipid Mediators is a Novel Effector Function of the Inflammasome *in vivo*

4.1 Introduction

Chapters 2 and 3 focused on the molecular mechanisms of inflammasome activation and regulation. I now turn my attention to the downstream effector functions of CASP1 and their impact *in vivo*. The consequences of IL-1β and IL-18 signaling remain the best characterized CASP1 effector functions; however, as discussed in chapter 1, there is ample evidence to suggest a role for cytokine-independent CASP1 activity. *In vitro,* pyroptosis has been shown to limit intracellular replication of pathogens, and recent evidence suggests this may occur *in vivo* as well[70]. Nonetheless, the pathology and immune responses associated directly with CASP1 activation *in vivo* have not been well characterized.

In this chapter I report the development of a novel protein toxin to selectively activate the NAIP5/NLRC4 inflammasome *in vivo*. Remarkably, systemic inflammasome activation by flagellin leads to loss of vascular fluid into the intestine and peritoneal cavity, resulting in rapid (<30 minutes) death in mice. This unexpected response is dependent on the inflammasome components NAIP5, NLRC4, and CASP1, but independent of IL-1b/-18 production. Instead, inflammasome activation in resident peritoneal macrophages results, within minutes, in an 'eicosanoid storm' – an unregulated and pathological release of signaling lipids that rapidly initiate inflammation and vascular fluid loss. Mice deficient in cyclooxygenase-1 (COX-1), a critical enzyme in prostaglandin biosynthesis, are resistant to these rapid pathological effects of systemic inflammasome activation by either flagellin or anthrax lethal toxin. Biosynthesis of eicosanoids downstream of the inflammasome depends on the activation of cPLA2 (cytosolic phospholipase A2) by CASP1-induced Ca^{2+} influx prior to cell lysis. Compared to other macrophage populations, resident peritoneal macrophages are specifically primed for production of eicosanoids by high expression of *Cox1* and other eicosanoid biosynthetic enzymes. Thus, these results identify eicosanoid production as a novel cell type-specific effector function of the inflammasome with dramatic physiological consequences *in vivo*.

The experiments reported in this chapter were performed in collaboration with Mahtab Moayeri in Stephen Leppla's group at the National Institutes of Health, and Norver Trinidad, a technician in the Vance Lab. Eicosanoid analysis was carried out in collaboration with Samantha Wang and Karsten Gronert in the Vision Sciences program at the Berkeley School of Optometry. Alex Kintzer (UC Berkeley), Bryan Krantz (UC Berkeley), Nico van Rooijen (Vrije Universiteit) and Charles Brown (U Missouri) provided reagents. These results are currently under review for publication.

4.2 Cytosolic Delivery of Flagellin in the Absence of Infection

Because pathogens trigger multiple and overlapping inflammatory pathways, we decided to take advantage of an established protein delivery system[119], based on *Bacillus anthracis* lethal toxin (LT), to deliver flagellin to the cytosol and thereby selectively activate NAIP5/NLRC4 in the absence of infection. We fused *Legionella pneumophila* flagellin (FlaA) to the N-terminal domain of *B. anthracis* lethal factor (LFn) that mediates cytosolic delivery through the protective antigen (PA) channel[19,22]. As expected, the combination of PA + LFn-

FlaA (here called FlaTox), but not PA or LFn-FlaA alone, activated the NAIP5/NLRC4 inflammasome in bone marrow derived macrophages (BMDM), as measured by cleavage of CASP1, release of lactate dehydrogenase, and secretion of IL-1β (Fig. 4.1a, c-e). Inflammasome activation was abrogated in *Casp1*$^{-/-}$, *Naip5*$^{-/-}$, and *Nlrc4*$^{-/-}$ BMDM (Fig. 4.1b). Importantly, a mutant form of FlaTox (FlaTox(AAA)), which is recognized by TLR5 but not NAIP5[19,120], did not activate pyroptosis (Fig. 4.1a).

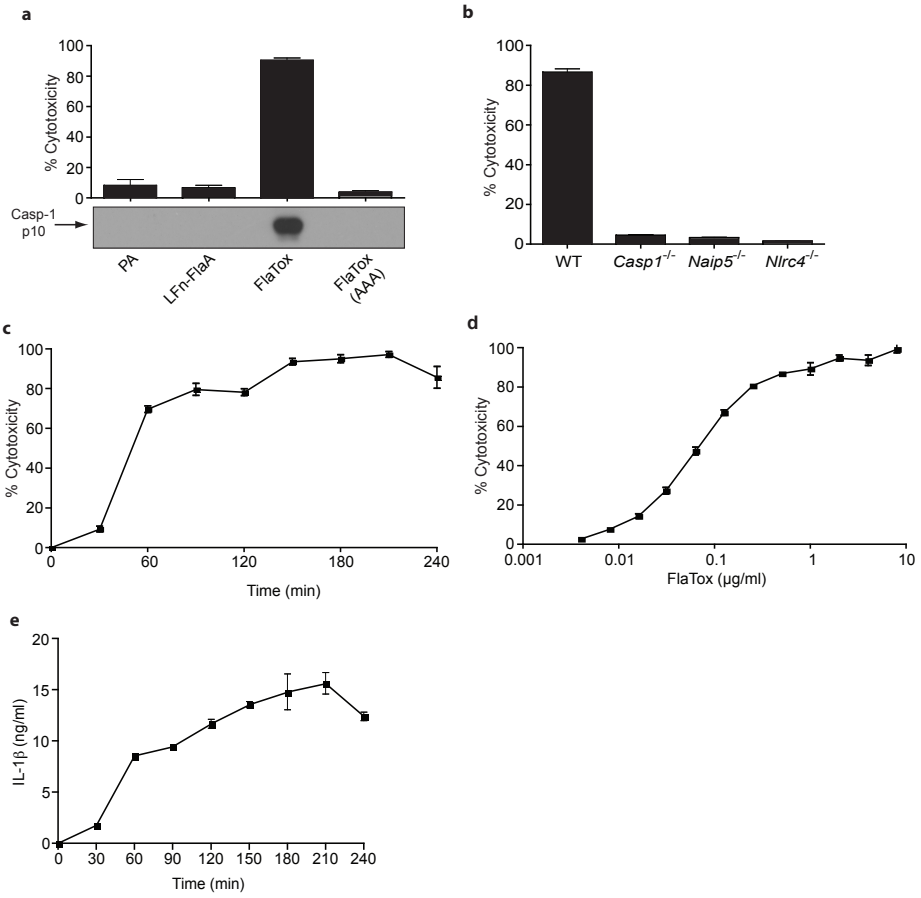

Figure 4.1 *In vitro* characterization of FlaTox
(a-d) Lysis of bone marrow derived macrophages (BMDM) was quantified by lactate dehydrogenase release assay. (a) Wild-type (B6) 4 h with 4 μg/ml PA, 2 μg/ml all others. Secreted proteins were probed with CASP1 p10 antibody (b) Indicated genotypes 4 h with FlaTox (4 μg/ml PA + 2 μg/ml LFn-FlaA). (c) Wild-type (B6) 4 h with FlaTox at indicated doses. (d) Wild-type (B6) with FlaTox (4 μg/ml PA + 2 μg/ml LFn-FlaA) for indicated times. (e) Wild-type (B6) pre-treated 4 h with 0.5 μg/ml PAM3CSK4 then FlaTox (4 μg/ml PA + 2 μg/ml LFn-FlaA) for indicated times. Processed IL-1β released into the supernatant was quantified by enzyme-linked immunosorbent assay (ELISA) as previously described[120]. Data shown (± s.e.m.) are representative of two (e) or three (a-d) independent experiments.

4.3 FlaTox Induces Inflammasome-dependent Fluid Loss and Death in Mice

We then determined the effect of FlaTox administration *in vivo*. Remarkably, intravenous delivery of FlaTox rapidly killed mice, causing signs of distress within 15 minutes and a mean time to death of ~30 minutes (Fig. 4.2a). Intraperitoneal injection of FlaTox was also lethal, but at higher doses and with slower kinetics (Fig. 4.2b). For all

subsequent experiments, we administered an intermediate intraperitoneal dose. Histological analysis (Fig. 4.4 and data not shown) of mice treated with FlaTox for 30 minutes revealed no signs of pathology; however, upon dissection we found fluid accumulation in the peritoneal cavity and in the intestine (Fig. 4.2c-d). Consistent with this observation, FlaTox-treated mice also rapidly developed diarrhea. We found no evidence of edema or fluid accumulation in the kidney or other organs of the peritoneal cavity, or in the lungs (Fig. 4.3).

To determine the origin of the accumulated fluid, we first measured the hematocrit (Hct), or percent volume of red blood cells. Remarkably, in mice injected with FlaTox, the Hct rose from a normal 45-50% to as high as 80% within 30-40 m.p.i (Fig. 4.2e), indicating fluid loss from the blood. As Hct rose, body temperature dropped, but with delayed kinetics. The loss of blood fluid was the earliest pathological event we could detect following FlaTox treatment, and we hypothesize that the resulting hemoconcentration and circulatory stress cause the drop in body temperature and death.

Using the rise in Hct and drop in body temperature as physiological markers, we further characterized the FlaTox response *in vivo*. As *in vitro*, only the complete toxin, and not individual subunits, induced a response *in vivo* (Fig. 4.2f-g). Mice were also completely non-responsive to FlaTox(AAA) (Fig. 4.2f-g; Fig. 4.5a), demonstrating that TLR signaling activated by flagellin or bacterial contaminants is not sufficient to cause pathology. *Nlrc4*$^{-/-}$ mice were completely protected at all doses and timepoints tested (Fig. 4.2h-i, and data not shown), but surprisingly, while *Naip5*$^{-/-}$ and *Casp1*$^{-/-}$ mice were completely protected in survival experiments (Fig. 4.5b), they were partially susceptible in Hct and body temperature assays, albeit with delayed kinetics (Fig. 4.2h-i). The moderate response of *Naip5*$^{-/-}$ mice may be due to the previously reported recognition of flagellin by NAIP6[19,22]. Importantly, mice deficient for both IL-1β and IL-18 were as sensitive as wild-type (B6) mice, ruling out a role for these cytokines in FlaTox-induced pathologies (Fig. 4.2j-k; Fig. 4.5b).

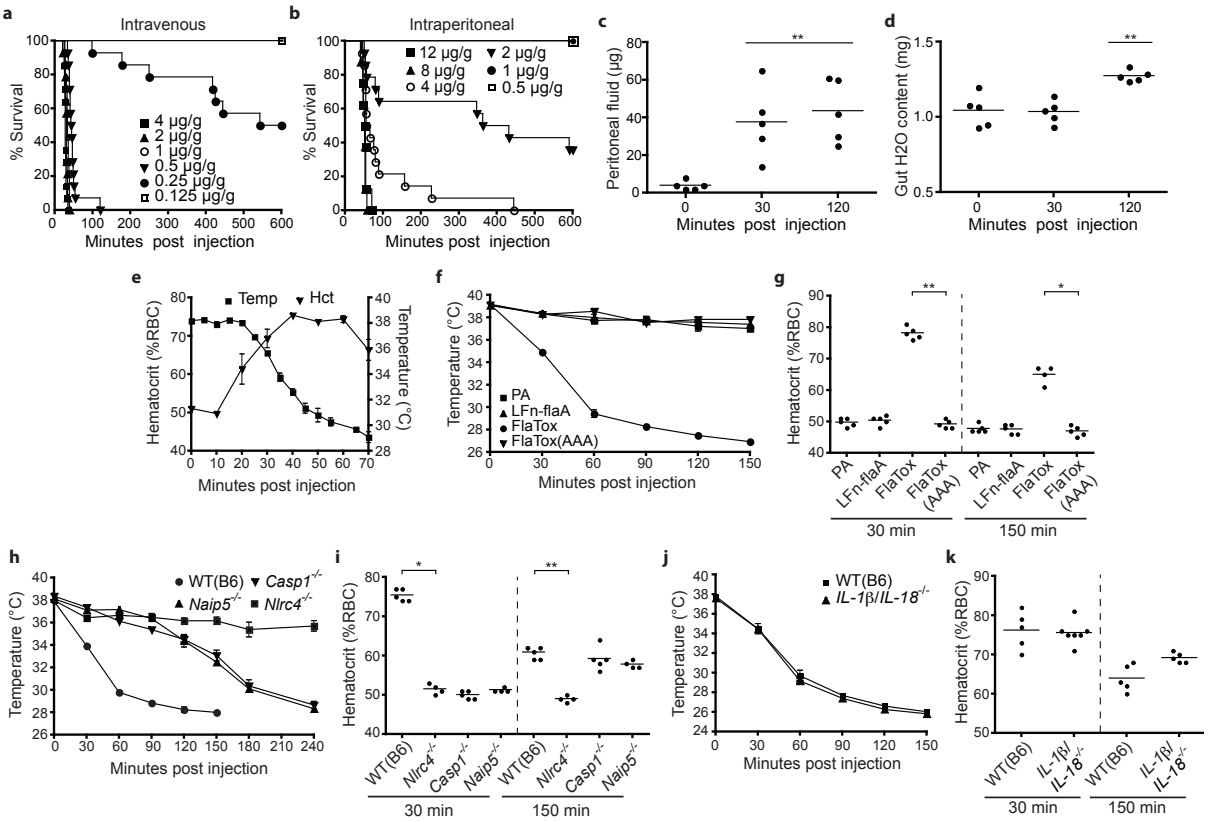

Figure 4.2 Systemic cytosolic delivery of flagellin *in vivo* induces NAIP5/NLRC4 inflammasome-dependent but IL-1b/IL-18-independent vascular leakage
(a-b) Wild-type (B6) mice were injected with FlaTox via tail-vein (a) or intraperitoneally (b) and monitored for survival (n=5-14). (c-d) Wild-type (B6) mice were injected intraperitoneally with FlaTox and peritoneal (c) and intestinal fluid (d) was quantified at indicated timepoints (n=5). (e-g) Wild-type (B6) mice were injected intraperitoneally with FlaTox or indicated proteins (4 µg/g PA; 2 µg/g all others) and rectal temperature (e, f) and hematocrit (e, g) were quantified over time (n=3 for (e); 4-5 for (f-g)). (h-k) Mice were injected intraperitoneally with FlaTox and analyzed as in (e-g) (n=4-7). Data shown (± s.e.m.) are pooled from multiple experiments (a-b) or representative of at least two independent experiments. * p = 0.016; ** p < 0.009 (Mann-Whitney t-test).

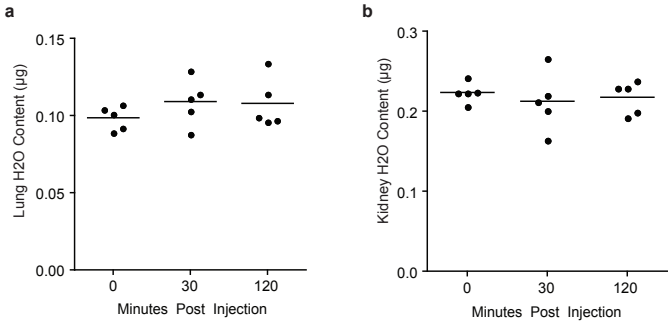

Figure 4.3 No evidence of fluid accumulation in kidneys and lung following FlaTox injection
(a-b) Wild-type (B6) mice were injected intraperitoneally with FlaTox (4 µg/g body weight PA + 2 µg/g body weight LFn-FlaA) and lung (a) and kidneys (b) were collected at the indicated times. Fluid content was determined by the difference between wet and dry organ weight (dried overnight at 37°C). Data shown are representative of three independent experiments.

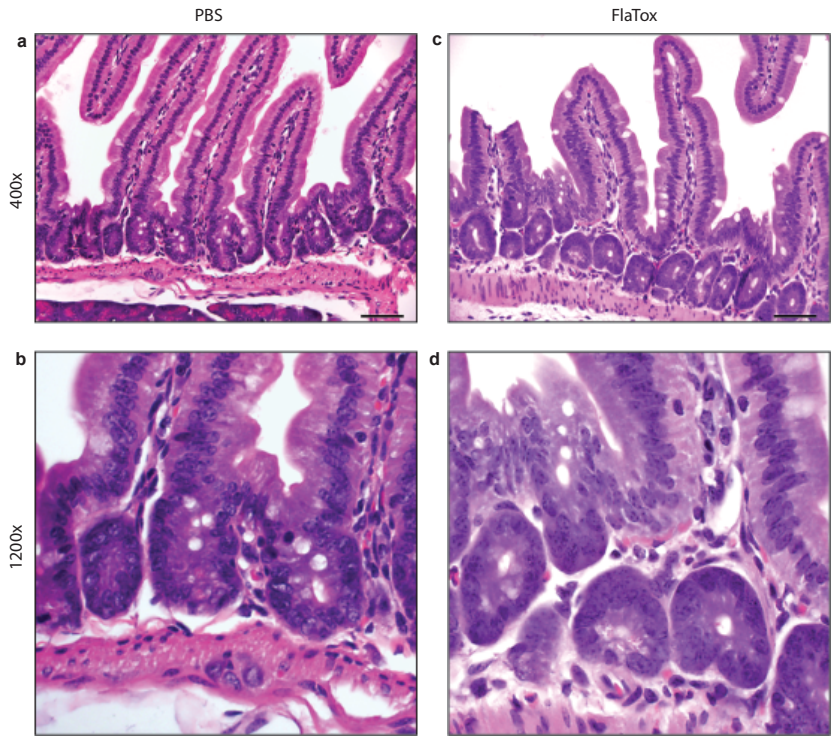

Figure 4.4 No histological changes detected in the intestine 30 minutes post FlaTox injection
(a-d) Wild-type (B6) mice were injected intraperitoneally with PBS (a-b) or FlaTox (4 μg/g body weight PA + 2 μg/g body weight LFn-FlaA) (c-d). After 30 minutes, intestinal tissues (cecum + small intestine + large intestine) were collected and fixed by gentle injection of 10% buffered formalin. Tissues were stored in 10% buffered formalin before being embedded in paraffin, sectioned, and stained with hematoxylin and eosin (University of Michigan Pathology Core). Sections were analyzed by board-certified pathologist (I. Bergin) blinded to experimental groups. No abnormalities were detected in any sections. Duodenal sections shown in figure are representative of entire intestinal tissue and experiment was repeated twice (n=1-2). A, C: x400, bar = 50μm; B, D: x1200.

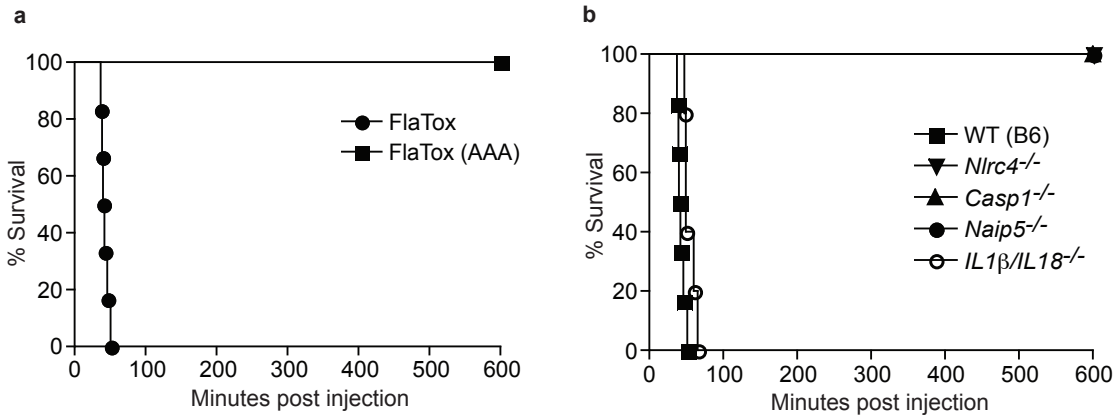

Figure 4.5 Time to morbidity
(a) Wild-type (B6) mice were injected intravenously (tail vein) with FlaTox or FlaTox(AAA) (1.0 μg/g PA + 0.5 μg/g LFn-FlaA or LFn-FlaA(AAA)) and monitored 10 h for morbidity. Time to morbidity was defined as the earliest time when mice failed to right themselves or had a rectal temperature < 25°C (n=5-6). (b) Mice of indicated genotypes were injected with FlaTox and monitored as in (a) (n=5-6). Data shown are representative of two independent experiments.

4.4 Resident Peritoneal Macrophages are Required for the Early FlaTox Response *In Vivo*

To identify the cell type(s) required for responsiveness to FlaTox, we generated bone marrow chimeras using susceptible wild-type (B6) mice and resistant *Nlrc4*$^{-/-}$ (KO) mice. *Nlrc4*$^{-/-}$ mice reconstituted with wild-type bone marrow were completely susceptible to FlaTox (Fig. 4.6a-b). Interestingly, wild-type mice reconstituted with *Nlrc4*$^{-/-}$ bone marrow also responded, but with delayed kinetics. These results suggest that at least two cell populations respond to FlaTox: (1) radio-sensitive cells of hematopoietic origin that are both necessary and sufficient for the early response to FlaTox (0-30 m.p.i.) and (2) radio-resistant cells that respond after 30 minutes. Here we decided to focus on the early hematopoietic response (EHR).

We sought to identify hematopoietic cell lineages required for the EHR. The EHR was intact in mice deficient in mast cells, lymphocytes, and neutrophils (Fig. 4.7). In contrast, wild-type mice depleted of macrophages using clodronate-loaded liposomes were almost completely protected from the EHR (Fig. 4.6c-d). Similarly, depletion of CD11b^{+} cells in FVB:CD11b-DTR mice conferred protection (Fig. 4.6e-f). Flow cytometric analysis revealed a near complete ablation of peritoneal resident CD11b/F4-80^{hi} macrophages by both treatments (Fig. 4.6g-h), while depletion of splenic and lamina propria macrophages was partial (clodronate) or not observed (CD11b-DTR) (Fig. 4.8a-b). We hypothesized therefore that resident peritoneal macrophages might be sufficient for responsiveness to FlaTox. Indeed, *Nlrc4*$^{-/-}$ mice injected with peritoneal cells from wild-type, but not *Nlrc4*$^{-/-}$, donors became sensitive to FlaTox (Fig. 4.6i). Surprisingly, intraperitoneal injection of wild-type thioglycollate-elicited or bone marrow derived macrophages into *Nlrc4*$^{-/-}$ hosts failed to transfer responsiveness (Fig. 4.6i). Transfer of entire splenic and bone marrow populations was also ineffective (Fig. 4.8c). These data demonstrate a unique and critical role for resident peritoneal macrophages in the inflammasome-dependent *in vivo* response to FlaTox; the apparent specialization of this cell type is discussed in more detail below.

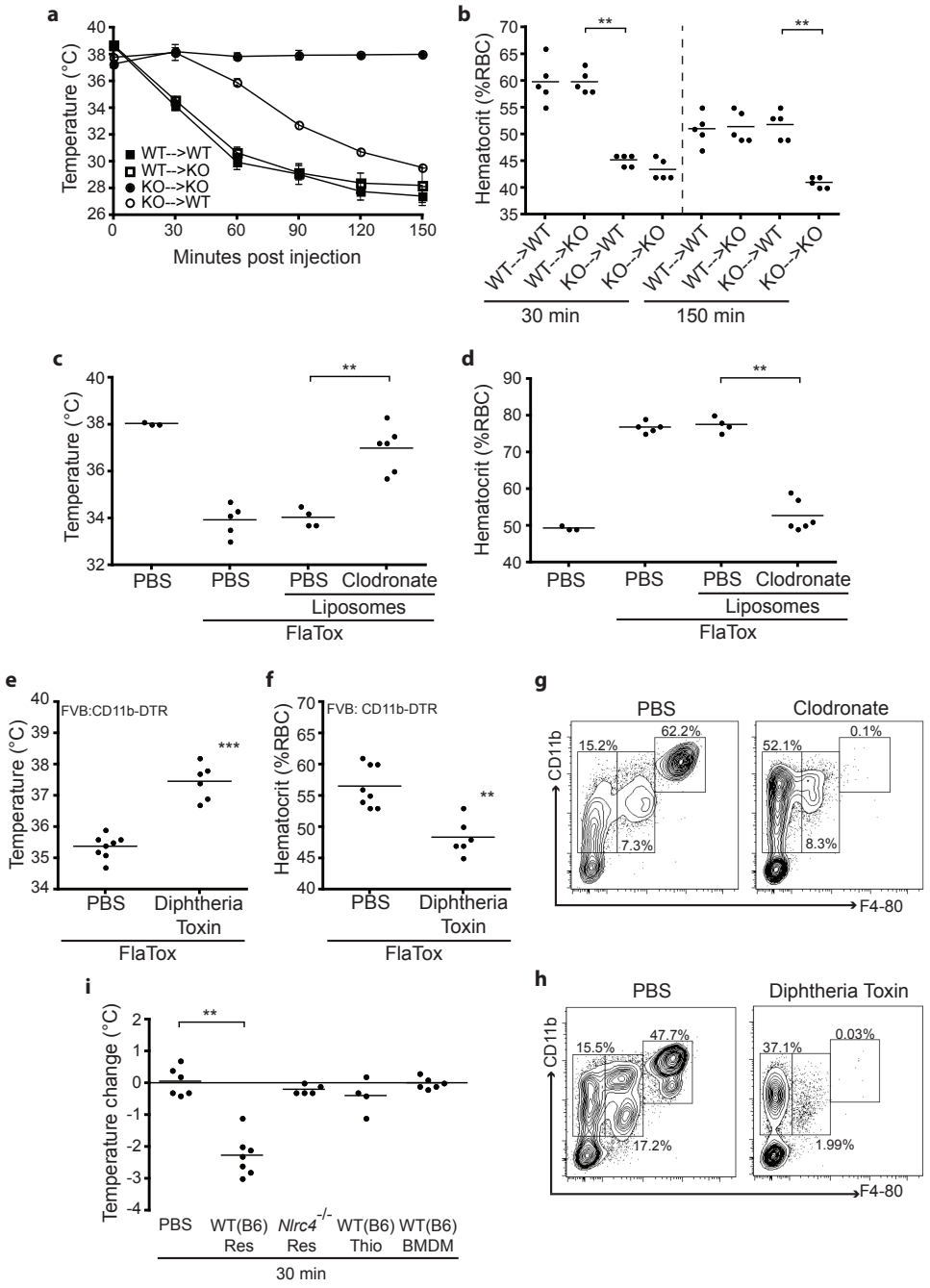

Figure 4.6 Resident peritoneal macrophages are critical for the early FlaTox response *in vivo*
(a-d) Bone marrow chimeric mice (KO = *Nlrc4*$^{-/-}$) (a, b) or naïve and macrophage-depleted wild-type (B6) (c, d) mice were injected intraperitoneally with FlaTox and rectal temperature (a, c) and hematocrit (b, d) were measured at 30 m.p.i. or otherwise indicated times (n=3-6). (e-f) FVB-Tg(CD11b-DTR) mice pre-treated with PBS or diphtheria toxin were analyzed as in (c-d) (n=6-8). (g-h) Resident peritoneal cells lavaged from macrophage-depleted wild-type (B6) mice (g) or diphtheria toxin-treated FVB-Tg(CD11b-DTR) mice (h) were labeled for CD11b and F4-80 and analyzed by flow cytometry. (i) 10^7 resident or thioglycollate-elicited peritoneal cells or BMDM were injected intraperitoneally into *Nlrc4*$^{-/-}$ recipients. After 2 h, mice were injected intraperitoneally with FlaTox (8 μg/g PA + 4 μg/g LFn-FlaA) and rectal temperature was measured at 30 m.p.i. Data shown (± s.e.m.) are pooled from multiple experiments (i) or representative of at least two (g-h) or three (a-f) independent experiments. ** $p < 0.01$; *** $p = 0.0007$ (Mann-Whitney t-test).

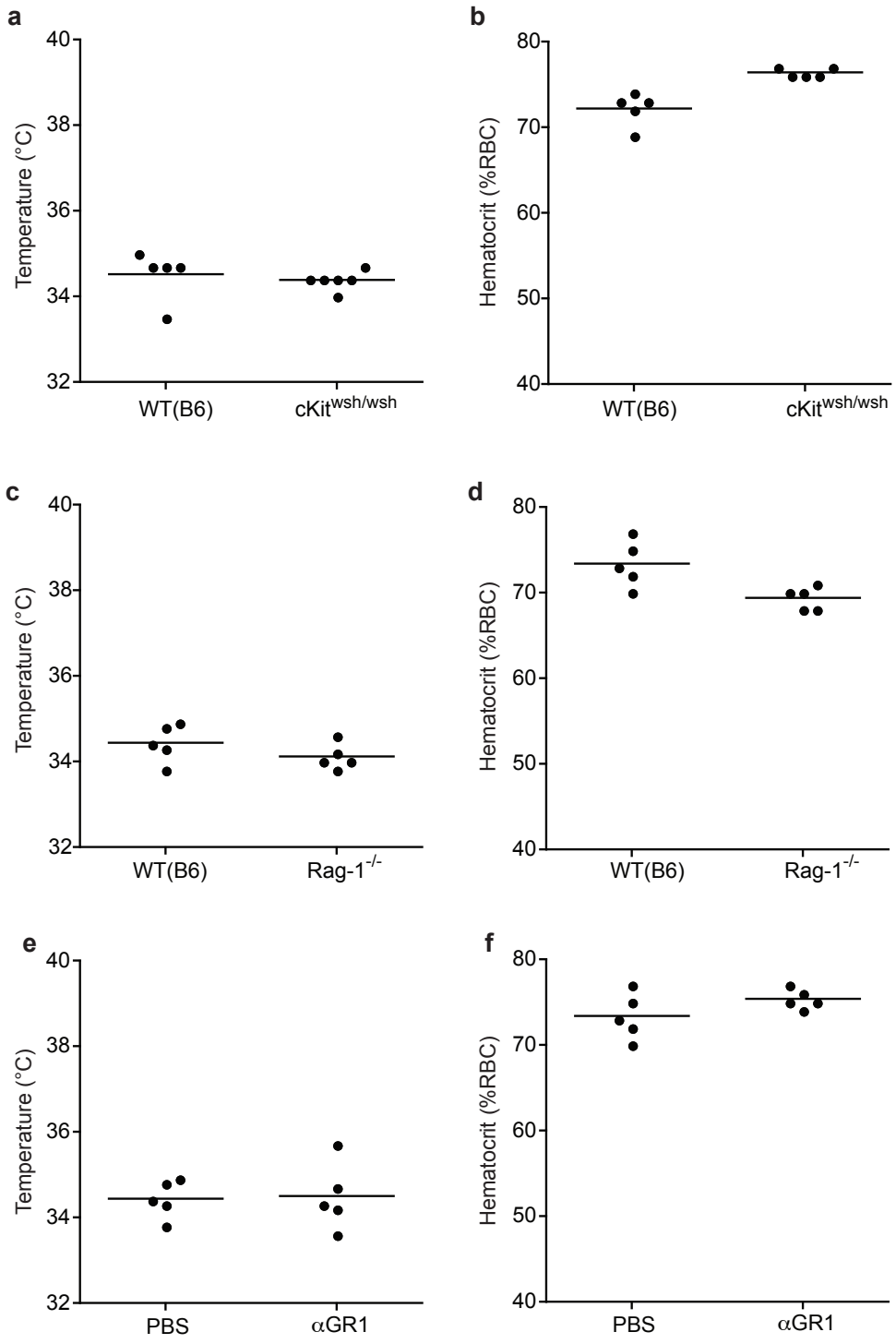

Figure 4.7 Mast cells, lymphocytes, and neutrophils are not required for early hematopoietic response to FlaTox

(a-b) Wild-type (B6) or mast cell deficient *cKit*$^{wsh/wsh}$ mice were injected intraperitoneally with FlaTox (4 μg/g body weight PA + 2 μg/g body weight LFn-FlaA) and rectal temperature (a) and hematocrit (b) were measured 30 minutes post injection (n=5-6). (b-c) Wild-type (B6) or lymphocyte-deficient *Rag1*$^{-/-}$ mice were analyzed as above (n=5). (e-f) Naïve or neutrophil-depleted (a-GR1) wild-type (B6) mice were analyzed as above (n=5). Data shown are representative of one (d; f) or at least two (a-c; e) independent experiments.

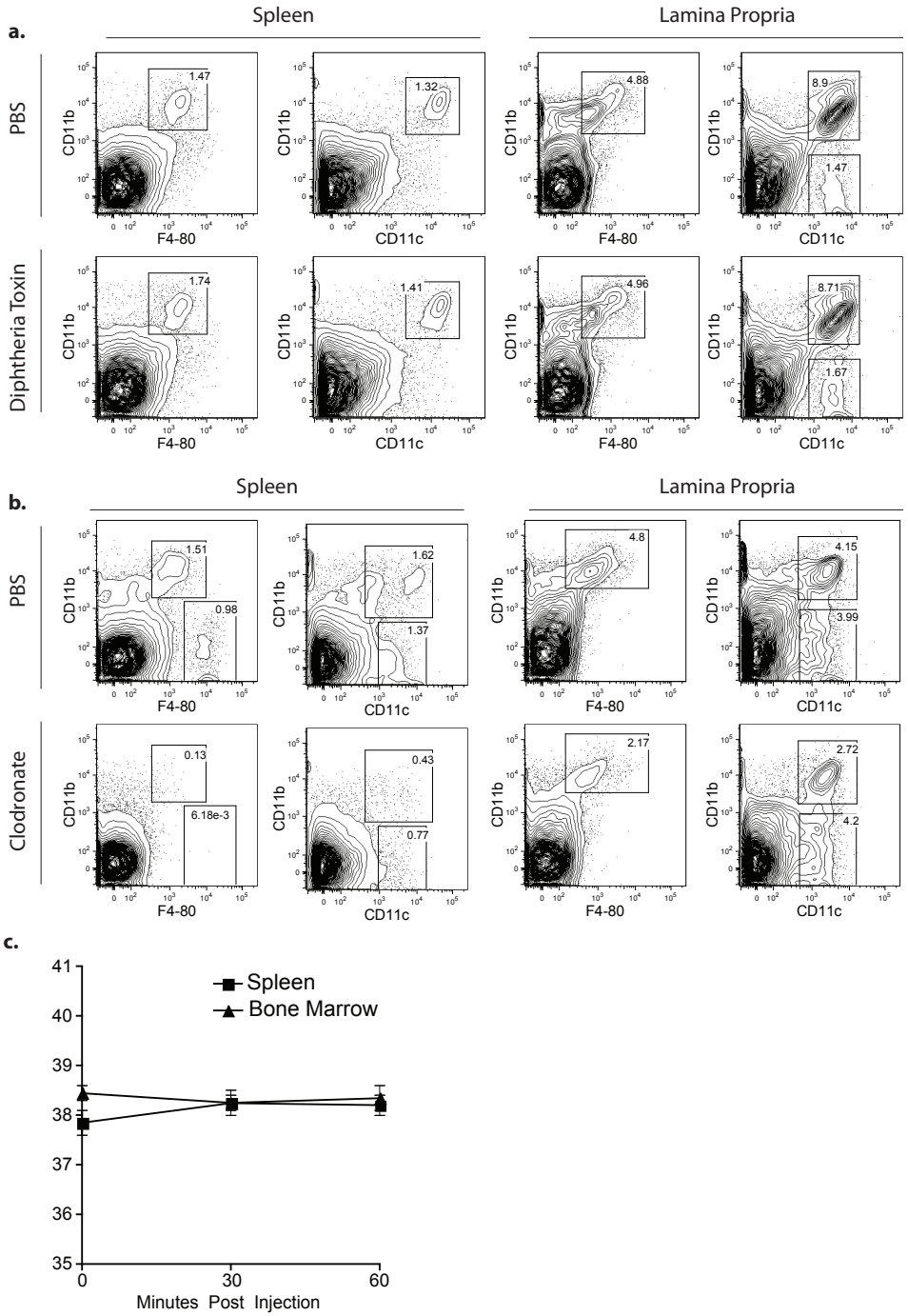

Figure 4.8 Depletion and transfer analysis
(a) FVB-Tg(CD11b/EGFP)34Lan/J (CD11b-DTR) mice were treated 24 h with diphtheria toxin (25 ng/g intraperitoneally). Splenic cells and isolated lamina propria lymphocytes were stained with CD11c, CD11b, and F4-80 antibodies and analyzed by flow cytometry. (b) Wild-type (B6) mice were treated 48 h with PBS or clodronate liposomes (200 µl intravenously + 500 µl intraperitoneally). Spleen and lamina propria were analyzed as in (a). (c) *Nlrc4*$^{-/-}$ mice were injected intravenously with bone marrow (2 femurs + 2 tibias) or spleen (entire spleen) cells from a wild-type (B6) mouse. After 30 min, mice were injected intraperitoneally with FlaTox and rectal temperature was monitored over time (n=2). Data shown (± s.e.m.) are representative of at least two independent experiments.

4.5 Inflammasome-dependent Eicosanoid Biosynthesis

Since IL-1β/IL-18 were not required, we hypothesized that resident peritoneal macrophages might initiate the EHR through secretion of a previously unidentified factor. After screening several candidate pathways associated with rapid response and vascular leakage, we focused on the eicosanoids, a family of lipid signaling molecules synthesized from arachidonic acid (AA). AA is released from cell membranes by phospholipases and converted into prostaglandins and thromboxanes downstream of the cyclooxygenases (COX-1 & COX-2), or into hydroxyeicosatetraenoic acids (HETEs) and leukotrienes downstream of the lipoxygenases (12/15-LOX & 5-LOX) (Fig. 4.9). Eicosanoids are critical for many aspects of inflammation, including vascular permeability, vasodilation, chemotaxis, and leukocyte regulation[121,122]. As a result, deficient eicosanoid responses result in impaired immune defense against numerous pathogens[123,124], while dysregulation of eicosanoid biosynthesis contributes to the pathogenesis of several inflammatory diseases[125-127]. Notably, direct intraperitoneal injection of prostaglandins leads to fluid accumulation in the gut[128].

We therefore investigated whether resident peritoneal macrophages, the specific cells required for the EHR (Fig. 4.6), produce eicosanoids in response to inflammasome activation. Liquid chromatography-tandem mass spectrometry (LC/MS/MS) lipidomic analysis was performed on supernatants of peritoneal lavage cells treated *ex vivo* with FlaTox. Remarkably, we found that these cells rapidly produce a broad spectrum of eicosanoids, including thromboxane, prostaglandins and leukotrienes (Fig. 4.10a). The eicosanoid response of peritoneal macrophages was almost completely inflammasome-dependent, as the FlaTox(AAA) mutant failed to induce a significant response (Fig. 4.10a). Consistent with LC/MS/MS results, enzyme immunoassay revealed that FlaTox-treated resident peritoneal macrophages secreted >10-fold more LTB_4 and PGE_2 than those treated with FlaTox(AAA), and moreover, eicosanoid induction was completely dependent on NAIP5, NLRC4 and CASP1 (Fig. 4.10b; Fig. 4.11a). We also detected inflammasome-dependent biosynthesis of cysteinyl leukotrienes, which were not included in our LC/MS/MS analysis, by immunoassay (Fig 4.10c). LTB_4 and PGE_2 induction by PA or LFn-FlaA alone was equivalent to FlaTox(AAA) or direct LPS stimulation, further demonstrating that TLR signaling cannot account for their biosynthesis (Fig. 4.10d; Fig. 4.11b). Importantly, the flagellated intracellular pathogen *Salmonella typhimurium* also elicited inflammasome-dependent eicosanoid biosynthesis similarly to FlaTox (Fig. 4.10e), demonstrating that this pathway is activated during infection with a natural pathogen.

Similar to the *ex vivo* response of resident peritoneal macrophages, LC/MS/MS analysis of peritoneal lavage fluid from mice treated with FlaTox for 20 minutes also revealed robust eicosanoid biosynthesis *in vivo* (Fig. 4.12). Compared to the *ex vivo* response of peritoneal macrophages, the *in vivo* response to FlaTox is potentially more complex since it represents the aggregate response of multiple cell types and host pathways. Thus, although the *in vivo* response was largely inflammasome dependent, some residual activation of eicosanoid (particularly PGE_2) biosynthesis by FlaTox(AAA) was observed and is likely due to TLR-dependent recognition of flagellin or residual bacterial products in our protein preps. However, as noted above, this residual response did not produce symptoms (Fig. 4.2f-g), suggesting that pathology may be due to the synergistic effects of multiple eicosanoids and their localized production by peritoneal macrophages.

Taken together, our results show that inflammasome activation results in an 'eicosanoid storm' *ex vivo* and *in vivo*, characterized by broad biosynthesis of both LOX and COX products, with a bias towards pro-inflammatory lipids such as leukotriene B_4 (LTB_4) and prostaglandin E_2 (PGE_2). Notably, inflammasome activation did not result in the production of lipoxins (Fig. 4.9), which are associated with the resolution of inflammation and counterbalance the pro-inflammatory and vascular actions of LTB_4 and PGE_2[129].

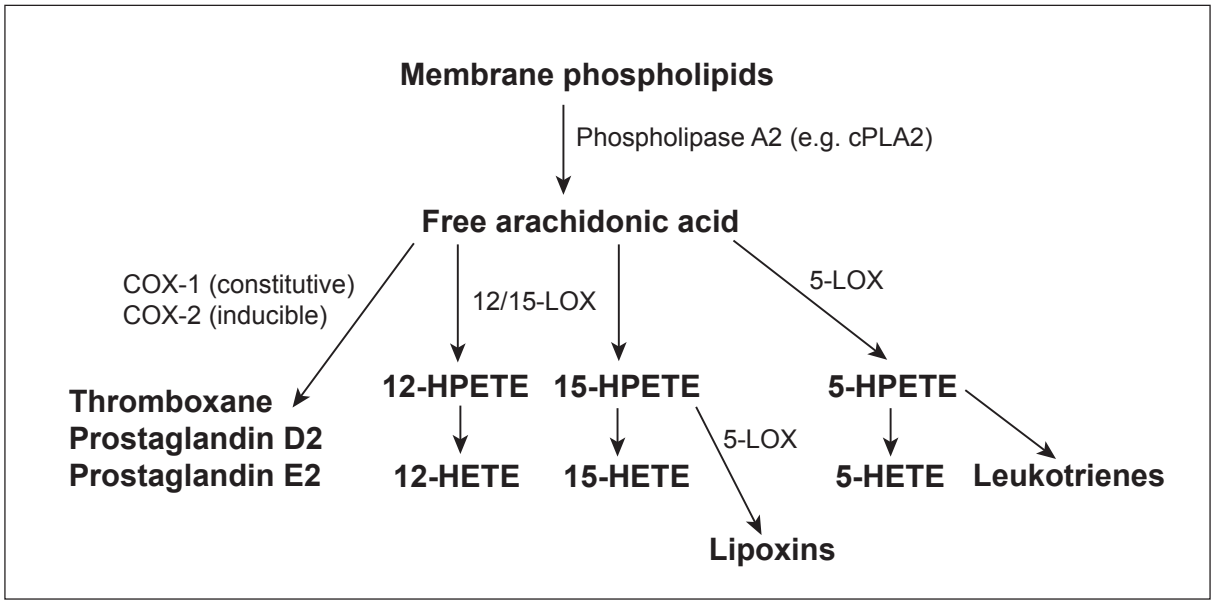

Figure 4.9 Major eicosanoid pathways in mouse macrophages
Eicosanoid biosynthesis is initiated by release of arachidonic acid from cell membranes by phospholipases, such as cPLA2. Free arachidonic acid is processed into thromboxanes and prostaglandins by the cyclooxygenase (COX, *Ptgs*) enzymes; into 12-HETE (12-hydroxyeicosatetraenoic acid) and 15-HETE by 12/15-LIPOXYGENASE (12/15-LOX, *Alox15*); and into 5-HETE and leukotrienes (e.g. LTB4) by 5-LIPOXYGENASE (5-LOX, *Alox5*). Lipoxins are synthesized from 15-HPETE (15-hydroperoxyeicosatetraenoic acid) by 5-LOX. Unlike the mixed 12/15-LOX activity of the mouse Alox15, human macrophages, depending on their phenotype, express two distinct 15-LOX enzymes (ALOX15, ALOX15B) that primarily generate 15-HPETE.

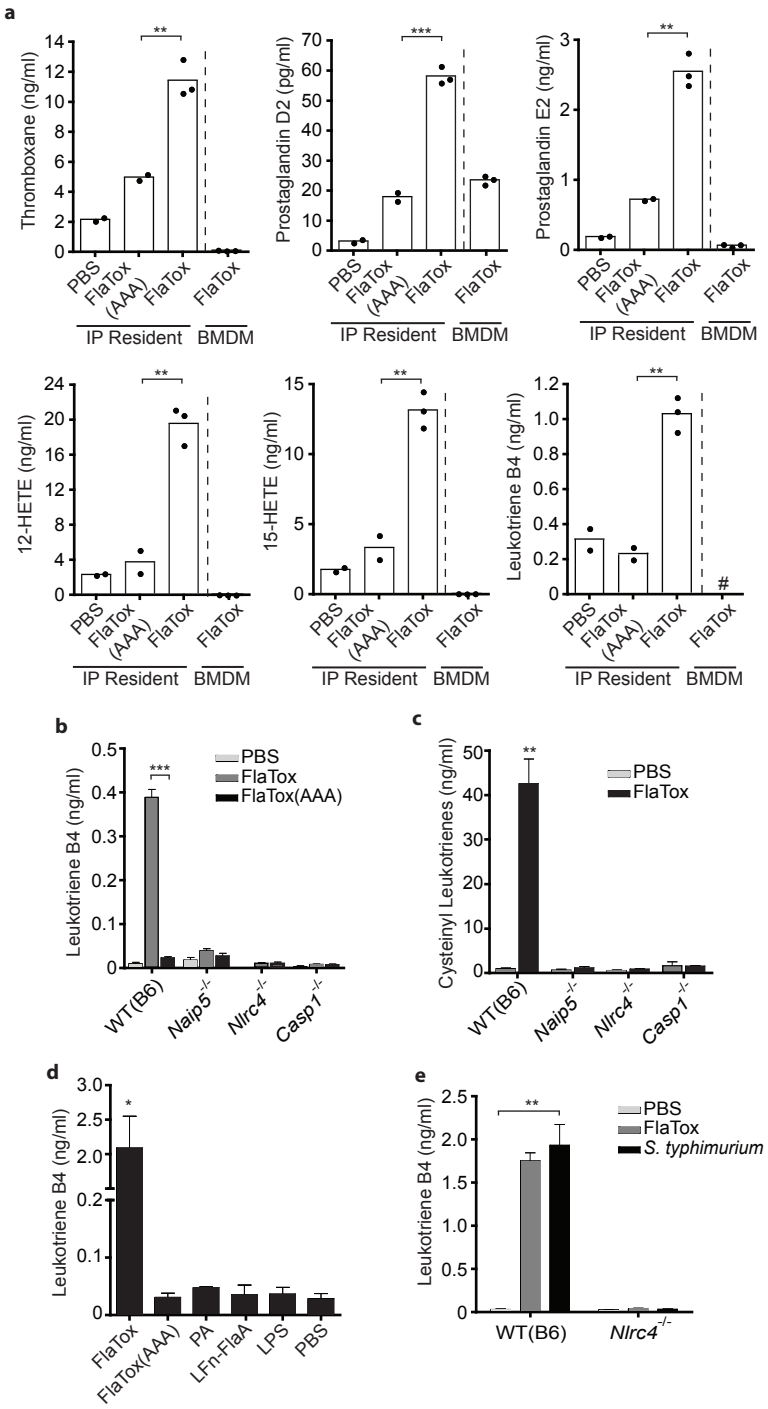

Figure 4.10 Inflammasome-dependent eicosanoid biosynthesis
(a) BMDM or resident peritoneal cells from wild-type (B6) mice were incubated 30 minutes with FlaTox (20 μg/ml PA + 10 μg/ml LFn-FlaA) and secreted eicosanoids were quantified by LC/MS/MS-based lipidomics. (b-e) Resident peritoneal macrophages were selected *ex vivo* by adherence to plastic and treated with FlaTox (b-e), indicated proteins (d: 10 μg/ml PA, 5 μg/ml all others), lipopolysaccharide (d: 1 μg/ml), or *S. typhimurium* (e: MOI=5). Leukotriene B_4 (b; d-e) or cysteinyl-leukotrienes (c) were measured by enzyme immunoassay 30 (b-d) or 180 (e) min after treatment. Data shown (± s.e.m.) are representative of at least two (c, e) or three (a, b, d) independent experiments. * $p < 0.04$; ** $p < 0.009$ *** $p < 0.0005$ (Student t-test). # = not detected.

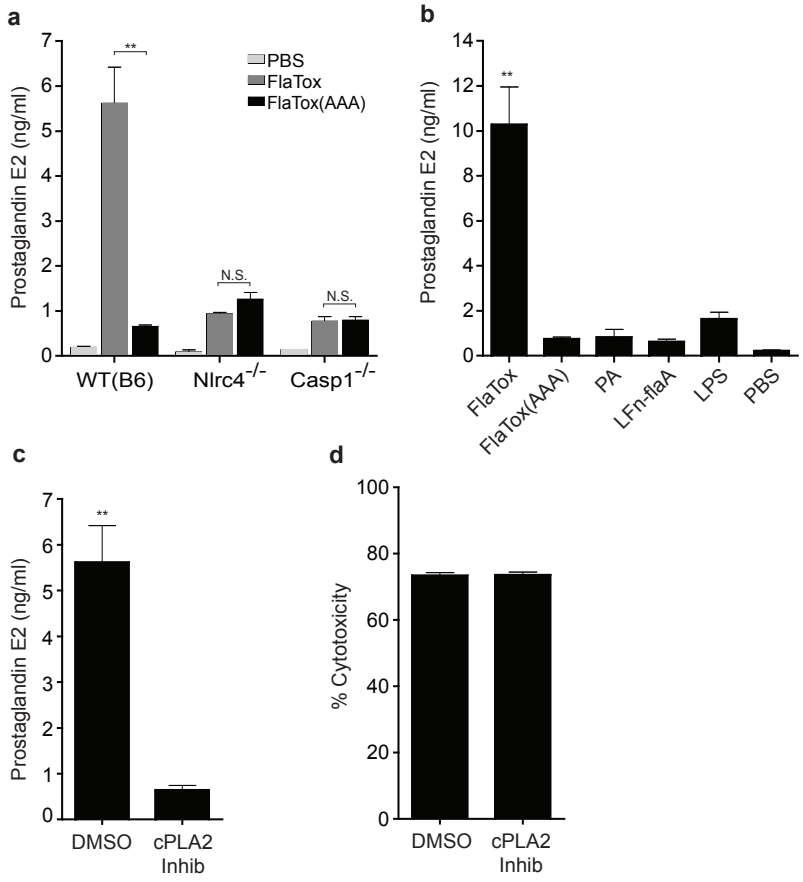

Figure 4.11 Inflammasome-dependent Prostaglandin E_2 production
(a-c) Resident peritoneal macrophages were selected *ex vivo* by adherence to plastic and treated 30 minutes with FlaTox (a, c: 10 μg/ml PA + 5 μg/ml LFn-FlaA), indicated proteins (b: 10 μg/ml PA, 5 μg/ml all others), or lipopolysaccharide (1 μg/ml). Prostaglandin E_2 was measured by enzyme immunoassay. (c) Cells were pre-treated for 30 minutes with DMSO or cPLA2 inhibitor (pyrrophenone, 0.2 μM) prior to addition of FlaTox (10 μg/ml PA + 5 μg/ml LFn-FlaA with DMSO or pyrrophenone) for 30 minutes. (d) Wild-type (B6) resident peritoneal macrophages were selected *in vitro* by adherence and pretreated 30 minutes with DMSO or cPLA2 inhibitor (pyrrophenone, 0.2 μM) before 2 h treatment with FlaTox (10 μg/ml PA + 5 μg/ml LFn-FlaA with DMSO or pyrrophenone). Cell lysis was quantified by release of lactate dehydrogenase. Data shown (± s.e.m.) are representative of two independent experiments. N.S. = not significant; * $p < 0.05$ (Student t-test).

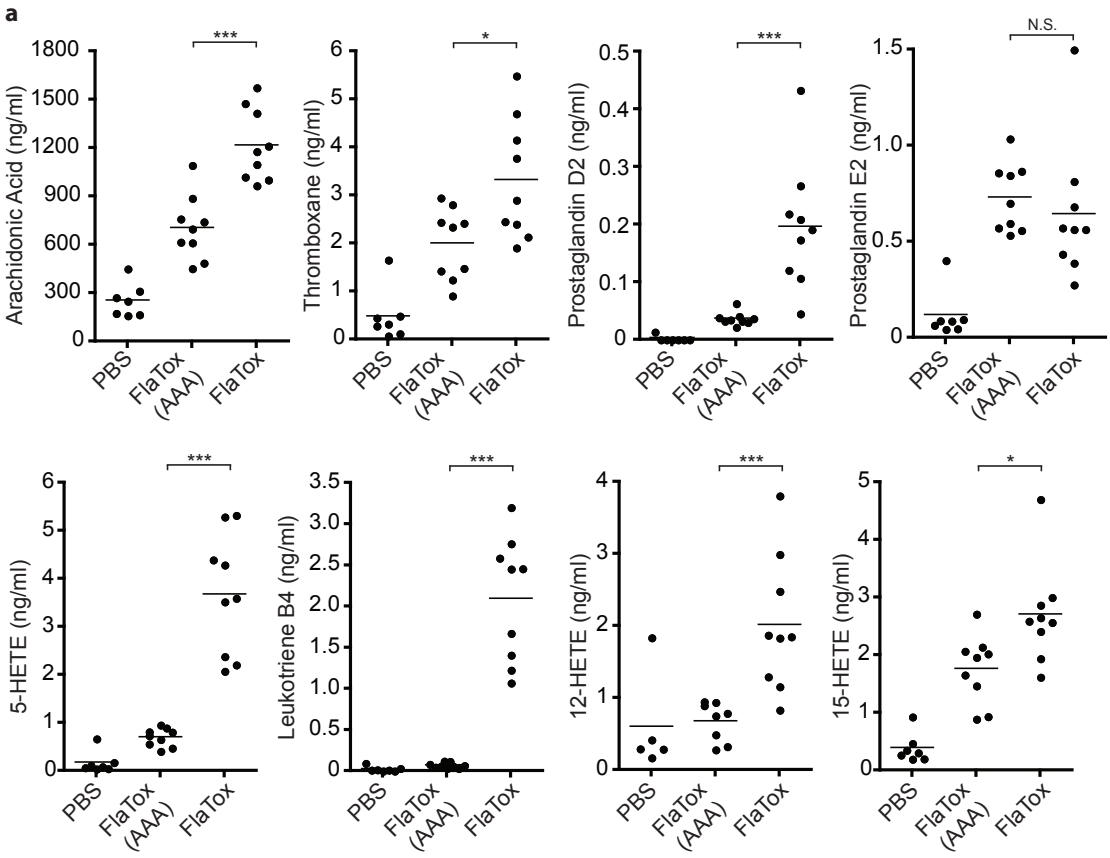

Figure 4.12 FlaTox induced eicosanoid biosynthesis *in vivo*
Wild-type (B6) mice were injected intraperitoneally with FlaTox or FlaTox (AAA) (4 μg/g PA + 2 μg/g LFn-FlaA or LFn-FlaA(AAA)) for 20 min. Peritoneal lavage was analyzed for eicosanoids by LC/MS/MS. Data shown are pooled from multiple experiments. N.S. = not significant; * $p < 0.04$; ** $p < 0.006$ *** $p < 0.0007$ (Mann-Whitney t-test).

4.6 Eicosanoid Biosynthesis Requires cPLA2 and CASP1-dependent Calcium Influx

To understand how inflammasome activation can induce eicosanoid biosynthesis, we considered the initiating A2 phospholipases. Although cells express several A2 phospholipases, the calcium-dependent cytosolic phospholipase cPLA2 is the most common initiator of eicosanoid biosynthesis[130] (Fig. 4.9). Indeed, inhibition of cPLA2 blocked LTB_4 and PGE_2 production in response to FlaTox without inhibiting pyroptosis, suggesting that it acts downstream of inflammasome activation (Fig. 4.13a; Fig. 4.11c-d). An increase in intracellular calcium (Ca^{2+}) concentration is both necessary and sufficient for cPLA2 activation[131]; therefore it is notable that the earliest detectable CASP1-dependent events (prior to cell lysis) in *S. typhimurium* infected BMDM are formation of plasma membrane pores and the influx of Ca^{2+} [89,90]. We observed that a similar CASP1-dependent Ca^{2+} influx preceded cell lysis in resident peritoneal macrophages (Fig. 4.13b-d) and was comparable in magnitude to an ionomycin control (Fig. 4.14). This Ca^{2+} influx appears to be critical for eicosanoid biosynthesis in response to FlaTox, as the intracellular Ca^{2+} chelator BAPTA-AM inhibited LTB_4 production without blocking pyroptosis (Fig. 4.13e).

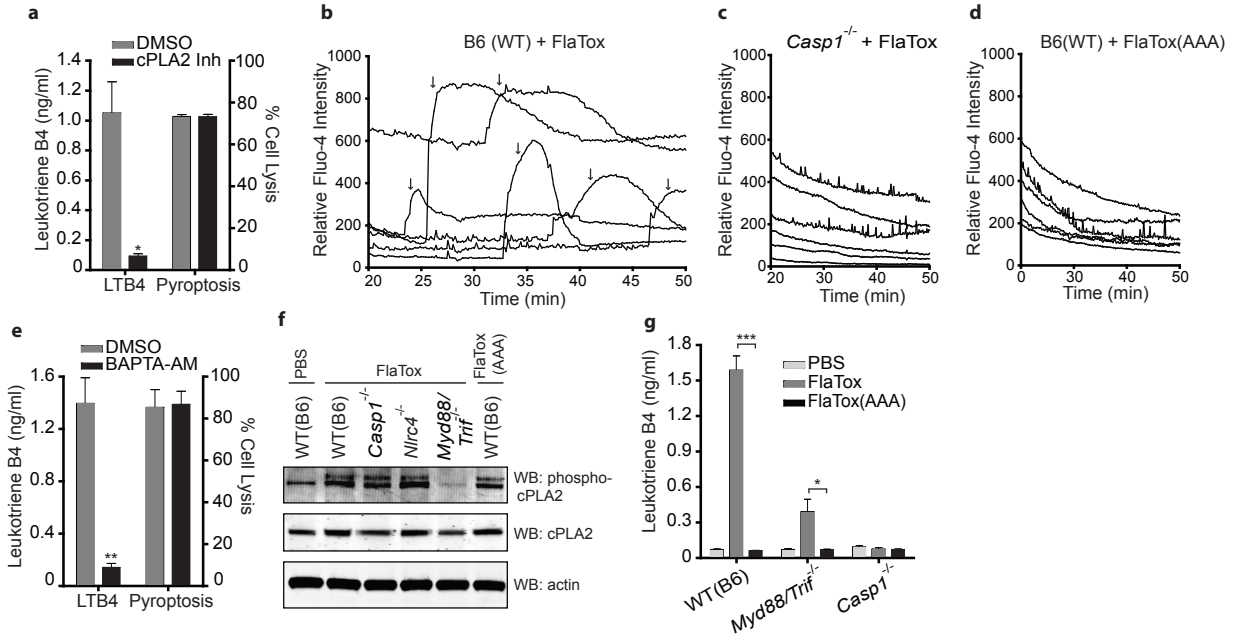

Figure 4.13 Mechanism of inflammasome-dependent eicosanoid production
(a-g) Resident peritoneal macrophages were selected *ex vivo* by adherence to plastic. (a) Pre-treated for 45 min with DMSO or cPLA2 inhibitor (pyrrophenone; 0.2 μM) prior to addition of FlaTox with DMSO or pyrrophenone. LTB_4 was measured by enzyme immunoassay after 30 min, and cell lysis was measured by lactate dehydrogenase release assay after 2.5 h. (b-d) Fluo-4 loaded wild-type (B6) cells (b, d) or *Casp1*$^{-/-}$ cells (c) were treated with FlaTox (b-c) or FlaTox(AAA) (d) and Fluo-4 fluorescence was imaged from 20-50 min post treatment. Each trace represents one cell over time. Arrows (b) indicate onset of membrane blebbing. (e) Pre-treated for 45 min with DMSO or BAPTA-AM (10 μM) prior to addition of FlaTox. Analysis as in (a). (f) Cells of indicated genotype were treated 30 min with FlaTox or FlaTox(AAA) or left untreated. Cell lysates were probed for indicated proteins by Western blot. (g) Cells of indicated genotype were treated as indicated. After 30 min LTB_4 was measured as in (a). Data shown (± s.e.m.) are representative of at least two (b-d) or three (a, e-g) independent experiments. * $p < 0.04$; ** $p < 0.006$ *** $p < 0.0007$ (k-n: Mann-Whitney t-test; a, e, g, j: Student t-test).

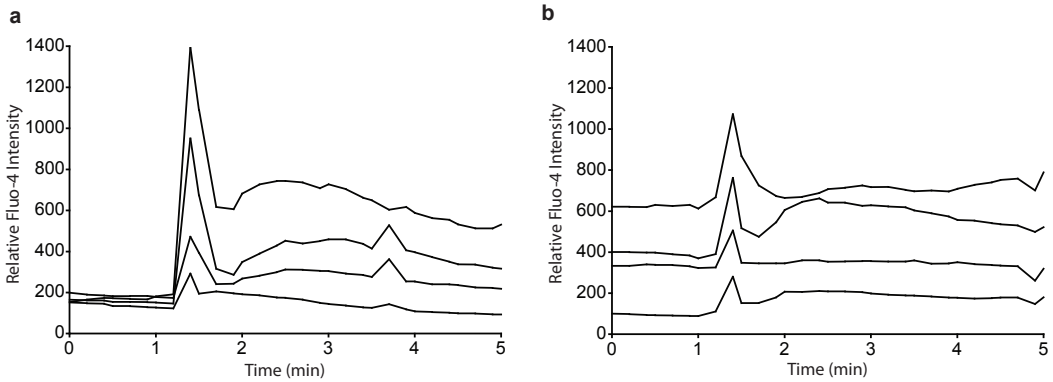

Figure 4.14 Ionomycin-induced calcium flux
(a-b) Wild-type (B6) (a) or *Casp1*$^{-/-}$ resident peritoneal macrophages loaded with Fluo-4 were imaged for 5 min and ionomycin (1 μM) was added after 1-2 min. Each trace represents one cell over time. Data shown are representative of >30 cells analyzed in two independent experiments.

4.7 TLR Signaling Synergizes with the Inflammasome to Induce Eicosanoid Biosynthesis

Although cPLA2 activity is regulated primarily by intracellular Ca^{2+} influx, its activity can be enhanced by mitogen activated map kinase (MAPK)-dependent phosphorylation[131]. Because TLR signaling rapidly activates MAPKs[132], we wondered if TLR-mediated recognition of flagellin or other ligands in our protein preps might enhance cPLA2 activity. Indeed, cPLA2 in resident peritoneal cells was phosphorylated following treatment with FlaTox, and this was inflammasome independent, but Myd88/Trif dependent (Fig 4.13f). Accordingly, LTB_4 production in response to FlaTox was partially attenuated in *Myd88/Trif*$^{-/-}$ cells (Fig. 4.13g) and *Myd88/Trif*$^{-/-}$ mice were partially protected *in vivo* (Fig. 4.15). These results indicate that although an inflammasome-dependent Ca^{2+} flux is both sufficient and necessary for eicosanoid production in response to FlaTox, TLR signaling can synergize with inflammasome activation to produce maximal responses. Such synergy is likely physiological, since during a natural infection, it is anticipated that both TLR and inflammasome activation will occur.

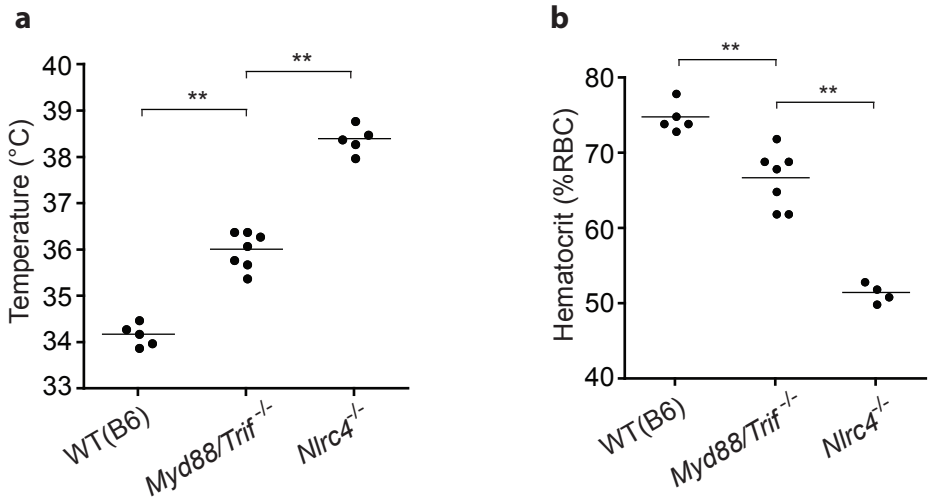

Figure 4.15 MYD88/TRIF-dependent signaling enhances FlaTox pathology
(a-b) Mice of indicated genotypes were injected intraperitoneally with FlaTox (4 μg/g PA + 2 μg/g LFn-FlaA) and rectal temperature (a) and hematocrit (b) were measured 30 m.p.i. Data shown (± s.e.m.) are representative of two independent experiments (n=5-7). ** $p < 0.006$ (Mann-Whitney t-test).

4.8 Resident Peritoneal Macrophages are Uniquely Primed for Inflammasome-dependent Eicosanoid Biosynthesis

We wished to further investigate the basis for the cell type specificity of inflammasome-dependent eicosanoid biosynthesis. Consistent with the inability of BMDM to transfer responsiveness to FlaTox *in vivo* (Fig. 4.6i), we observed no eicosanoid production by LC/MS/MS in BMDM treated 30 min with FlaTox (Fig. 4.10a), and even after two hours of treatment, when a majority of BMDM have undergone pyroptosis, we could not detect LTB_4 production (Fig. 4.16a-b). Since BMDM exhibit inflammasome-dependent Ca^{2+} flux[89], we hypothesized that eicosanoid production in BMDM is regulated downstream

of Ca^{2+} flux. Transcriptional analysis revealed that *Cox1*, *Alox12/15*, and *Alox5*, which encode key enzymes required for eicosanoid biosynthesis, were expressed at much (10- to 1,000-fold) higher levels in CD11b/F4-80^{hi} resident peritoneal macrophages than in BMDM or thioglycollate-elicited CD11b/F4-80^{hi} cells (Fig. 4.16c). Resident peritoneal macrophages therefore appear uniquely primed for inflammasome-dependent eicosanoid responses. Most *in vitro* characterization of inflammasomes has relied on BMDM, perhaps explaining why a link to eicosanoid biosynthesis has not been discovered previously.

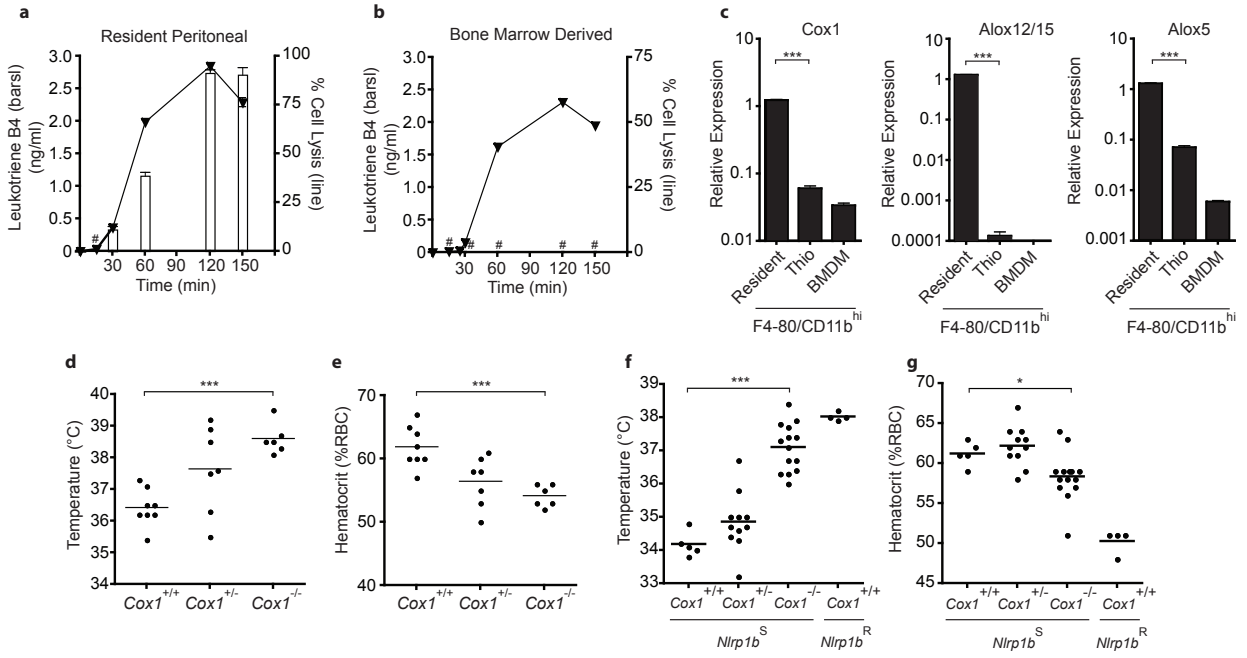

Figure 4.16 Cell-type specificity and *in vivo* role of eicosanoid production
(a-b) Resident peritoneal macrophages (a) or BMDM (b) were treated with FlaTox. LTB_4 (bars) was measured by enzyme immunoassay and cell lysis (lines) was measured by lactate dehydrogenase release assay at indicated timepoints. (c) cDNA was prepared from BMDM and from sorted resident or thioglycollate-elicited CD11b/F4-80^{hi} peritoneal cells. Gene expression was measured by quantitative RT-PCR. (d-e) B6;129P2-*Cox1*$^{-/-}$ mice and littermate controls were injected with FlaTox and rectal temperature (d) and hematocrit (e) were measured 30 m.p.i. (f-g) *Cox-1*$^{-/-}$ mice and littermate controls expressing a lethal toxin sensitive (S) or resistant (R) *Nlrp1b* allele were injected with anthrax lethal toxin (200 µg PA + 100 µg lethal factor) and analyzed as in (e-f) 45 m.p.i. Data shown (± s.e.m.) are pooled from multiple experiments (d-g) or representative of at least two (a-c) independent experiments. * $p < 0.04$; ** $p < 0.006$ *** $p < 0.0007$ (k-n: Mann-Whitney t-test; a, e, g, j: Student t-test). # = not detected.

4.9 *In Vivo* Role of Inflammasome-dependent Eicosanoid Biosynthesis

To test the role of eicosanoids in FlaTox-induced pathology directly, we injected B6;129P2.*Cox1*$^{-/-}$ mice and littermate controls with FlaTox, and found that the EHR was significantly attenuated in these mice ($p<0.0007$; Fig. 4.16d-e). As expected, given that FlaTox induces broad biosynthesis of both COX-1-dependent and -independent eicosanoids, the role of COX-1 was masked at high doses of FlaTox or at later timepoints (data not shown), suggesting a contribution of COX-1-independent eicosanoids or other as yet unidentified factors. Importantly, pyroptosis was unaffected by *Cox1* deficiency, further demonstrating that pyroptosis is not sufficient for pathology in FlaTox-treated mice

(Fig.4.17). Furthermore, chemical inhibition of COX-1 protected mice from a low dose of FlaTox (Fig. 4.18). Inhibition of COX-2, which is undetectable in resting macrophages, or genetic deletion of *Alox5* had no effect, although a contribution may have been masked by functional redundancy with other eicosanoids (Fig. 4.18). These data link inflammasome-dependent eicosanoid production by peritoneal macrophages to the pathology associated with *in vivo* delivery of FlaTox, and particularly implicate COX-1 dependent eicosanoids, i.e. prostaglandins, in the resulting vascular leakage.

Since eicosanoid production occurred downstream of CASP1, we hypothesized that other inflammasomes might also lead to eicosanoid production *in vivo*. It is well established that LT-induced lethality in mice is inflammasome-independent[133], however a recent report demonstrated a rapid and transient inflammasome-dependent hypothermic response in LT-treated mice[134]. Since C57BL/6 mice express a non-functional allele of *Nlrp1b* (*Nlrp1b*^{R}), we injected *Cox1*$^{+/+}$ mice expressing the sensitive 129 allele of *Nlrp1b* (*Nlrp1b*^{S}*).* In addition to a drop in body temperature, these mice developed diarrhea, which coincided with an inflammasome-dependent increase in hematocrit (Fig. 4.16f-g). As in FlaTox-treated mice, deletion of *Cox1* attenuated these early pathologies of lethal toxin (Fig. 4.16f-g), indicating that in mice this naturally occurring bacterial toxin activates a similar, although non-lethal, inflammasome pathway.

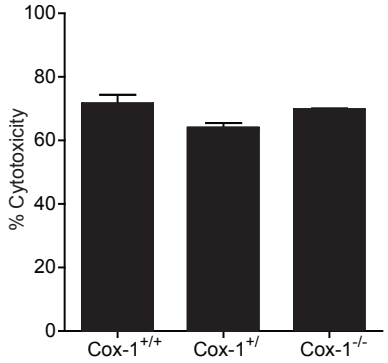

Figure 4.17 Pyroptosis is COX-1 independent
BMDM from B6;129P2-*Cox1*$^{-/-}$ mice and littermate controls were incubated 4 h with FlaTox (4 μg/ml PA + 2 μg/ml LFn-FlaA). Cell lysis was quantified by release of lactate dehydrogenase. Data shown (± s.e.m.) are representative of three independent experiments.

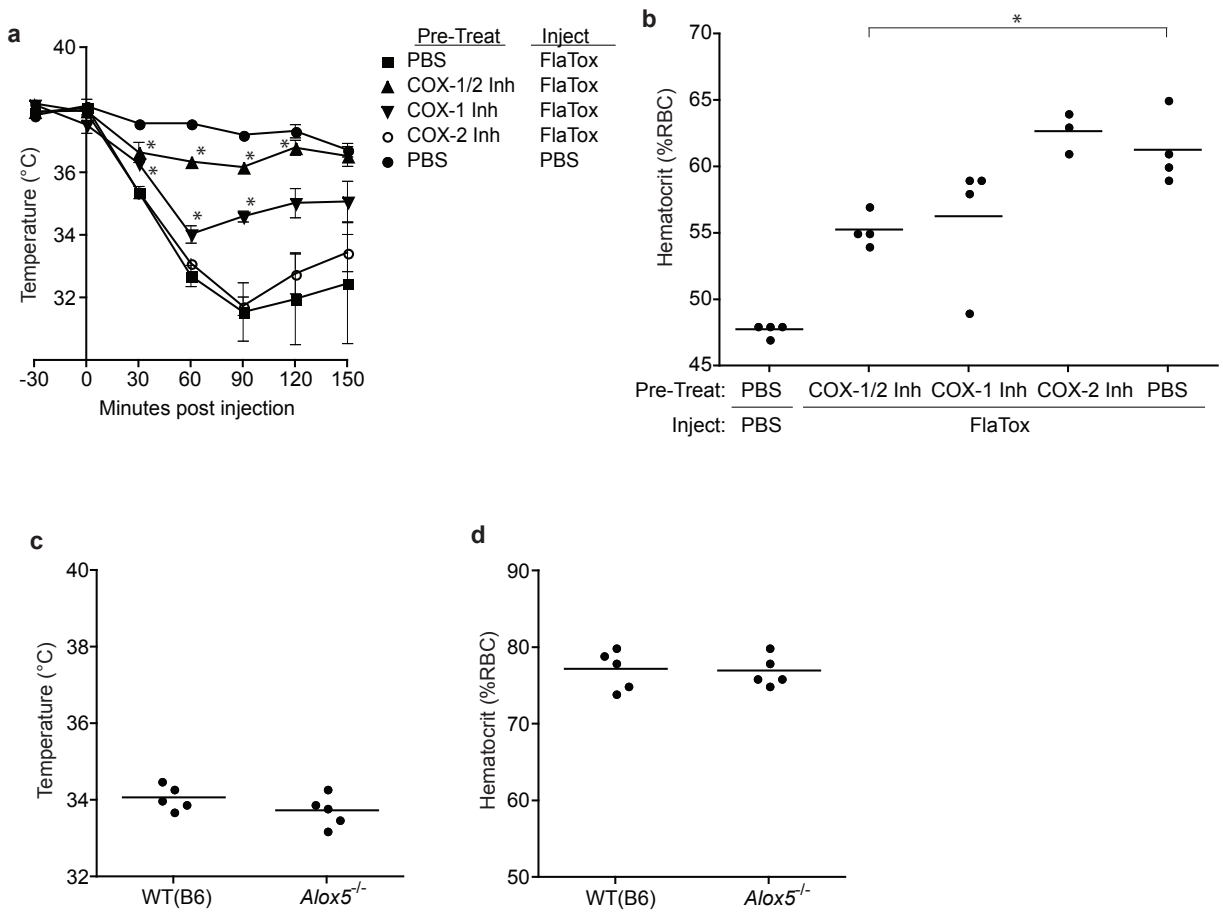

Figure 4.18 COX-1 inhibition but not COX-2 inhibition or LOX-5 deletion protects mice from FlaTox
(a-b) Wild-type (B6) mice were pretreated intraperitoneally for 30 minutes with 1 µg/g body weight of COX-1/2 non-specific (indomethacin), COX-1 specific (SC-560) or COX-2 specific (Cay-10404) inhibitors. 5 µg of FlaTox (5 µg PA + 5 µg LFn-FlaA) was delivered in 200 µl PBS by tail vein injection. (a) Rectal temperature was monitored over time. (b) Hematocrit was measured 60 minutes post injection. (c-d) Mice of indicated genotypes were injected intraperitoneally with FlaTox (4 µg/g PA + 2 µg/g LFn-FlaA) and temperature (c) and hematocrit (d) were measured 30 m.p.i. Data shown (± s.e.m.) are representative of at least two independent experiments. * p = 0.029 (Mann-Whitney t-test).

4.10 Discussion

In summary, our results suggest a model (Fig. 4.19) in which CASP1 activation results in a rapid calcium influx (Fig. 4.13b) that is necessary for cPLA2 activation (Fig. 4.13e) and downstream eicosanoid biosynthesis. Identification of a CASP1 substrate required for calcium influx is an important, but technically challenging area for future research, as proteomic studies to identify novel substrates of CASP1[58-60] have so far yielded limited insight into its cytokine-independent activities.

To our knowledge, this is the first demonstrated direct link between inflammasome activation and eicosanoid biosynthesis. Moreover, this link appears to be of great physiological significance *in vivo*, since our data show that inappropriate inflammasome-dependent eicosanoid production contributes to lethal and rapid vascular leakage. Interestingly, inflammasome-dependent eicosanoid production appears to be cell-type

specific, as peritoneal macrophages express higher levels than BMDM of the lipoxygenase and cyclooxygenase enzymes required for eicosanoid biosynthesis. The primed state of resting peritoneal macrophages may be a general characteristic of resident macrophages guarding sites of pathogen entry, and it will be important to further explore the concept of cell lineage-specific regulation of inflammasome function *in vivo* (see section 5.2.1). Indeed, our experiments using bone marrow chimeras suggest that another cell type, likely of non-hematopoietic origin, also responds to FlaTox (see section 5.2.2). The dichotomy between inflammasome responses in resident peritoneal macrophages and BMDM also highlights the importance of using *in vivo* models to study immune responses.

While many cellular immune responses require *de novo* transcription, the NAIP5/NLRC4 and NLRP1B inflammasomes assemble from preformed protein components to activate a proteolytic cascade. As such, these inflammasomes are ideally positioned to mediate rapid responses to infection. Initiated within minutes of flagellin detection, the inflammasome-dependent eicosanoid production described here represents one of the most rapid *in vivo* innate immune cellular responses known. When restricted to the site of infection, this inflammasome effector function may play an important role in host protection (see section 5.3). For example, eicosanoids rapidly increase local vascular permeability, allowing antibody, complement, and immune cells to access the site of infection. Additionally, the diarrhea associated with FlaTox injection may represent an inflammasome-mediated mechanism for secretion of pathogens and toxins, as is seen in response to parasites. Because our data show that eicosanoids are produced downstream of CASP1 activation, we suggest it will be important to evaluate a role for eicosanoids in other inflammasome-dependent phenotypes that have previously been described *in vivo*. Indeed, our results suggest that the effector functions of inflammasomes are much broader, and have more dramatic effects on host physiology, than has been previously appreciated.

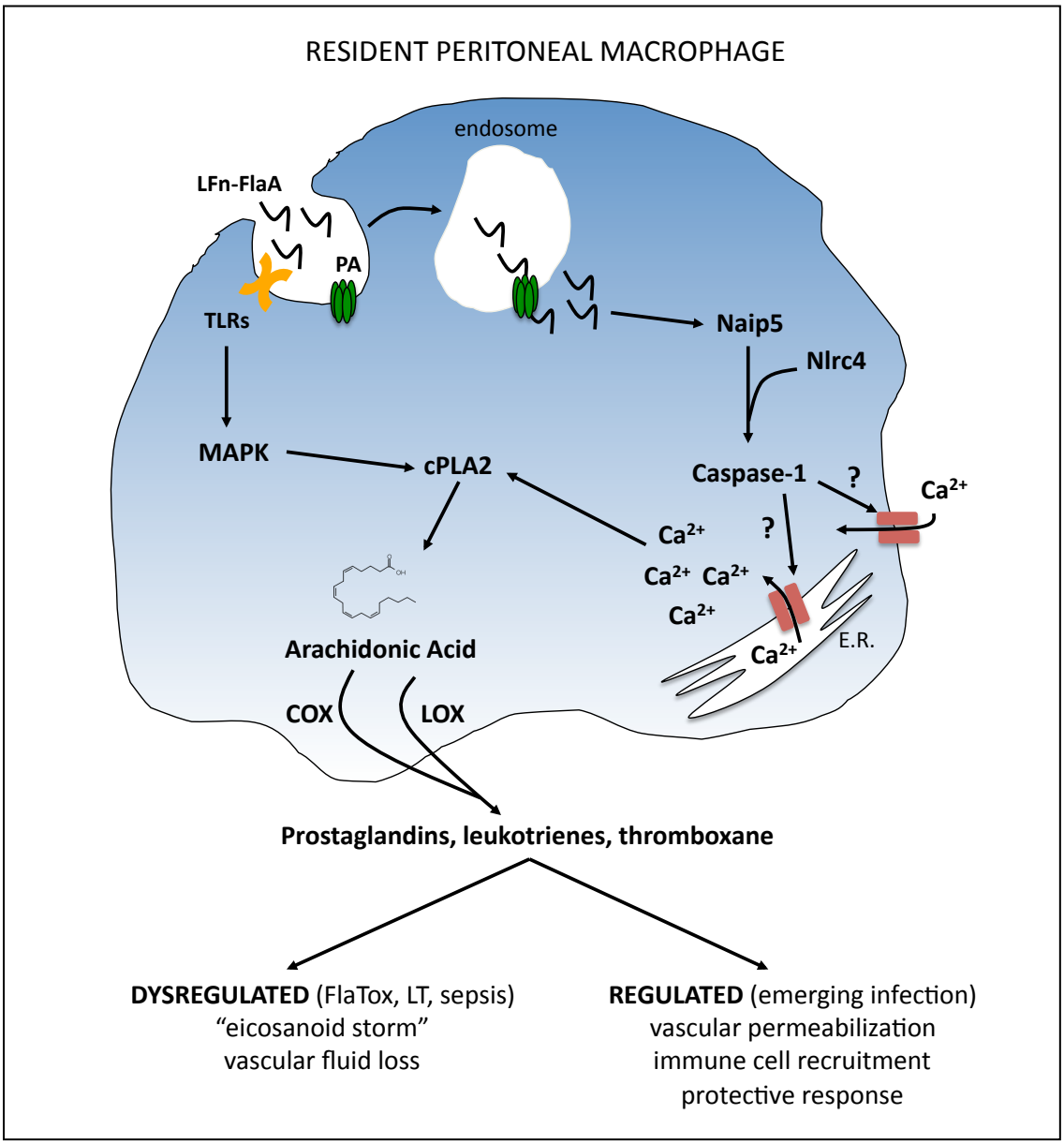

Figure 4.19 Model of inflammasome-dependent eicosanoid biosynthesis
LFn-FlaA and protective antigen (PA) are taken up into endosomes, where the PA channel inserts into the membrane and translocates LFn-FlaA to the cytosol. Once in the cytosol, LFn-FlaA is detected by the NAIP5/NLRC4 inflammasome leading to recruitment and activation of CASP1. Activated CASP1 targets as yet unidentified substrates to cause an influx of cytosolic calcium (Ca^{2+}). The rise in Ca^{2+} activates the cytosolic phospholipase A2 (cPLA2), which processes membrane phospholipids to release arachidonic acid (AA). cPLA2 activity is further enhanced by phosphorylation downstream of TLR-signaling. Cyclooxygenase (COX) and lipoxygenase (LOX) enzymes then process AA into the eicosanoids - prostaglandins, thromboxanes, and leukotrienes. Outside the cell, these eicosanoids have potent inflammatory effects. When activated systemically, this pathway leads to an "eicosanoid storm" with devastating effects that include vascular collapse and possible death in mice. On the other hand, we predict that localized activation of eicosanoid biosynthesis in infected cells protects the host by opening the site of infection and recruiting an appropriate immune response. This inflammasome-dependent induction of eicosanoid biosynthesis is absent in bone marrow derived macrophages, but may be a general phenotype of resident macrophages, such as those in the peritoneum, that express high levels of the COX and LOX enzymes.

Chapter 5: Future Directions and Development of Mouse Models

In this final chapter I address some of the future directions suggested by the findings presented in this dissertation. In particular, I am developing three knock-in mouse models that will allow us to further dissect inflammasome responses *in vivo,* and that promise to reveal new insights into inflammasome function.

5.1 The Search for Novel CASP1 Substrates

5.1.1 Pooled shRNA Screening

The identification of novel CASP1 substrates remains a central challenge for the inflammasome field. Despite the failures of our siRNA screen, an unbiased approach probably still offers the best chance of success. As discussed in chapter 2, the whole-genome screen almost certainly suffered from a high rate of false positives and false negatives. Some of this is inevitable due to the high-throughput nature of the screen and the inherent limitations of the RNAi technology; however, two recent advances provide an exciting opportunity to revisit the screening approach.

The siRNA library I used contained 3-4 pooled oligos targeting each gene. Not only does this increase the chances of false negatives, it also makes it more difficult to identify false positives if, for example, two out of four oligos give a phenotype. Several groups, including the McManus lab at UCSF, have recently addressed this limitation by developing pooled lentiviral libraries with ~30 shRNA targeting each gene[135]. After establishing stable knockdown by transduction, cells are cultured with and without selection (e.g. FlaTox to induce pyroptosis). Following selection, the shRNA inserts are amplified and subjected to deep sequencing. By comparing the frequency of each shRNA in the selected cells with unselected cells, it is possible to identify shRNAs that confer either a gain or loss of fitness. Identification of multiple shRNAs targeting the same gene gives high confidence of a real result.

One important limitation of this pooled shRNA screening approach is that the library is currently only available for human genes. Unfortunately, FlaTox and lethal toxin, the most robust inducers of pyroptosis, do not activate human inflammasomes. Therefore, it has been difficult to identify an appropriate selective pressure to pair with the human-targeted shRNA library. Recently, however, Zhao et al identified CprI, a needle protein from the type-three secretion apparatus of *C. violaceum*, as an agonist of the human NAIP/NLRC4 inflammasome. The authors also showed that a LFn-CprI fusion protein could be delivered to the cell cytosol and induce pyroptosis in the human macrophage-like cell line U937[19]. The high-coverage shRNA library and this "CprI-Tox" therefore provide an excellent opportunity to revisit RNAi screening to identify novel components of inflammasome pathways.

5.1.2 Biochemical Approaches

There are also several experimental modifications that might make biochemical approaches for the identification of novel CASP1 substrates more promising, despite past failures. I believe that formation of the ASC-focus in activated cells has hindered the identification of CASP1 substrates required for pyroptosis. As described in chapter 3, pyroptosis can be initiated from NAIP/NLRC4/CASP1 complexes in the absence of ASC. In

fact, the ASC-focus appears to be a structure that is largely dedicated to the processing of IL-1β/IL-18. This complex also presents many technical challenges due to its megadalton size. Most notably, the ASC focus is difficult to separate from membranes and other debris in a cell lysate. It is likely that many investigators have unknowingly pelleted the ASC focus (and all associated proteins) when trying to clear their cell lysate.

I propose, therefore, to repeat proteomics in *Asc*$^{-/-}$ cells to bias towards the identification of CASP1 substrates required for pyroptosis. As an important control, I have also generated *Asc/Casp1*$^{-/-}$ mice, so that CASP1-specific substrates can be isolated. These cells would also allow for complementation with a protease dead allele of *Casp1* or other genetic modifications that might facilitate the trapping of CASP1 substrates. As an additional control, it would be interesting to probe *Casp1*$^{-/-}$ cells treated to activate the recently identified non-canonical CASP11 inflammasome[62]. Although CASP11 requires CASP1 for cytokine processing, it can activate pyroptosis independently. The protein required for pyroptosis should therefore be a substrate of both CASP1 and CASP11.

5.2 Cell Type Specific Inflammasome Diversity

5.2.1 Lineage Differentiation and the Inflammasome

Since the inflammasome was first identified in THP-1 cells, a monocyte-like human cell line, the overwhelming majority of research in the field has been carried out in myeloid lineages. Immortalized macrophages or bone marrow derived macrophages and dendritic cells have been the model of choice. Although these cells facilitated many important advances in our understanding of inflammasomes, their limitations are becoming evident. In particular, the resulting model of inflammasome activation and downstream effector functions is likely over-simplified. In this section I will explore two emerging concepts related to the idea of inflammasome diversity: (1) inflammasome activation and effector functions vary within myeloid lineages depending on differentiation state, and (2) inflammasomes also assemble in non-hematopoietic lineages.

Several examples of differentiation-state associated diversity in inflammasome activation and function have been reported in the literature. Netea et al found that in human monocytes, LPS is sufficient to induce secretion of bioactive IL-1β, while in tissue-culture differentiated macrophages or dendritic cells a second stimulus, such as ATP, is required in addition to LPS[136]. Since the levels of pro-IL-1β were equivalent in all LPS-treated cells, the authors suspected regulation at the processing stage. Indeed, active CASP1 was constitutively detected in monocytes, but not macrophages or dendritic cells[136]. This finding has important implications for pathogen surveillance by monocytes and macrophages. Perhaps circulating blood monocytes are primed to respond to a bacterial product, such as LPS, since its presence in the blood suggests a systemic invasion.

Gabriel Nuñez, Luigi Franchi and colleagues recently presented a reciprocal model, showing that unlike monocytes or macrophages studied *in vitro*, tissue resident macrophages in the intestine constitutively express pro-IL-1β and are therefore primed to secrete the cytokine immediately following inflammasome activation (Keystone Symposia – 2012 Innate Immunity).

Another interesting example is provided by Kupz et al. The authors show that intravenous injection of *S. typhimurium* or even purified flagellin leads to NLRC4-

dependent IL-18 secretion in the spleen that promotes IFN-γ production by memory $CD4^+$ T-cells[87]. The authors find that IL-18 is secreted selectively by splenic $CD8\alpha^+$ dendritic cells, which are known for their ability to cross-present exogenous antigen on MHC-1[87]. The transit of antigen through the cytosol during cross-presentation might explain the ability of purified flagellin to activate CASP1, and has exciting implications for the interaction of inflammasomes with commensal bacteria. For example, the NLRP6 inflammasome is required to maintain a normal microbiota, but it remains unclear how this crosstalk is achieved[45]. Cross-presenting dendritic cells in the lamina propria might provide a clue to this mechanism.

Finally, our own findings reported in chapter 4 also support the idea of differentiation-state specific specialization of the inflammasome. While resident peritoneal macrophages secrete eicosanoids following CASP1 activation, this response is completely absent in BMDM and also reduced in thioglycollate-elicited peritoneal macrophages. This difference seems to arise at least in part from the differential expression of *Cox1*, *Alox5*, and *Alox12/15* (Fig. 4.16). It will be interesting to test if changes in culturing conditions that drive BMDMs into different activation states (e.g. "classical", "regulatory", "wound-healing"[137]) enhance expression of these genes and confer the eicosanoid phenotype. It will also be important to test if inflammasome-dependent eicosanoid biosynthesis is a general phenotype of resident macrophages (e.g. alveolar, lamina propria), and if this extends to other cell lineages.

5.2.2 Inflammasomes in Non-hematopoietic Cells

In addition to inflammasome specialization within hematopoietic lineages, it has also become clear that inflammasomes assemble in non-hematopoietic cells. This finding has long been suggested by the expression patterns of inflammasome components. For example, some of the highest levels of *Naip5* transcript are detected in the intestine (REV unpublished data from whole tissue homogenate), and *Casp1* is widely expressed outside the hematopoietic compartment[138]. The best functional evidence of inflammasome activation in non-hematopoietic cells has come from bone marrow chimera experiments and suggests that stromal cells of the intestine are particularly important. For example, *Casp1*$^{-/-}$ mice have enhanced intestinal tumor formation in the AOM/DSS model of inflammation-induced tumorigenesis. This phenotype is replicated by neither the WT-->*Casp1*$^{-/-}$ nor the *Casp1*$^{-/-}$-->WT chimeras, suggesting inflammasome activation is required in both radio sensitive and radio resistant cells[139]. Expression of *Nlrp6*, meanwhile, is almost undetectable in the hematopoietic compartment, but abundant in gut epithelium[45].

Again, our data from chapter 4 also suggest a role for inflammasome activation in radio-resistant cells, likely of non-hematopoietic origin. Wild-type mice reconstituted with *Nlrc4*$^{-/-}$ bone marrow respond robustly to FlaTox, although with delayed kinetics (Fig. 4.6). Since much of the fluid accumulation is observed in the intestine and *Nlrc4* is expressed in these tissues, we speculate that inflammasome activation in the intestinal epithelium might contribute to the late FlaTox pathology. While we could not detect any pathology by histology at 30 minutes post FlaTox treatment, analysis of the small intestine at 120 minutes post injection provided an interesting observation. A blinded clinical pathologist (Ingrid Bergin at U. Mich.) readily identified FlaTox treated tissues by observing pyknotic, often crescent-shaped nuclei in the gut epithelium, suggesting cell death (Fig. 5.1). These

dead cells seemed to cluster in the villus crypts, where cell division is most rapid. In one FlaTox-treated sample we also observed large amounts of dead cells sloughed off into the gut lumen (Fig. 5.2).

Both observations warrant further analysis as they provide only indirect evidence of inflammasome activation in these cells. It will be important to study epithelial cells in isolation, either through *ex vivo* culturing and treatment, or by identifying epithelium-derived cell lines that activate the inflammasome. Once the tools are available, it will be interesting to identify the inflammasome effector functions that operate in these cells. To our knowledge, pyroptosis has not been directly documented in non-hematopoietic cells, although our histology in Fig. 5.1 suggests it might occur. Fluorescent reagents being developed by Matt Bogyo's lab at Stanford might allow us to observe active CASP1 in these cells(A. Puri, personal communication).

It also remains to be determined if delayed FlaTox pathology mediated by radio resistant cells is also eicosanoid-dependent. The fact that *Cox1*$^{-/-}$ mice are fully responsive to FlaTox after 30 minutes (data not shown) suggests the involvement of other COX1-independent eicosanoid pathways or of a different effector function. It is also tempting to speculate that the delayed FlaTox responsiveness observed in *Casp1*$^{-/-}$ and *Naip5*$^{-/-}$ mice (Fig. 4.2) is mediated by the late-responding radio resistant cells. Perhaps *Naip6* expression is higher in these cells. In any case, the partial responsiveness of *Naip5*$^{-/-}$ and *Casp1*$^{-/-}$ mice suggests the assembly of diverse flagellin-responsive inflammasomes and extends the idea of cell-type specific inflammasome diversity.

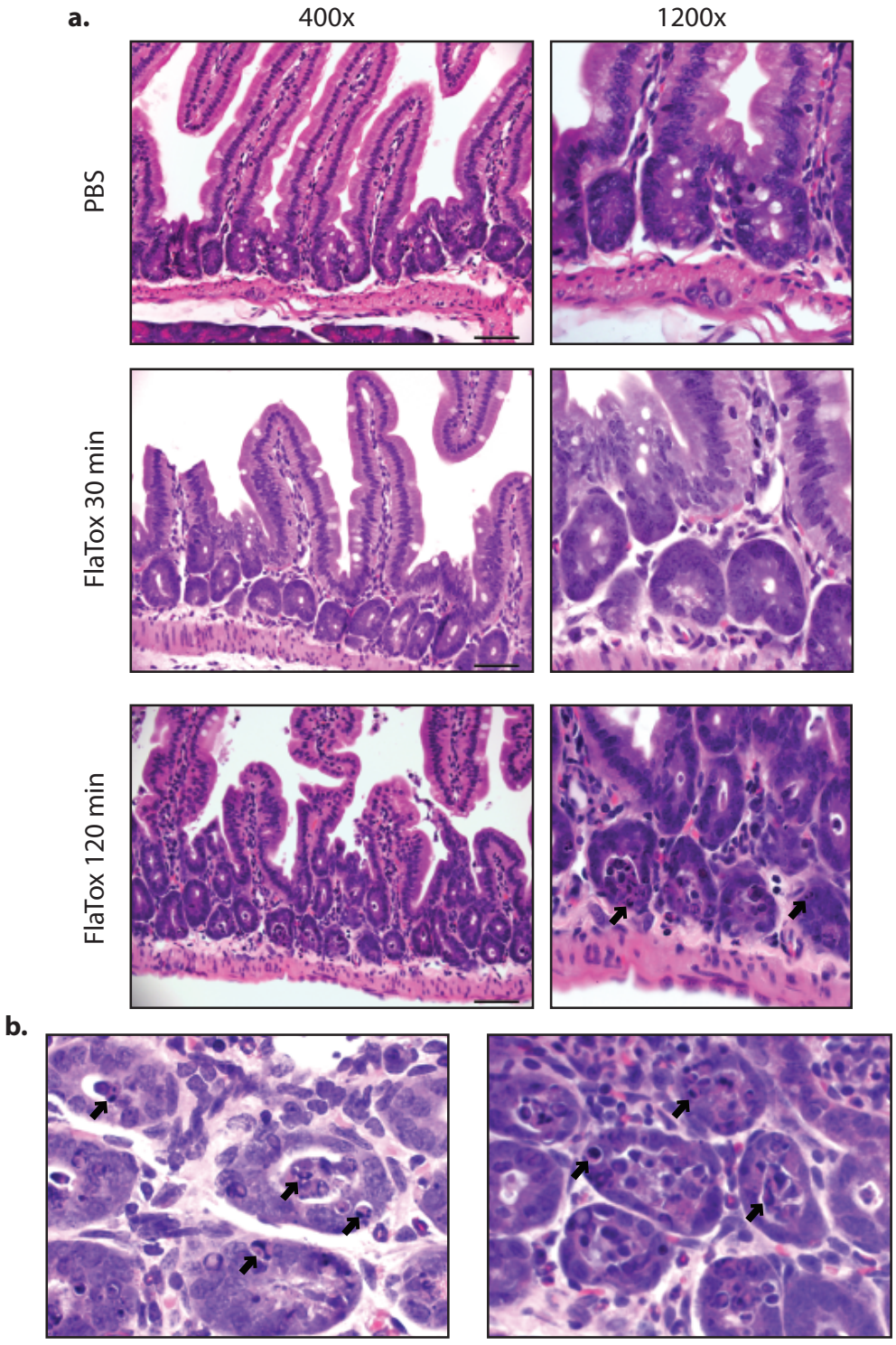

Figure 5.1 FlaTox-induced epithelial cell death in intestinal tissues at late timepoints
(a-b) Wild-type (B6) mice were injected intraperitoneally with FlaTox (4 μg/g PA; 2 μg/g LFn-FlaA). Intestinal tissues were fixed at the indicated timepoints and stained with hematoxylin and eosin. (b) Additional images (1200x) from 120 m.p.i. Arrowheads indicate pyknotic nuclei. Duodenal sections shown in figure are representative of entire intestinal tissue and experiment was repeated twice (n=1-2). Bar = 50μm.

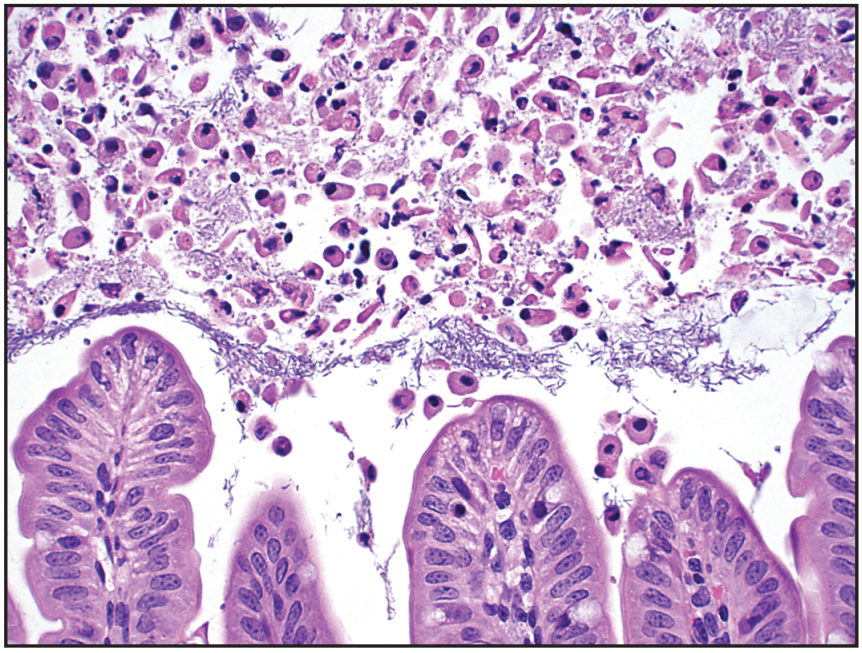

Figure 5.2 Sloughing of dead cells into intestinal lumen
Wild-type (B6) mice were injected intraperitoneally with FlaTox (4 μg/g PA; 2 μg/g LFn-FlaA). After 120 minutes the intestinal tissues were fixed, sectioned, and stained with hematoxylin and eosin. Image is representative of one experiment.

5.2.3 Knock-in Mouse Models

In order to interrogate cell lineage-specific inflammasome functions *in vivo,* we are developing two knock-in mouse models (Fig 5.3). These models take advantage of robust gene expression at the *Rosa26* locus[140]. The *Rosa26*-targeted construct encodes a loxP-flanked transcriptional stop cassette upstream of wild-type *Nlrc4* or *Casp1*. We have also included an IRES-GFP to mark cells that have undergone CRE-mediated recombination and excised the stop cassette. By crossing these mice onto the appropriate knockout background (*Nlrc4*$^{-/-}$ or *Casp1*$^{-/-}$) and then using lineage-restricted CRE recombinase drivers, we will be able to reconstitute a functional inflammasome in select cell types. These mice should provide an excellent tool for many *in vivo* models of inflammasome activation. In the FlaTox model, a *Villin*-CRE driver to restrict the NLRC4 inflammasome to the gut epithelium will be of particular interest.

In collaboration with the Mouse Biology Program at UC Davis, we have completed gene targeting in JM8.F6 (B6 background) cells using both the STOP$^{fl/fl}$-*Casp1* and STOP$^{fl/fl}$-*Nlrc4* construct (Fig. 5.4). After selecting three positive clones for injection (Fig. 5.4, asterisk), we have generated >18 chimeras for each knock-in. These mice display up to 80% chimerism and are currently being tested for germline transmission. Appendix F summarizes the karyotyping and injection results.

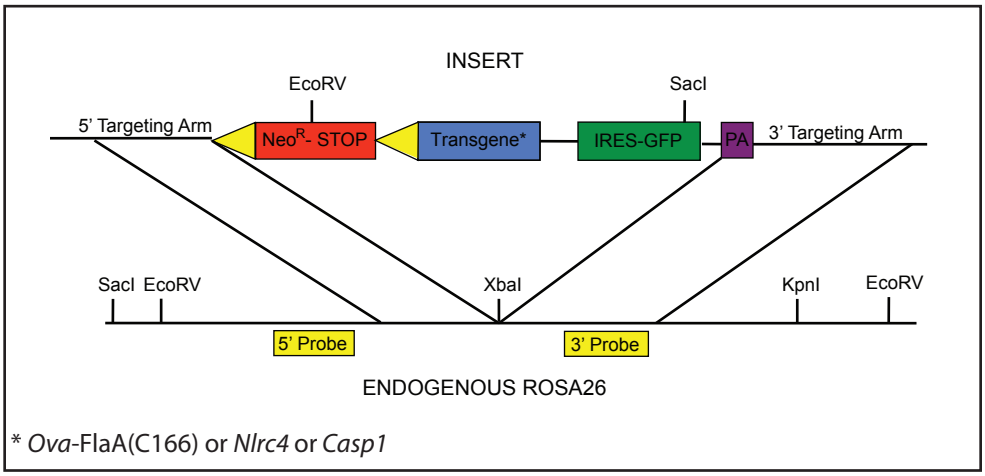

Figure 5.3 *Rosa26* targeting strategy
The *Rosa26* locus was targeted for genomic insertion of a construct encoding a loxP-flanked (yellow triangles) transcriptional STOP cassette upstream of a transgene of choice. An IRES-GFP was included to mark cells in which the STOP cassette has been excised. For 5' prime southern analysis gDNA was digested with EcoRV, giving rise to 12kb (wt) and 5kb (knock-in) bands. For 3' prime southern analysis gDNA was digested with KpnI and SacI, giving rise to 10.3kb (wt) and 7.9kb (knock-in) bands. Note that due to technical difficulties, the 3' probe was re-designed within the 3' targeting arm.

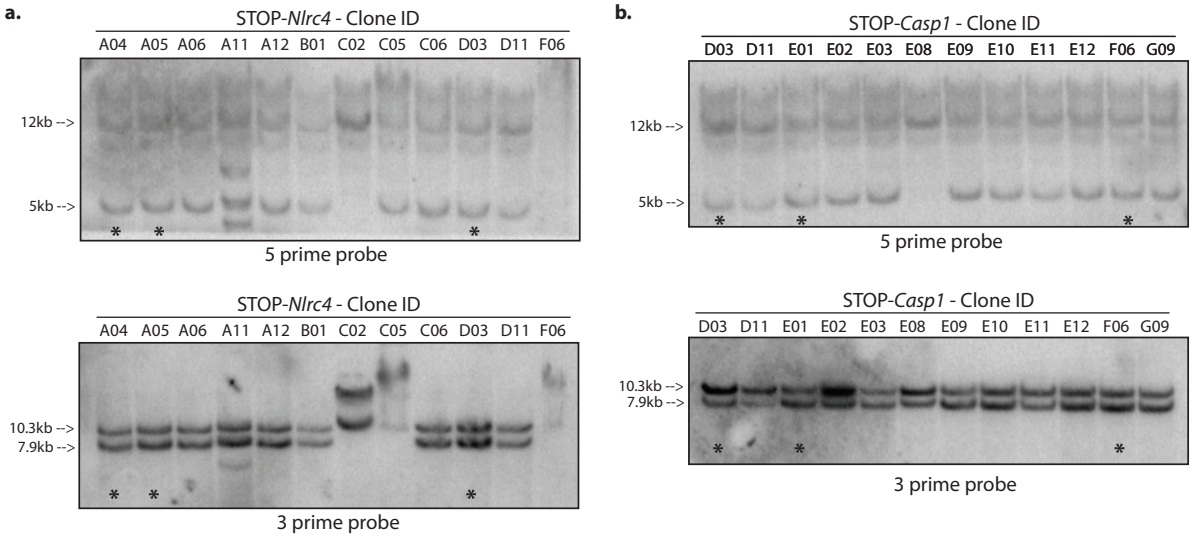

Figure 5.4 Gene targeting results (STOP-*Nlrc4* & STOP-*Casp1*)
JM8.F6 ES cells targeted with the STOP-Nlrc4 (a) or STOP-Casp1 (b) construct were screened by southern blot using the 5 prime and 3 prime probes (Fig. 5.3). Asterisks indicate clones selected for karyotyping and injection. Blots shown are from second round of screening.

5.3 The Role of Eicosanoids in Inflammasome-dependent Immunity and Disease

Our discovery of inflammasome-dependent eicosanoid biosynthesis described in chapter 4 provides a conceptually satisfying link between the rapid sensing capacity of inflammasomes and the inflammatory potential of eicosanoids. While our model of systemic FlaTox delivery has uncovered important biological pathways and highlights the risk of dysregulated inflammasome activation, the physiological relevance of this toxin remains uncertain. Data from COX1-deficient mice injected with the naturally occurring anthrax lethal toxin (Fig. 4.16) support a broader role for inflammasome-dependent eicosanoids, but here too the contribution of this response to host immunity is unclear given that the lethal effects of lethal toxin are entirely inflammasome independent[133]. Therefore, a primary objective of our future research will be to characterize the contribution of eicosanoid biosynthesis in models of inflammasome-dependent immunity and disease.

One model of particular interest is LPS-induced sepsis-like disease. As mentioned in chapter 1, deletion of CASP1 or NLRP3 but not IL-1β/IL-18 is protective in this model, suggesting a cytokine-independent inflammasome effector function. In fact, previous studies have demonstrated a partial contribution of COX or LOX pathways to this endotoxemia. For example, *Alox5*$^{-/-}$ mice showed reduced organ dysfunction and *Cox2*$^{-/-}$ mice survived longer than wild-type mice following LPS administration[141,142]. However, given that the inflammasome-dependent "eicosanoid-storm" is comprised of both COX and LOX products, it is important to eliminate both branches of eicosanoid biosynthesis. *Cpla2*$^{-/-}$ mice provide an ideal opportunity to investigate the role of eicosanoids in endotoxemia, and to our knowledge this experiment has not yet been done[130].

Although perhaps clinically relevant in sepsis, the systemic delivery of FlaTox only models dysregulated inflammasome function. But immune pathology is often the consequence of hyperactivating a normally beneficial process. Accordingly, I hypothesize that in the context of an emerging infection, where only a few cells are infected, the inflammasome-dependent production of eicosanoids will be protective by initiating inflammation, and perhaps even shaping adaptive immunity.

The role of eicosanoids in inflammation is well established, and they contribute to all classical signs of inflammation – heat (fever), pain, redness, and swelling. This inflammatory response represents the aggregate effects of the individual eicosanoids. Since the half-life of eicosanoids is generally very short *in vivo*, they act primarily near the site of synthesis[121]. Eicosanoid receptors are responsive to nanomolar concentrations of ligand, however their expression pattern provides important regulation of tissue tropism for each eicosanoid[121]. By acting on neuronal tissues, PGE_2 is the primary eicosanoid associated with fever and pain sensitization, but as noted earlier, in the gut PGE_2 causes vascular fluid loss and diarrhea[121,143]. PGD_2 is a less potent diarrhetic, but is important in lymphocyte chemotaxis[121,128]. Thromboxane acts through its receptor on vascular smooth muscle to induce vasoconstriction[121]. LTB_4 stimulates leukocyte adhesion to local endothelial cells and is a potent chemoattractant for neutrophils[121]. The cysteinyl-leukotrienes are important in allergic response, causing bronchoconstriction, and cause edema by triggering plasma leakage from postcapillary venules[121] .

Although their role in inflammation is undisputed, the contribution of eicosanoids to the final outcome of infectious disease is less clear. There are few examples in the literature

where eicosanoid knockout (e.g. *Alox5*$^{-/-}$, *Cox2*$^{-/-}$, *Cpla2*$^{-/-}$) mice are tested for susceptibility to bacterial pathogens. It is unclear if these experiments have not been performed, or if they resulted in negative results that went unreported. It is also possible that the contributions of individual pathways are masked by functional redundancies or by the route of infection. For example, eicosanoids might be particularly important for initiating early inflammation following bacterial invasion at epithelial barriers. However, these pathways are bypassed in many models of bacterial pathogenesis that deliver thousands of infectious organisms directly into the blood stream or peritoneal cavity.

One interesting link between eicosanoids and bacterial restriction comes from work in zebrafish. Using a forward genetic screen and the *M. marinum* model of tuberculosis infection, Tobin and colleagues discovered a hypersusceptible mutant with a loss of function mutation in *lta4h*, which encodes the leukotriene A_4 hydrolase[123]. Interestingly, the susceptibility results not directly from the loss of LTB_4, but rather an imbalance of pro- and anti-inflammatory eicosanoids.

The discovery of a link between inflammasome activation and eicosanoid biosynthesis provides a renewed opportunity to investigate the role of inflammatory lipids in innate immunity. The challenge will be to develop good models of localized and regulated inflammasome-dependent eicosanoid biosynthesis, and to eliminate redundancies. Vascular permeabilization by prostaglandins, which can be measured by extravasation of Evan's Blue dye, and the recruitment of neutrophils by LTB_4, are promising experimental endpoints. Since IL-1β is itself known to recruit neutrophils, it will be important to examine early timepoints, or to use *IL-1β*$^{-/-}$ mice. With careful experimental design, it should be possible to characterize if and how inflammasome-dependent eicosanoids orchestrate immune responses.

5.4 Inflammasomes and the Adaptive Immune Response

The contribution of IL-1β and IL-18 to T-cell differentiation and the inflammatory nature of pyroptosis and eicosanoids suggest a possible link between inflammasome activation and the adaptive immune response. Indeed, the contribution of CASP1 and NLRP3 to the adjuvanticity of alum has been an active, albeit controversial, area of research [see ref #144 for review]. One particularly interesting example of inflammasome-dependent adaptive immunity comes from an influenza model. The recruitment of leukocytes to the lung was reduced in *Asc*$^{-/-}$, *Casp1*$^{-/-}$, and *IL-1R*$^{-/-}$ mice infected with A/PR8 influenza virus, and these mice died beginning around day 8, when the adaptive immune system normally clears the virus in wild-type mice[145]. This was consistent with decreased T-cell responses and a lack of IgA in inflammasome deficient mice[145].

Relatively little work has examined the requirement of inflammasomes for adaptive immunity to bacterial pathogens; however protective immunity to Helicobacter infections requires IL-1R[146]. Conversely, mice infected with a strain of *L. monocytogenes* engineered to hyper-induce the NAIP5/NLRC4 inflammasome fail to develop protective immunity[75]. Clearly, many unanswered questions remain about the crosstalk between inflammasomes and adaptive immunity.

Along these lines, we have been interested in the potential adjuvanticity of pyroptosis, particularly in the context of sterile inflammation. It has been well documented that sterile but lytic cell death can release endogenous adjuvants such as high-mobility

group box 1, heat shock proteins, and DNA that can activate dendritic cells and macrophages[147]. It remains unclear, however, if pyroptosis can have a similar effect.

To address this question, we have developed a knock-in mouse model that allows us to induce pyroptosis in the absence of infection, and in the absence of TLR-ligands that inevitably contaminate our FlaTox preps. These mice were targeted at the *Rosa26* locus with a construct encoding a loxP-flanked transcriptional stop cassette upstream of an *Ova*-FlaA(C166) fusion and an IRES-GFP (Fig. 5.3). This fusion protein lacks the OVA secretion signal, but includes both the MHC-I and MHC-II OVA peptides. The C-terminal 166 amino acids of *L. pneumophila* flagellin included in the construct are sufficient for NAIP5/NLRC4 inflammasome activation, but lack the TLR5 recognition sequence. This construct was successfully targeted in PrxB6T (B6-derived) ES cells and two injected clones (Fig. 5.5, asterisk) gave rise to 8 chimeras. Three of the 8 chimeras transmitted the knock-in construct.

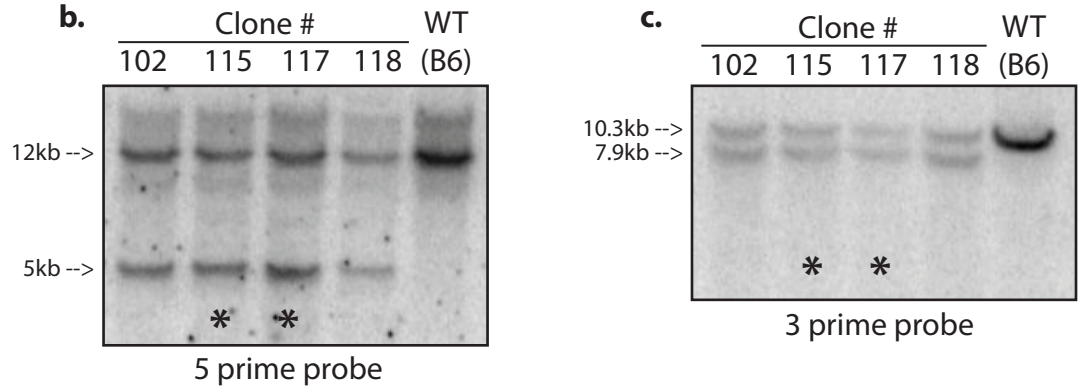

Figure 5.5 Gene targeting results (STOP-*Ova*-FlaA)
PrxB6T ES cells targeted with the STOP-*Ova*-FlaA(C166) construct were screened by southern blot using the 5 prime (a) and 3 prime (b) probes (Fig. 5.3). Asterisks indicate clones selected for karyotyping and injection. Blots shown are from second round of screening.

For initial characterization, we have crossed these STOP$^{fl/fl}$-*Ova*-FlaA mice to CRE-ER mice that express a tamoxifen-inducible CRE recombinase ubiquitously. Tail fibroblasts generated from these mice and treated with tamoxifen are 30-40% GFP$^+$ after 5 days (Fig 5.6a). The small number of GFP$^+$ cells in the absence of tamoxifen likely represent leakiness of the CRE-ER protein, which requires sequestration in the cytosol, rather than leakiness of the transcriptional stop cassette. Interestingly, BMDM generated from these mice and treated up to 72 hours with tamoxifen show only trace induction of GFP (Fig. 5.6b). Further experiments will be needed to determine if this results from a failure of induction, or if GFP$^+$ cells are eliminated by pyroptosis. It will also be important to confirm that OVA is not expressed during immunological development and that STOP$^{fl/fl}$-*Ova*-FlaA;CRE-ER mice can still generate an anti-OVA immune response.

If these initial characterizations of the STOP$^{fl/fl}$-*Ova*-FlaA mice remain encouraging, we will have an excellent tool to interrogate the contribution of pyroptosis to adaptive immune responses. For example, we could apply tamoxifen topically to the skin and look for OVA responses in the draining lymph nodes. Alternatively, we could transfer macrophages or dendritic cells from STOP$^{fl/fl}$-*Ova*-FlaA;CRE-ER mice to naïve B6 mice and

treat systemically with tamoxifen to induce pyroptosis. Eventually we hope to also generate STOP$^{fl/fl}$-*Ova*-diphtheria toxin mice to ask if the apoptosis-like death triggered by diphtheria toxin also triggers anti-OVA immunity; however, we predict that this capacity is unique to lytic cell death like pyroptosis. If our sterile pyroptosis model proves sufficient to initiate anti-OVA immunity, we can use additional knockout mice or antibody depletion (e.g. α-HMGB1) to interrogate the pathways that are activated downstream of pyroptosis to prime adaptive immune responses.

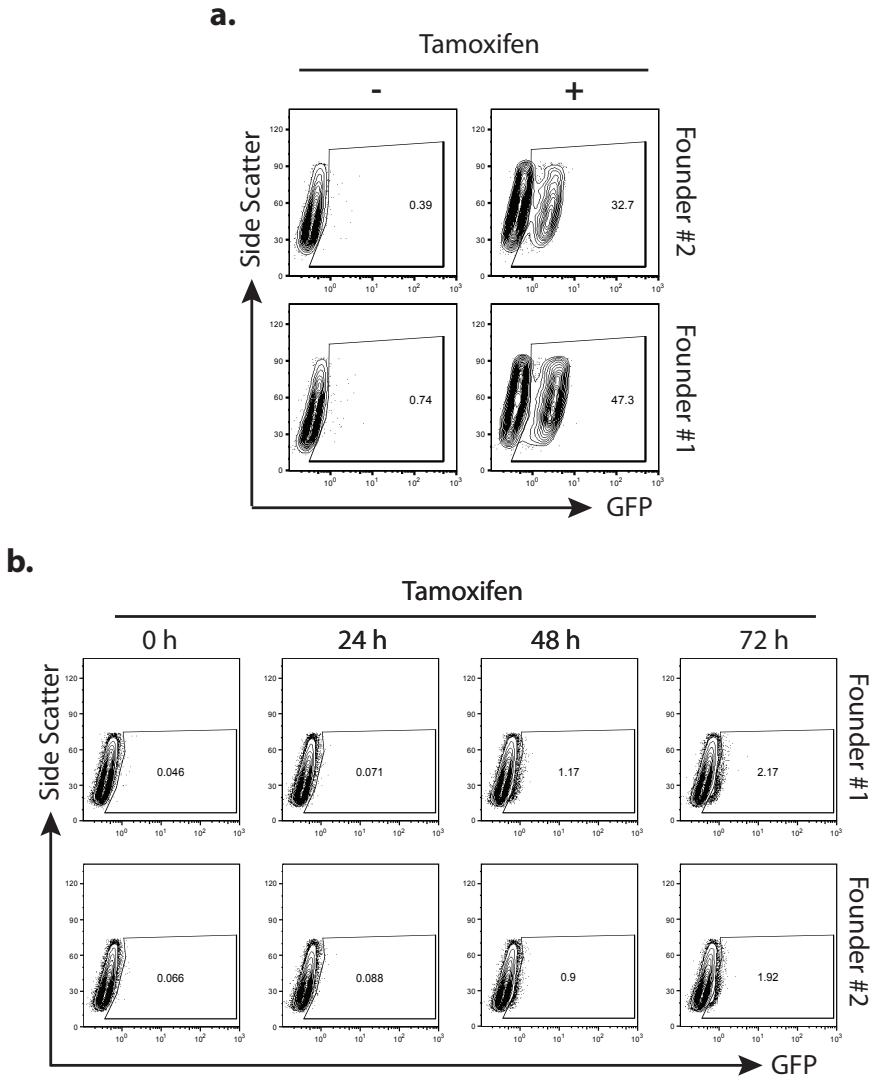

Figure 5.6 Initial characterization of STOP$^{fl/fl}$-*Ova*-FlaA(C166);CRE-ER cells
(a) Tails fibroblasts generated from STOP^{flfl}-*Ova*-FlaA(C166);CRE-ER mice were treated 5 days with tamoxifen (2 μM) or left untreated. Cells were analyzed for GFP fluorescence by flow cytometry. (b) Bone marrow macrophages were differentiated from STOP^{flfl}-*Ova*-FlaA(C166);CRE-ER with M-CSF and then treated with tamoxifen (2 μM) for the indicated times. Cells were analyzed as in (a). Data shown are representative of one experiment.

5.5 Concluding Remarks

In this dissertation I have presented findings that add significantly to our understanding of inflammasome function and regulation, with a particular emphasis on cytokine-independent activity. In chapter 2, I presented results from an siRNA screen to identify genes required for anthrax lethal toxin-induced pyroptosis in immortalized BMDM. To our knowledge, this was the first whole-genome siRNA screen carried out in bone marrow derived macrophages. Although the screen identified several known components of the inflammasome pathway, the novel candidates have unfortunately failed to validate and the identification of CASP1 substrates required for pyroptosis remains a primary challenge for the inflammasome field.

In chapter 3 we showed that CASP1 autoproteolysis is required for cytokine processing but not pyroptosis, thereby resolving a long-standing mystery in the inflammasome field. Furthermore, CARD-containing NBD-LRR proteins can initiate pyroptosis from "death-complexes" that are spatially and structurally distinct from the ASC-containing speck. Our results suggest that both host cells and invading pathogens could tune inflammasome outputs by regulating ASC. It will be interesting to investigate why uncleaved CASP1 can not process IL-1β and IL-18.

In chapter 4, I reported the identification of eicosanoid biosynthesis as a novel inflammasome effector function. Remarkably, when activated systemically *in vivo*, this response promotes massive loss of vascular fluid and contributes to rapid death. This dramatic pathology highlights the importance of regulating inflammasomes, but also suggests that inflammasomes are critical for initiating localized inflammation during infection. Our results also demonstrate the cell-type specific nature of inflammasome responses, since eicosanoid biosynthesis is completely absent in bone marrow derived macrophages cultured *in vitro*.

It is likely that other inflammasome functions have gone unnoticed because of the emphasis on *in vitro* experiments, and in chapter 5 I discuss the development of three knock-in mouse strains that will allow us to further dissect inflammasome activation *in vivo*. Using these mice, we hope to determine the contributions of individual cell lineages to inflammasome-dependent phenotypes, and to investigate the potential of inflammasome activation to promote adaptive immune responses.

FlaTox-mediated delivery of flagellin bypasses numerous immune barriers, but in the course of a natural infection the detection of flagellin in the cell cytosol indicates a severe breach. Therefore, it is perhaps not surprising that the inflammasome is licensed to activate potent countermeasures. The secretion of IL-1β and IL-18 serves as a systemic alarm, but is relatively slow when compared to the biosynthesis of eicosanoids. The most rapid inflammasome responses are therefore cytokine-independent, and it will be important to determine how these contribute to host immunity.

Materials & Methods

Chapter 2

Lethal Toxin
Recombinant proteins (PA and LF) were purified from *E. coli* in the Krantz Lab at UC Berkeley, as previously described[148]

Macrophage Immortalization
129 WT bone marrow was infected with the v-myc/v-raf expressing J2 retrovirus[108], and differentiated in 10% L929-MCSF supernatant. After 30d in culture, L929-MCSF supernatant was removed from the media and the surviving immortalized macrophage lines were cultured in RPMI with 10% FCS.

Cell Viability
Lactate dehydrogenase (LDH) release assay (Promega) was performed according to the manufacturer's protocol. For neutral red assay, 1 µl of neutral red (Sigma-Aldrich) was added to each well in a 96-well plate and cells were incubated for an additional 1-2 h. Live cells that had taken up the dye were manually counted on a dissecting microscope at 40x magnification. One field of view was counted for each triplicate well. For Guava viability assay, cells were treated with LT in 200 µl in 1.5 ml tubes at 37°C. After 2-3 h, 10 µl of cells was diluted in 140 µl of ViaCount solution (Millipore) and incubated 10 min at room temperature. Then 50 µl of 16% PFA was added and cells were incubated an additional 10 min before analysis on a Guava EasyCyte Plus using the manufacturer's viability protocol.

Timelapse Microscopy
8-chamber glass slides (Thermo-Fisher) were pre-treated with poly-D-lysine (0.1 mg/ml). 2.5x10^4 cells were plated in each well and incubated overnight. Cells were treated with lethal toxin (1 µg/ml PA + 1 µg/ml LF) or staurosporine (2.5 µM) in the presence of 1 µM ethidium bromide homodimer. Imaging on a Nikon Eclipse TE 2000-E microscope was started 1 hour post treatment and continued for 3 hours with images taken every 5 minutes. Cells were maintained at 37°C with ~5% CO_2 throughout the imaging.

siRNA Transfection
30 picomoles of siRNA (Qiagen) were complexed with 1.5 µl of RNAiMAX lipofectamine (Invitrogen) in 100 µl Optimem in a 24-well plate. After 15 minutes 2.5x10^4 cells were plated on top of transfection mixture in 500 µl media + antibiotics. Cells were incubated for 52 h before quantification of knockdown.

qPCR
RNA was isolated with the RNeasy kit (Qiagen) according to the manufacturer's protocol. RNA samples were treated with RQ1 DNase (Promega) prior to reverse transcription with Superscript III (Invitrogen). cDNA reactions were primed with poly dT for measurement of mature transcripts, and with random hexamers (Invitrogen) for measurement of unspliced transcripts. Quantitative PCR was performed as described[149] using the Step One Plus RT

PCR System (Applied Biosystems) with Platinum Taq DNA polymerase (Invitrogen) and EvaGreen (Biotium). Transcript levels were normalized to *Rps17*. See Appendix XX for primer sequences.

Stable shRNA Cell Lines
Oligo sequences from the Qiagen siRNA library (Appendix C) were cloned into the pLKO.1 vector (Addgene.org). Infectious lentivirus was generated in HEK-293T cells. $5x10^5$ cells were plated in a 6-well dish and incubated overnight. The next day these cells were calcium-phosphate transfected with 2 µg pLKO.1 + siRNA insert, 1.5 µg psPAX2 (Addgene.org), and 0.5 µg pMD2.6 (Addgene.org). After 8 h the transfection media was replaced with 2 ml fresh media and the cells were incubated overnight. The next day the supernatants were sterile filtered and 0.5 ml of supernatant was used to transduce $4x10^5$ i129-#22 cells. After 24 h these cells were placed under selection using 5 µg/ml puromycin.

Chapter 3

Bacterial Strains
Bacterial strains include WT *Salmonella enterica* serovar *Typhimurium* SL1344, WT *Francisella tularensis* subspecies *novicida* U112, *Pseudomonas aeruginosa* PAO1 and WT *Legionella pneumophila*.

Mice
Mice lacking Nlrc4, Caspase-1, Aim2 or Asc have been described before (Jones et al., 2010; Mariathasan et al., 2004). Mice were maintained following the guidelines approved by the institutional animal care and use committees of Stanford University and University of California, Berkeley.

DNA Transfections
Macrophages were transfected with 1 g/ml (final concentration) of poly(dA:dT). or poly(dG:dC) in OptiMEM (Gibco) using Lipofectamine 2000 (Invitrogen).

Cytokine and LDH Release Measurement
IL-1 (R&D systems) was measured by ELISA. LDH was measured using CytoTox 96 (Non-Radioactive Cytotoxicity Assay, Promega). To normalize for spontaneous lysis, the percentage of LDH release was calculated as follows: (LDH infected - LDH uninfected / LDH total lysis - LDH uninfected)*100.

Immunofluorescence
BMDMs were seeded onto glass cover slips and infected with *S. typhimurium* at an MOI of 20 for 2h, resulting in >99% infected cells. Cover slips were fixed and stained as described previously (Broz et al., 2010). Rat anti-mouse Caspase-1 p20 (clone 4B4; Genentech) was used at 1:200. Cells were imaged with a Zeiss LSM700 confocal microscope. For FAM-YVAD-FMK stainings (FLICA, ImmunoChemistry Technologies), medium was replaced with fresh DMEM containing 5 M FLICA 1h before fixation.

Western Blotting
Caspase-1 and IL-1 processing in supernatant and lysate samples was determined by western blotting with rabbit anti-mouse Caspase-1 p10 antibody (sc514, Santa Cruz Biotech) at 1:200, rat anti-mouse Caspase-1 p20 (4B4, Genentech) at 1:2000, rabbit anti-Aim2 (9A8, Genentech) at 1:1000 and goat anti-mouse IL-1 antibody (AF-401-NA, R&D Systems) at 1:1000. Cell lysates were probed with anti-actin antibodies (1:500, M-2 Santa Cruz Biotech) to ensure equal loading.

Quantitative RT-PCR
Macrophage RNA was harvested from the indicated cell lines (2x106 cells) and isolated with the RNeasy kit (Qiagen) according to the manufacturer's protocol. RNA samples were treated with RQ1 DNase (Promega) prior to reverse transcription with Superscript III (Invitrogen). cDNA reactions were primed with poly dT. Quantitative PCR was performed using the Step One Plus RT PCR System (Applied Biosystems) with Platinum Taq DNA polymerase (Invitrogen) and EvaGreen (Biotium). Transcript levels were normalized to *Rps17*. The following primers were used: *Flag-Nlrp1b* fusion, 5'-AGGATGACGATGACAAGGAAGAATCCC-3' and 5'- CTCCTCTCTCAATGACTGTGCTGG-3'; *Rps17,* 5'-CGCCATTATCCCCAGCAAG-3' and 5'-TGTCGGGATCCACCTCAATG-3'.

Macrophage Immortalization
C57BL/6 WT, Aim2$^{-/-}$, Asc$^{-/-}$ and Caspase -1$^{-/-}$ bone marrow was infected with the v-myc/v-raf expressing J2 retrovirus[108], and differentiated in 10% L929-MCSF supernatant. After 30d in culture, L929-MCSF supernatant was removed from the media and the surviving immortalized macrophage lines were cultured in RPMI with 10% FCS.

Retroviral Transductions
Genes encoding Caspase-1, Aim2, Nlrc4, Flag-Nlrp1b or CARD-Aim2 were cloned into a replication-defective mouse stem cell retroviral construct (pMSCV2.2). Site directed mutagenesis was performed using QuickChange (Stratagene). For transduction of primary bone marrow cells, retroviral particles were generated with Phoenix-Eco packaging cells and used to transduce bone marrow cells after 48h and 72h of culture in medium with 10% L929-MCSF supernatant. Cells were typically infected 4d after the first transduction. Immortalized macrophages were transduced with vesicular stomatitis virus pseudotyped virus packaged in GP2 cells, and sorted by FACS to enrich to >80% GFP^{+} cells.

Cell Culture and Infections
Bone marrow was isolated from femurs of 6-8 week old C57BL/6 mice, differentiated and cultured as described previously[53]. For Caspase-1 inhibitor treatments, the macrophages were cultured in 100 μM Z-YVAD-FMK in DMSO or DMSO 1h before the infection and throughout the infection. For infections with *S. typhimurium*, *P. aeruginosa* and *F. novicida* macrophages were prestimulated with 0.1 μM LPS for 16h, for *L. pneumophila* infections with 0.5 μg/ml PAM3CSK4 for 4h. *S. typhimurium* and *P. aeruginosa* were grown overnight in LB at 37°C, sub-cultured for 3-4h. *F. novicida* were grown overnight in Tryptic Soy Broth (TSB). *L. pneumophila* (*Lp02 or Lp02ΔflaA)* were grown overnight in BYE to post-log phase (OD > 3.8).

Chapter 4

Statistical Analysis

Statistical differences were calculated with an unpaired two-tailed Student's *t*-test (*in vitro/ex vivo)* or two-tailed non-parametric Mann-Whitney test (*in vivo*) using GraphPad Prism 4.0b.

Mice & Cell Culture

Except bone marrow chimeras, all mice were sex and age-matched at 5-8 weeks old. C57BL/6J (B6) and B6.*cKit*$^{wsh/wsh}$ mice were purchased from Jackson Labs. B6;129P2-*Ptgs1*^{tm1Unc} *(Cox1)* mice were purchased from Taconic. B6.*Nlrc4*$^{-/-}$ mice[112] were from S. Mariathasan and V. Dixit. B6.*Casp1*$^{-/-}$ mice[150] were a gift from A. Van der Velden and M. Starnbach. B6.*MyD88/Trif*$^{-/-}$ and FVB-Tg(CD11b/EGFP)34Lan/J were a gift from G. Barton. B6.*Rag1*$^{-/-}$ mice were a gift from D. Raulet. B6.IL-1b/IL-18$^{-/-}$ mice were a gift from D. Portnoy. B6.*Alox5*$^{-/-}$ mice were a gift from C. Brown. B6.*Naip5*$^{-/-}$ mice were described previously[120]. For bone marrow chimeras, mice were irradiated 2x with 600 Rad 4 h apart and reconstituted with 5x10^6 donor cells by tail vein injection. Chimeric mice were assayed >12 weeks post irradiation. Bone marrow macrophages were differentiated from bone-marrow-derived precursor cells using macrophage colony stimulating factor as described previously[120]. For thioglycollate-elicited macrophages, mice were injected intraperitoneally with 2 ml of 4% aged thioglycollate media (BD Diagnostics) 4 days before peritoneal lavage. Cell lysis was measured by lactate dehydrogenase (LDH) release assay (Promega) according to the manufacturer's protocol. Animal experiments were approved by the Animal Care and Use Committee of the National Institute of Allergy and Infectious Diseases, National Institutes of Health (Fig. 4.2a-b) and the UC Berkeley Animal Care and Use Committee (all other figures).

FlaTox Injections & Pathology

Recombinant proteins (PA, LFn-FlaA, LFn-FlaA(AAA), and LF) were purified from *E. coli* as previously described[148]. Endotoxin was removed from these proteins using Detoxi-Gel (Pierce) according to the manufacturer's protocol. LFn-FlaA(AAA) was generated by mutating the three C-terminal leucines of *L. pneumophila* flagellin to alanine[120]. Toxin was injected intraperitoneally or intravenously (tail vein) in 200 µl PBS. Unless otherwise noted, standard doses were 2 µg/g body weight LFn-FlaA *in vivo* (intraperitoneally) and 5 µg/ml LFn-FlaA *in vitro*. PA dose was always 2x LFn-FlaA. Rectal temperature was measured using a MicroTherma 2T thermometer (Braintree Scientific) with a lubricated RET-3 probe. For hematocrit measurement, mice were briefly anesthetized with isoflurane and blood was collected in a heparinized StatSpin 40 mm tube (Fisher Scientific) by retroorbital-bleed. The tube was sealed at one end with StatSpin sealant (Fisher Scientific) and centrifuged 10 minutes at 9,000g. The percentage of red blood cells was quantified using a StatSpin card hematocrit reader.

Fluid Loss
Peritoneal fluid was collected with a 1-ml insulin syringe (BD Biosciences) and quantified by weight. Intestines (small intestine + cecum + colon) were harvested and immediately weighed. Harvested tissues were then dried uncovered overnight at 37°C and weighed again. Fluid volume was calculated as wet weight - dry weight.

Cell Depletions
Neutrophils were depleted by injecting B6 mice with 200 µg (intraperitoneal; 36 h before treatment) and 150 µg (intravenous; 6 h before treatment) of RB6-8C5 antibody (a-GR1; gift from D. Portnoy[151]). Macrophages were depleted by injecting B6 mice intraperitoneally with 500 µl and intravenously with 200 µl of liposome encapsulated Clodronate (N. van Rooijen) 48 h before FlaTox treatment. Clodronate liposomes were prepared as previously described[152]. $CD11b^+$ cells were depleted by injecting FVB:CD11b-DTR mice intraperitoneally with 25 ng/g of body weight diphtheria toxin (Sigma-Aldrich) 24 h before FlaTox treatment.

Eicosanoid Analysis
For *ex vivo* analysis, total resident peritoneal cells were lavaged from euthanized mice and macrophage numbers estimated by counting only large cells. 1-2x10^6 macrophages (~2-4x10^6 total cells) were aliquoted to 1.5 ml eppendorf tubes. Toxin treatments were carried out in 1 ml pre-warmed Dulbecco's-PBS with Ca^{2+} and Mg^{2+}. After 30 minutes, cells were pelleted by centrifugation and the supernatant was immediately transferred to 2 ml cold methanol for storage at -80°C. For *in vivo* analysis, mice were injected intraperitoneally with FlaTox. After 20 minutes, mice were euthanized and the peritoneum was lavaged with 1 ml cold PBS, which was immediately transferred to 2 ml cold methanol for storage at -80°C. Before analysis, 400 pg each of the deuterated internal standards prostaglandin E_2 (PGE_2-d4), 15(S)-hydroxyeicosatetraenoic acid [15(S)-HETE-d8], and leukotriene B_4 (LTB_4-d4) were added to each sample to calculate the recovery of different classes of oxygenated fatty acid. Lipid autacoids were extracted by solid phase with SampliQ ODS-C18 cartridges (Agilent Technologies). Eicosanoids and docosanoids were identified and quantified by LC/MS/MS-based lipidomics[153-156]. In brief, we analyzed extracted samples by a triple-quadrupole linear ion trap LC/MS/MS system (MDS SCIEX 3200 QTRAP) equipped with a Kinetex C18 mini-bore column. The mobile phase was a gradient of A [water/acetonitrile/acetic acid (72:28:0.01, v:v:v)] and B [isopropanol/acetonitrile (60:40, v:v)] with a 450 µl/min flow rate. MS/MS analyses were performed in negative ion mode and prominent fatty acid metabolites were quantified by multiple reaction monitoring (MRM mode) using established transitions (*2,4,5,6*) for PGE_2/PGD_2 (351→271, 351→189 *m/z*), TXB_2 (369→169 *m/z*), $PGF_{2\alpha}$ (353→193*m/z*), 5-HETE (319→115 *m/z*), 12-HETE (319→179 *m/z*), 15-HETE (319→175 *m/z*), 5,12-DiHETE/LTB_4 (335→195 *m/z*), LXA_4 (351→115 *m/z*), PGE_2-d4 (335→275 *m/z*), LTB_4-d4 (339→197 *m/z*), and 15-HETE-d8 (327→182 *m/z*). Calibration curves (1 to 1000 pg) and specific LC retention times for each compound were established with synthetic standards (Cayman Chemical, Ann Arbor, MI). Structures were confirmed for selected autacoids by MS/MS analyses using enhanced product ion mode with appropriate selection of the parent ion in quadrupole 1.

For enzyme immunoassay (EIA) of LTB_4, PGE_2, and cysteinyl leukotrienes, total resident peritoneal cells were collected by lavage as above. $2x10^5$ macrophages were seeded into 96-well plates and incubated 4 h in RPMI, 10% FBS, 100 units/ml penicillin, 100 µg/ml streptomycin, 2 mM L-glutamine. Before assay, cells were washed 1x with PBS to select for adherent macrophages. Cells were treated for 30 minutes in 100 µl DPBS with Ca^{2+} and Mg^{2+}. PGE_2, LTB_4, and cysteinyl leukotrienes in supernatants were measured by EIA (Cayman Chemicals).

Flow Cytometry

Leukocytes were collected from the peritoneal cavity by lavage with 7 ml PBS, from spleen passed through a nylon mesh (BD Falcon) to establish a single cell suspension, or from the lamina propria as previously described[157]. Cells were stained with a-F4-80-APC (eBiosciences; BM8; 1:200), a-CD11b-PE (eBiosciences; M1/70; 1:400), and a-CD11c-PE-Cy7 (eBiosciences; N418; 1:100), and analyzed using standard flow cytometry protocols. F4-80/CD11b^{hi} cells were isolated by fluorescence-activated cell sorting.

Quantitative RT-PCR

CD11b/F4-80^{hi} cells were sorted from total peritoneal cells lavaged from naïve or thioglycollate-injected (2 ml injected intraperitoneally four days in advance) mice. Bone marrow derived macrophages are >95% CD11b/F4-80^{hi} and were used without sorting. RNA was isolated with the RNeasy kit (Qiagen) according to the manufacturer's protocol. RNA samples were treated with RQ1 DNase (Promega) prior to reverse transcription with Superscript III (Invitrogen). cDNA reactions were primed with poly dT for measurement of mature transcripts, and with random hexamers (Invitrogen) for measurement of unspliced transcripts. Quantitative PCR was performed as described[149] using the Step One Plus RT PCR System (Applied Biosystems) with Platinum Taq DNA polymerase (Invitrogen) and EvaGreen (Biotium). Transcript levels were normalized to *Rps17*. The following primers were used in this study. *Rps17* sense: CGCCATTATCCCCAGCAAG; *Rps17* antisense: TGTCGGGATCCACCTCAATG; *Ptgs1(Cox1)* sense: ATGAGTCGAAGGAGTCTCTCG; *Ptgs1(Cox1)* antisense: GCACGGATAGTAACAACAGGGA; *Alox5* sense: ACTACATCTACCTCAGCCTCATT; *Alox5* antisense: GGTGACATCGTAGGAGTCCAC; *Alox12/15* sense: GGCTCCAACAACGAGGTCTAC; *Alox12/15* antisense: AGGTATTCTGACACATCCACCTT

Western Blotting

Secreted proteins from FlaTox-treated cells were collected and probed with a-CASP1 p10 (Santa Cruz; sc-514) as previously described[2]. Cell lysates from ~$2x10^6$ resident peritoneal cells were probed with a-cPLA2 (Cell Signaling; 2832), a-phospho-cPLA2 (Cell Signaling; 2831), and a-beta-actin (Santa Cruz; sc-47778).

Calcium Flux

Resident peritoneal macrophages were selected from total peritioneal lavage by overnight plating on untreated petri dishes followed by replating onto 8-chamber glass slides (Thermo Scientific) coated with poly-D-lysine (Sigma-Aldrich). After overnight incubation, cells were incubated 45 min at 37°C with 2.5 mM Fluo-4 (Invitrogen) + 0.02% pluronic (Invitrogen) in Ringer's buffer containing 2 mM Ca^{2+}. Cells were washed twice and

incubated for 45 min in Ringer's buffer at 37°C before transfer to microscope for imaging. Cells were maintained at 37°C with CO_2 throughout imaging. Fluorescent (470/520) and differential interference contrast images were collected every 10 seconds on a Nikon Eclipse TE 2000-E microscope and analyzed using NIS Elements AR 3.2 software. At least 30 cells were analyzed for each replicate.

Chapter 5

Tissue Staining & Analysis

Wild-type (B6) mice were injected intraperitoneally with FlaTox (4 μg/g body weight PA + 2 μg/g body weight LFn-FlaA). After 120 minutes, intestinal tissues (cecum + small intestine + large intestine) were collected and fixed by gentle injection of 10% buffered formalin. Tissues were stored and shipped in 10% buffered formalin before being embedded in paraffin, sectioned, and stained with hematoxylin and eosin (University of Michigan Pathology Core). Sections were analyzed by board-certified pathologist (I. Bergin) blinded to experimental groups.

Cloning

OVA-FlaA(C166) was cloned into pBigT (Addgene.org) using XhoI (5') and NotI (3'). Next, the NotI-IRES-GFP-NotI fragment from STOP-eGFP-ROSA26TV (Addgene.org) was sub-cloned into pBigT+OVA-FlaA(C166) and checked for correct orientation. Finally, the PacI/AscI fragment from pBigT+OVA-FlaA(C166)-IRES-GFP was sub-cloned into pROSA26-PA (Addgene.org). The final targeting plasmid (pRosa26-STOP-OVA-FlaA(C166)-IRES-GFP) was linearized using SacII. STOP-Nlrc4 and STOP-Casp1 constructs were generated the same way except XhoI was replaced by NheI in the first cloning step for Nlrc4.

Southern Blotting

Genomic DNA from targeted embryonic stem cell clones was digested with EcoRV (5' probe) or KpnI and SacI (3' probe) and run on a 1% TAE agarose gel at 60V for 6-8 hours. The gel was incubated 45 min in denaturing buffer (NaOH) and then DNA was transferred to Zeta-probe membrane (BioRad) overnight. After transfer, membranes were incubated 5 min in neutralization buffer and then crosslinked in UV oven. Membranes were incubated 6 h to overnight at 42°C in pre-hybridization buffer. Radiolabeled probes were synthesized from template (see below) using the RadPrime DNA Labeling System (Invitrogen) and P-32 dCTP (3000 Ci/mmol, 10 mCi/ml; Perkin Elmer). Unincorporated nucleotides were removed with a ProbeQuant G-50 Micro Column (GE Healthcare). Membranes were hybridized overnight with probe at 42°C. The next day, membranes were washed at 68°C, 3x in 2X SSC/0.1%SDS and 1x in 1X SSC/0.1%SDS. Membranes were exposed overnight on phosphor screen (GE Healthcare) and analyzed on a Typhoon Scanner (GE Healthcare). 5' probe template was the 337 bp NotI fragment of the pROSA-26-promoter plasmid (Addgene.org). 3' probe template (1214 nt) was synthesized from pROSA26-PA using: 5'-GACAGCAAGGGGGAGGATTG -3' and 5'-CAAGCCAGTCCAAGAGAAAGCAC-3'.

Tail Fibroblasts

1-2 cm of tail were cleaned of hair and blood and then minced using two sterile razor blades. The minced tissue was transferred to 2 ml McCoy's 5A media supplemented with 320 U collagenase and 0.5 mg self-digested pronase and incubated 75 min at 37°C with shaking. 5 ml of cold McCoy's complete media (McCoy's 5A + 10% FBS + 1% pen/strep + 1% glutamine + 1% amphotericin B) was added to digestion and tissue was pelleted. The pellet was resuspended in 2 ml McCoy's complete media and strained through a 70 μM nylon mesh into 2 wells of a 6-well dish for culturing.

Bone Marrow Derived Macrophages

Bone marrow macrophages were differentiated from bone-marrow-derived precursor cells using macrophage colony stimulating factor as described previously[120]

References

1 Vance, R.E., Isberg, R.R., & Portnoy, D.A., Patterns of pathogenesis: discrimination of pathogenic and nonpathogenic microbes by the innate immune system. *Cell Host Microbe* 6 (1), 10-21 (2009).

2 Brodsky, I.E. & Monack, D., NLR-mediated control of inflammasome assembly in the host response against bacterial pathogens. *Semin Immunol* 21 (4), 199-207 (2009).

3 Yoon, S.I. *et al.*, Structural basis of TLR5-flagellin recognition and signaling. *Science* 335 (6070), 859-864 (2012).

4 Kim, H.M. *et al.*, Crystal structure of the TLR4-MD-2 complex with bound endotoxin antagonist Eritoran. *Cell* 130 (5), 906-917 (2007).

5 Faustin, B. *et al.*, Reconstituted NALP1 inflammasome reveals two-step mechanism of caspase-1 activation. *Mol Cell* 25 (5), 713-724 (2007).

6 Schroder, K. & Tschopp, J., The inflammasomes. *Cell* 140 (6), 821-832 (2010).

7 Poyet, J.L. *et al.*, Identification of Ipaf, a human caspase-1-activating protein related to Apaf-1. *J Biol Chem* 276 (30), 28309-28313 (2001).

8 Mariathasan, S. *et al.*, Cryopyrin activates the inflammasome in response to toxins and ATP. *Nature* 440 (7081), 228-232 (2006).

9 Strowig, T., Henao-Mejia, J., Elinav, E., & Flavell, R., Inflammasomes in health and disease. *Nature* 481 (7381), 278-286 (2012).

10 Ren, T., Zamboni, D.S., Roy, C.R., Dietrich, W.F., & Vance, R.E., Flagellin-deficient Legionella mutants evade caspase-1- and Naip5-mediated macrophage immunity. *PLoS Pathog* 2 (3), e18 (2006).

11 Sutterwala, F.S. *et al.*, Immune recognition of Pseudomonas aeruginosa mediated by the IPAF/NLRC4 inflammasome. *J Exp Med* 204 (13), 3235-3245 (2007).

12 Molofsky, A.B. *et al.*, Cytosolic recognition of flagellin by mouse macrophages restricts Legionella pneumophila infection. *J Exp Med* 203 (4), 1093-1104 (2006).

13 Amer, A. *et al.*, Regulation of Legionella phagosome maturation and infection through flagellin and host Ipaf. *J Biol Chem* 281 (46), 35217-35223 (2006).

14 Wu, J., Fernandes-Alnemri, T., & Alnemri, E.S., Involvement of the AIM2, NLRC4, and NLRP3 inflammasomes in caspase-1 activation by Listeria monocytogenes. *J Clin Immunol* 30 (5), 693-702 (2010).

15 Miao, E.A. *et al.*, Cytoplasmic flagellin activates caspase-1 and secretion of interleukin 1beta via Ipaf. *Nat Immunol* 7 (6), 569-575 (2006).

16 Franchi, L. *et al.*, Cytosolic flagellin requires Ipaf for activation of caspase-1 and interleukin 1beta in salmonella-infected macrophages. *Nat Immunol* 7 (6), 576-582 (2006).

17 Suzuki, T. *et al.*, Differential regulation of caspase-1 activation, pyroptosis, and autophagy via Ipaf and ASC in Shigella-infected macrophages. *PLoS Pathog* 3 (8), e111 (2007).

18 Huang, S., Scharf, J.M., Growney, J.D., Endrizzi, M.G., & Dietrich, W.F., The mouse Naip gene cluster on Chromosome 13 encodes several distinct functional transcripts. *Mamm Genome* 10 (10), 1032-1035 (1999).

19 Zhao, Y. *et al.*, The NLRC4 inflammasome receptors for bacterial flagellin and type III secretion apparatus. *Nature* (2011).

[20] Miao, E.A. *et al.*, Innate immune detection of the type III secretion apparatus through the NLRC4 inflammasome. *Proc Natl Acad Sci U S A* 107 (7), 3076-3080 (2010).
[21] Lightfield, K.L. *et al.*, Differential requirements for NAIP5 in activation of the NLRC4 inflammasome. *Infect Immun* 79 (4), 1606-1614 (2011).
[22] Kofoed, E.M. & Vance, R.E., Innate immune recognition of bacterial ligands by NAIPs determines inflammasome specificity. *Nature* (2011).
[23] Endrizzi, M.G., Hadinoto, V., Growney, J.D., Miller, W., & Dietrich, W.F., Genomic sequence analysis of the mouse Naip gene array. *Genome Res* 10 (8), 1095-1102 (2000).
[24] Boyden, E.D. & Dietrich, W.F., Nalp1b controls mouse macrophage susceptibility to anthrax lethal toxin. *Nat Genet* 38 (2), 240-244 (2006).
[25] Milne, J.C., Furlong, D., Hanna, P.C., Wall, J.S., & Collier, R.J., Anthrax protective antigen forms oligomers during intoxication of mammalian cells. *J Biol Chem* 269 (32), 20607-20612 (1994).
[26] Duesbery, N.S. *et al.*, Proteolytic inactivation of MAP-kinase-kinase by anthrax lethal factor. *Science* 280 (5364), 734-737 (1998).
[27] Fink, S.L., Bergsbaken, T., & Cookson, B.T., Anthrax lethal toxin and Salmonella elicit the common cell death pathway of caspase-1-dependent pyroptosis via distinct mechanisms. *Proc Natl Acad Sci U S A* 105 (11), 4312-4317 (2008).
[28] Wickliffe, K.E., Leppla, S.H., & Moayeri, M., Anthrax lethal toxin-induced inflammasome formation and caspase-1 activation are late events dependent on ion fluxes and the proteasome. *Cell Microbiol* 10 (2), 332-343 (2008).
[29] Jones, J.D. & Dangl, J.L., The plant immune system. *Nature* 444 (7117), 323-329 (2006).
[30] Sutterwala, F.S. *et al.*, Critical role for NALP3/CIAS1/Cryopyrin in innate and adaptive immunity through its regulation of caspase-1. *Immunity* 24 (3), 317-327 (2006).
[31] Hornung, V. *et al.*, Silica crystals and aluminum salts activate the NALP3 inflammasome through phagosomal destabilization. *Nat Immunol* 9 (8), 847-856 (2008).
[32] Cassel, S.L. *et al.*, The Nalp3 inflammasome is essential for the development of silicosis. *Proc Natl Acad Sci U S A* 105 (26), 9035-9040 (2008).
[33] Cruz, C.M. *et al.*, ATP activates a reactive oxygen species-dependent oxidative stress response and secretion of proinflammatory cytokines in macrophages. *J Biol Chem* 282 (5), 2871-2879 (2007).
[34] Dostert, C. *et al.*, Innate immune activation through Nalp3 inflammasome sensing of asbestos and silica. *Science* 320 (5876), 674-677 (2008).
[35] Warren, S.E. *et al.*, Cutting edge: Cytosolic bacterial DNA activates the inflammasome via Aim2. *J Immunol* 185 (2), 818-821 (2010).
[36] Tsuchiya, K. *et al.*, Involvement of absent in melanoma 2 in inflammasome activation in macrophages infected with Listeria monocytogenes. *J Immunol* 185 (2), 1186-1195 (2010).
[37] Sauer, J.D. *et al.*, Listeria monocytogenes triggers AIM2-mediated pyroptosis upon infrequent bacteriolysis in the macrophage cytosol. *Cell Host Microbe* 7 (5), 412-419 (2010).

[38] Kim, S. *et al.*, Listeria monocytogenes is sensed by the NLRP3 and AIM2 inflammasome. *Eur J Immunol* 40 (6), 1545-1551 (2010).
[39] Jones, J.W. *et al.*, Absent in melanoma 2 is required for innate immune recognition of Francisella tularensis. *Proc Natl Acad Sci U S A* 107 (21), 9771-9776 (2010).
[40] Fernandes-Alnemri, T. *et al.*, The AIM2 inflammasome is critical for innate immunity to Francisella tularensis. *Nat Immunol* 11 (5), 385-393 (2010).
[41] Rathinam, V.A. *et al.*, The AIM2 inflammasome is essential for host defense against cytosolic bacteria and DNA viruses. *Nat Immunol* 11 (5), 395-402 (2010).
[42] Hornung, V. *et al.*, AIM2 recognizes cytosolic dsDNA and forms a caspase-1-activating inflammasome with ASC. *Nature* 458 (7237), 514-518 (2009).
[43] Chen, G.Y., Liu, M., Wang, F., Bertin, J., & Nunez, G., A functional role for Nlrp6 in intestinal inflammation and tumorigenesis. *J Immunol* 186 (12), 7187-7194 (2011).
[44] Zaki, M.H. *et al.*, The NOD-like receptor NLRP12 attenuates colon inflammation and tumorigenesis. *Cancer Cell* 20 (5), 649-660 (2011).
[45] Elinav, E. *et al.*, NLRP6 inflammasome regulates colonic microbial ecology and risk for colitis. *Cell* 145 (5), 745-757 (2011).
[46] Henao-Mejia, J. *et al.*, Inflammasome-mediated dysbiosis regulates progression of NAFLD and obesity. *Nature* 482 (7384), 179-185 (2012).
[47] Arthur, J.C. *et al.*, Cutting edge: NLRP12 controls dendritic and myeloid cell migration to affect contact hypersensitivity. *J Immunol* 185 (8), 4515-4519 (2010).
[48] Murdoch, S. *et al.*, Mutations in NALP7 cause recurrent hydatidiform moles and reproductive wastage in humans. *Nat Genet* 38 (3), 300-302 (2006).
[49] Khare, S. *et al.*, An NLRP7-Containing Inflammasome Mediates Recognition of Microbial Lipopeptides in Human Macrophages. *Immunity* (2012).
[50] Masumoto, J. *et al.*, ASC, a novel 22-kDa protein, aggregates during apoptosis of human promyelocytic leukemia HL-60 cells. *J Biol Chem* 274 (48), 33835-33838 (1999).
[51] Srinivasula, S.M. *et al.*, The PYRIN-CARD protein ASC is an activating adaptor for caspase-1. *J Biol Chem* 277 (24), 21119-21122 (2002).
[52] Bao, Q. & Shi, Y., Apoptosome: a platform for the activation of initiator caspases. *Cell Death Differ* 14 (1), 56-65 (2007).
[53] Broz, P. *et al.*, Redundant roles for inflammasome receptors NLRP3 and NLRC4 in host defense against Salmonella. *J Exp Med* 207 (8), 1745-1755 (2010).
[54] Fernandes-Alnemri, T. *et al.*, The pyroptosome: a supramolecular assembly of ASC dimers mediating inflammatory cell death via caspase-1 activation. *Cell Death Differ* 14 (9), 1590-1604 (2007).
[55] Thornberry, N.A., Caspases: key mediators of apoptosis. *Chem Biol* 5 (5), R97-103 (1998).
[56] Thornberry, N.A. *et al.*, A novel heterodimeric cysteine protease is required for interleukin-1 beta processing in monocytes. *Nature* 356 (6372), 768-774 (1992).
[57] Martinon, F., Burns, K., & Tschopp, J., The inflammasome: a molecular platform triggering activation of inflammatory caspases and processing of proIL-beta. *Mol Cell* 10 (2), 417-426 (2002).
[58] Lamkanfi, M. *et al.*, Targeted peptidecentric proteomics reveals caspase-7 as a substrate of the caspase-1 inflammasomes. *Mol Cell Proteomics* 7 (12), 2350-2363 (2008).

[59] Agard, N.J., Maltby, D., & Wells, J.A., Inflammatory stimuli regulate caspase substrate profiles. *Mol Cell Proteomics* 9 (5), 880-893 (2010).
[60] Shao, W., Yeretssian, G., Doiron, K., Hussain, S.N., & Saleh, M., The caspase-1 digestome identifies the glycolysis pathway as a target during infection and septic shock. *J Biol Chem* 282 (50), 36321-36329 (2007).
[61] Kang, S.J. *et al.*, Dual role of caspase-11 in mediating activation of caspase-1 and caspase-3 under pathological conditions. *J Cell Biol* 149 (3), 613-622 (2000).
[62] Kayagaki, N. *et al.*, Non-canonical inflammasome activation targets caspase-11. *Nature* 479 (7371), 117-121 (2011).
[63] Mayer-Barber, K.D. *et al.*, Caspase-1 independent IL-1beta production is critical for host resistance to mycobacterium tuberculosis and does not require TLR signaling in vivo. *J Immunol* 184 (7), 3326-3330 (2010).
[64] Greten, F.R. *et al.*, NF-kappaB is a negative regulator of IL-1beta secretion as revealed by genetic and pharmacological inhibition of IKKbeta. *Cell* 130 (5), 918-931 (2007).
[65] Coeshott, C. *et al.*, Converting enzyme-independent release of tumor necrosis factor alpha and IL-1beta from a stimulated human monocytic cell line in the presence of activated neutrophils or purified proteinase 3. *Proc Natl Acad Sci U S A* 96 (11), 6261-6266 (1999).
[66] Gringhuis, S.I. *et al.*, Dectin-1 is an extracellular pathogen sensor for the induction and processing of IL-1beta via a noncanonical caspase-8 inflammasome. *Nat Immunol* 13 (3), 246-254 (2012).
[67] Brodsky, I.E. *et al.*, A Yersinia effector protein promotes virulence by preventing inflammasome recognition of the type III secretion system. *Cell Host Microbe* 7 (5), 376-387 (2010).
[68] Sansonetti, P.J. *et al.*, Caspase-1 activation of IL-1beta and IL-18 are essential for Shigella flexneri-induced inflammation. *Immunity* 12 (5), 581-590 (2000).
[69] Mariathasan, S., Weiss, D.S., Dixit, V.M., & Monack, D.M., Innate immunity against Francisella tularensis is dependent on the ASC/caspase-1 axis. *J Exp Med* 202 (8), 1043-1049 (2005).
[70] Miao, E.A. *et al.*, Caspase-1-induced pyroptosis is an innate immune effector mechanism against intracellular bacteria. *Nat Immunol* 11 (12), 1136-1142 (2010).
[71] Case, C.L., Shin, S., & Roy, C.R., Asc and Ipaf Inflammasomes direct distinct pathways for caspase-1 activation in response to Legionella pneumophila. *Infect Immun* 77 (5), 1981-1991 (2009).
[72] Pereira, M.S. *et al.*, Activation of NLRC4 by flagellated bacteria triggers caspase-1-dependent and -independent responses to restrict Legionella pneumophila replication in macrophages and in vivo. *J Immunol* 187 (12), 6447-6455 (2011).
[73] Lara-Tejero, M. *et al.*, Role of the caspase-1 inflammasome in Salmonella typhimurium pathogenesis. *J Exp Med* 203 (6), 1407-1412 (2006).
[74] Raupach, B., Peuschel, S.K., Monack, D.M., & Zychlinsky, A., Caspase-1-mediated activation of interleukin-1beta (IL-1beta) and IL-18 contributes to innate immune defenses against Salmonella enterica serovar Typhimurium infection. *Infect Immun* 74 (8), 4922-4926 (2006).

[75] Sauer, J.D. *et al.*, Listeria monocytogenes engineered to activate the Nlrc4 inflammasome are severely attenuated and are poor inducers of protective immunity. *Proc Natl Acad Sci U S A* 108 (30), 12419-12424 (2011).
[76] Dorhoi, A. *et al.*, Activation of the NLRP3 inflammasome by Mycobacterium tuberculosis is uncoupled from susceptibility to active tuberculosis. *Eur J Immunol* 42 (2), 374-384 (2012).
[77] Mishra, B.B. *et al.*, Mycobacterium tuberculosis protein ESAT-6 is a potent activator of the NLRP3/ASC inflammasome. *Cell Microbiol* 12 (8), 1046-1063 (2010).
[78] Koo, I.C. *et al.*, ESX-1-dependent cytolysis in lysosome secretion and inflammasome activation during mycobacterial infection. *Cell Microbiol* 10 (9), 1866-1878 (2008).
[79] Weber, A., Wasiliew, P., & Kracht, M., Interleukin-1beta (IL-1beta) processing pathway. *Sci Signal* 3 (105), cm2 (2010).
[80] Chung, Y. *et al.*, Critical regulation of early Th17 cell differentiation by interleukin-1 signaling. *Immunity* 30 (4), 576-587 (2009).
[81] Mortensen, R.F., C-reactive protein, inflammation, and innate immunity. *Immunol Res* 24 (2), 163-176 (2001).
[82] LeibundGut-Landmann, S., Weidner, K., Hilbi, H., & Oxenius, A., Nonhematopoietic cells are key players in innate control of bacterial airway infection. *J Immunol* 186 (5), 3130-3137 (2011).
[83] Moayeri, M. *et al.*, Inflammasome sensor Nlrp1b-dependent resistance to anthrax is mediated by caspase-1, IL-1 signaling and neutrophil recruitment. *PLoS Pathog* 6 (12), e1001222 (2010).
[84] Ceballos-Olvera, I., Sahoo, M., Miller, M.A., Del Barrio, L., & Re, F., Inflammasome-dependent pyroptosis and IL-18 protect against Burkholderia pseudomallei lung infection while IL-1beta is deleterious. *PLoS Pathog* 7 (12), e1002452 (2011).
[85] Carlsson, F. *et al.*, Host-detrimental role of Esx-1-mediated inflammasome activation in mycobacterial infection. *PLoS Pathog* 6 (5), e1000895 (2010).
[86] Arend, W.P., Palmer, G., & Gabay, C., IL-1, IL-18, and IL-33 families of cytokines. *Immunol Rev* 223, 20-38 (2008).
[87] Kupz, A. *et al.*, NLRC4 inflammasomes in dendritic cells regulate noncognate effector function by memory CD8 T cells. *Nat Immunol* 13 (2), 162-169 (2012).
[88] Cookson, B.T. & Brennan, M.A., Pro-inflammatory programmed cell death. *Trends Microbiol* 9 (3), 113-114 (2001).
[89] Bergsbaken, T., Fink, S.L., den Hartigh, A.B., Loomis, W.P., & Cookson, B.T., Coordinated host responses during pyroptosis: caspase-1-dependent lysosome exocytosis and inflammatory cytokine maturation. *J Immunol* 187 (5), 2748-2754 (2011).
[90] Fink, S.L. & Cookson, B.T., Caspase-1-dependent pore formation during pyroptosis leads to osmotic lysis of infected host macrophages. *Cell Microbiol* 8 (11), 1812-1825 (2006).
[91] MacKenzie, A. *et al.*, Rapid secretion of interleukin-1beta by microvesicle shedding. *Immunity* 15 (5), 825-835 (2001).
[92] Brough, D. *et al.*, Ca2+ stores and Ca2+ entry differentially contribute to the release of IL-1 beta and IL-1 alpha from murine macrophages. *J Immunol* 170 (6), 3029-3036 (2003).

93 Andrei, C. *et al.*, The secretory route of the leaderless protein interleukin 1beta involves exocytosis of endolysosome-related vesicles. *Mol Biol Cell* 10 (5), 1463-1475 (1999).
94 Lamkanfi, M. *et al.*, Inflammasome-dependent release of the alarmin HMGB1 in endotoxemia. *J Immunol* 185 (7), 4385-4392 (2010).
95 Keller, M., Ruegg, A., Werner, S., & Beer, H.D., Active caspase-1 is a regulator of unconventional protein secretion. *Cell* 132 (5), 818-831 (2008).
96 Akhter, A. *et al.*, Caspase-7 activation by the Nlrc4/Ipaf inflammasome restricts Legionella pneumophila infection. *PLoS Pathog* 5 (4), e1000361 (2009).
97 Buzzo, C.L. *et al.*, A novel pathway for inducible nitric-oxide synthase activation through inflammasomes. *J Biol Chem* 285 (42), 32087-32095 (2010).
98 Gurcel, L., Abrami, L., Girardin, S., Tschopp, J., & van der Goot, F.G., Caspase-1 activation of lipid metabolic pathways in response to bacterial pore-forming toxins promotes cell survival. *Cell* 126 (6), 1135-1145 (2006).
99 Eriksson, S., Lucchini, S., Thompson, A., Rhen, M., & Hinton, J.C., Unravelling the biology of macrophage infection by gene expression profiling of intracellular Salmonella enterica. *Mol Microbiol* 47 (1), 103-118 (2003).
100 Dons, L., Rasmussen, O.F., & Olsen, J.E., Cloning and characterization of a gene encoding flagellin of Listeria monocytogenes. *Mol Microbiol* 6 (20), 2919-2929 (1992).
101 Master, S.S. *et al.*, Mycobacterium tuberculosis prevents inflammasome activation. *Cell Host Microbe* 3 (4), 224-232 (2008).
102 Schotte, P. *et al.*, Targeting Rac1 by the Yersinia effector protein YopE inhibits caspase-1-mediated maturation and release of interleukin-1beta. *J Biol Chem* 279 (24), 25134-25142 (2004).
103 Zhou, H. *et al.*, Genome-scale RNAi screen for host factors required for HIV replication. *Cell Host Microbe* 4 (5), 495-504 (2008).
104 Li, Q. *et al.*, A genome-wide genetic screen for host factors required for hepatitis C virus propagation. *Proc Natl Acad Sci U S A* 106 (38), 16410-16415 (2009).
105 Brass, A.L. *et al.*, Identification of host proteins required for HIV infection through a functional genomic screen. *Science* 319 (5865), 921-926 (2008).
106 Kumar, D. *et al.*, Genome-wide analysis of the host intracellular network that regulates survival of Mycobacterium tuberculosis. *Cell* 140 (5), 731-743 (2010).
107 Agaisse, H. *et al.*, Genome-wide RNAi screen for host factors required for intracellular bacterial infection. *Science* 309 (5738), 1248-1251 (2005).
108 Blasi, E. *et al.*, Selective immortalization of murine macrophages from fresh bone marrow by a raf/myc recombinant murine retrovirus. *Nature* 318 (6047), 667-670 (1985).
109 Pelegrin, P., Barroso-Gutierrez, C., & Surprenant, A., P2X7 receptor differentially couples to distinct release pathways for IL-1beta in mouse macrophage. *J Immunol* 180 (11), 7147-7157 (2008).
110 Broz, P., von Moltke, J., Jones, J.W., Vance, R.E., & Monack, D.M., Differential requirement for Caspase-1 autoproteolysis in pathogen-induced cell death and cytokine processing. *Cell Host Microbe* 8 (6), 471-483 (2010).
111 Hu, H. & Leppla, S.H., Anthrax toxin uptake by primary immune cells as determined with a lethal factor-beta-lactamase fusion protein. *PLoS One* 4 (11), e7946 (2009).

[112] Mariathasan, S. *et al.*, Differential activation of the inflammasome by caspase-1 adaptors ASC and Ipaf. *Nature* 430 (6996), 213-218 (2004).
[113] Wang, S. *et al.*, Murine caspase-11, an ICE-interacting protease, is essential for the activation of ICE. *Cell* 92 (4), 501-509 (1998).
[114] Ramage, P. *et al.*, Expression, refolding, and autocatalytic proteolytic processing of the interleukin-1 beta-converting enzyme precursor. *J Biol Chem* 270 (16), 9378-9383 (1995).
[115] Boatright, K.M. *et al.*, A unified model for apical caspase activation. *Mol Cell* 11 (2), 529-541 (2003).
[116] Stennicke, H.R. *et al.*, Caspase-9 can be activated without proteolytic processing. *J Biol Chem* 274 (13), 8359-8362 (1999).
[117] Elliott, J.M., Rouge, L., Wiesmann, C., & Scheer, J.M., Crystal structure of procaspase-1 zymogen domain reveals insight into inflammatory caspase autoactivation. *J Biol Chem* 284 (10), 6546-6553 (2009).
[118] Taxman, D.J., Huang, M.T., & Ting, J.P., Inflammasome inhibition as a pathogenic stealth mechanism. *Cell Host Microbe* 8 (1), 7-11 (2010).
[119] Arora, N. & Leppla, S.H., Residues 1-254 of anthrax toxin lethal factor are sufficient to cause cellular uptake of fused polypeptides. *J Biol Chem* 268 (5), 3334-3341 (1993).
[120] Lightfield, K.L. *et al.*, Critical function for Naip5 in inflammasome activation by a conserved carboxy-terminal domain of flagellin. *Nat Immunol* 9 (10), 1171-1178 (2008).
[121] Funk, C.D., Prostaglandins and leukotrienes: advances in eicosanoid biology. *Science* 294 (5548), 1871-1875 (2001).
[122] Samuelsson, B., From studies of biochemical mechanism to novel biological mediators: prostaglandin endoperoxides, thromboxanes, and leukotrienes. Nobel Lecture, 8 December 1982. *Biosci Rep* 3 (9), 791-813 (1983).
[123] Tobin, D.M. *et al.*, The lta4h locus modulates susceptibility to mycobacterial infection in zebrafish and humans. *Cell* 140 (5), 717-730 (2010).
[124] Mancuso, P., Lewis, C., Serezani, C.H., Goel, D., & Peters-Golden, M., Intrapulmonary administration of leukotriene B4 enhances pulmonary host defense against pneumococcal pneumonia. *Infect Immun* 78 (5), 2264-2271 (2010).
[125] FitzGerald, G.A., COX-2 and beyond: Approaches to prostaglandin inhibition in human disease. *Nat Rev Drug Discov* 2 (11), 879-890 (2003).
[126] Penrose, J.F., Austen, K.F., & Lam, B.K. eds., Leukotrienes: Biosynthetic pathways, release, and receptor-mediated actions with relevance to disease states. (Lippincott Williams & Wilkins, Philadelphia, 1999).
[127] Serhan, C.N. & Z., H.J. eds., Lipid Mediators in Acute Inflammation and Resolution: Eicosanoids, PAF, Resolvins and Protectins. . (Cambridge University Press, New York, 2011).
[128] Robert, A., Nezamis, J.E., Lancaster, C., Hanchar, A.J., & Klepper, M.S., Enteropooling assay: a test for diarrhea produced by prostaglandins. *Prostaglandins* 11 (5), 809-828 (1976).
[129] Serhan, C.N. *et al.*, Resolution of inflammation: state of the art, definitions and terms. *FASEB J* 21 (2), 325-332 (2007).

130 Bonventre, J.V. *et al.*, Reduced fertility and postischaemic brain injury in mice deficient in cytosolic phospholipase A2. *Nature* 390 (6660), 622-625 (1997).
131 Gijon, M.A., Spencer, D.M., & Leslie, C.C., Recent advances in the regulation of cytosolic phospholipase A(2). *Adv Enzyme Regul* 40, 255-268 (2000).
132 Akira, S. & Takeda, K., Toll-like receptor signalling. *Nat Rev Immunol* 4 (7), 499-511 (2004).
133 Moayeri, M., Haines, D., Young, H.A., & Leppla, S.H., Bacillus anthracis lethal toxin induces TNF-alpha-independent hypoxia-mediated toxicity in mice. *J Clin Invest* 112 (5), 670-682 (2003).
134 Terra, J.K. *et al.*, Cutting edge: resistance to Bacillus anthracis infection mediated by a lethal toxin sensitive allele of Nalp1b/Nlrp1b. *J Immunol* 184 (1), 17-20 (2010).
135 Bassik, M.C. *et al.*, Rapid creation and quantitative monitoring of high coverage shRNA libraries. *Nat Methods* 6 (6), 443-445 (2009).
136 Netea, M.G. *et al.*, Differential requirement for the activation of the inflammasome for processing and release of IL-1beta in monocytes and macrophages. *Blood* 113 (10), 2324-2335 (2009).
137 Mosser, D.M. & Edwards, J.P., Exploring the full spectrum of macrophage activation. *Nat Rev Immunol* 8 (12), 958-969 (2008).
138 Lin, X.Y., Choi, M.S., & Porter, A.G., Expression analysis of the human caspase-1 subfamily reveals specific regulation of the CASP5 gene by lipopolysaccharide and interferon-gamma. *J Biol Chem* 275 (51), 39920-39926 (2000).
139 Hu, B. *et al.*, Inflammation-induced tumorigenesis in the colon is regulated by caspase-1 and NLRC4. *Proc Natl Acad Sci U S A* 107 (50), 21635-21640 (2010).
140 Soriano, P., Generalized lacZ expression with the ROSA26 Cre reporter strain. *Nat Genet* 21 (1), 70-71 (1999).
141 Ejima, K. *et al.*, Cyclooxygenase-2-deficient mice are resistant to endotoxin-induced inflammation and death. *FASEB J* 17 (10), 1325-1327 (2003).
142 Collin, M. *et al.*, Reduction of the multiple organ injury and dysfunction caused by endotoxemia in 5-lipoxygenase knockout mice and by the 5-lipoxygenase inhibitor zileuton. *J Leukoc Biol* 76 (5), 961-970 (2004).
143 Riviere, P.J., Farmer, S.C., Burks, T.F., & Porreca, F., Prostaglandin E2-induced diarrhea in mice: importance of colonic secretion. *J Pharmacol Exp Ther* 256 (2), 547-552 (1991).
144 Spreafico, R., Ricciardi-Castagnoli, P., & Mortellaro, A., The controversial relationship between NLRP3, alum, danger signals and the next-generation adjuvants. *Eur J Immunol* 40 (3), 638-642 (2010).
145 Ichinohe, T., Lee, H.K., Ogura, Y., Flavell, R., & Iwasaki, A., Inflammasome recognition of influenza virus is essential for adaptive immune responses. *J Exp Med* 206 (1), 79-87 (2009).
146 Hitzler, I. *et al.*, Caspase-1 Has Both Pro-Inflammatory and Regulatory Properties in Helicobacter Infections, Which Are Differentially Mediated by Its Substrates IL-1beta and IL-18. *J Immunol* (2012).
147 Rock, K.L., Lai, J.J., & Kono, H., Innate and adaptive immune responses to cell death. *Immunol Rev* 243 (1), 191-205 (2011).
148 Krantz, B.A. *et al.*, A phenylalanine clamp catalyzes protein translocation through the anthrax toxin pore. *Science* 309 (5735), 777-781 (2005).

149 Monroe, K.M., McWhirter, S.M., & Vance, R.E., Identification of host cytosolic sensors and bacterial factors regulating the type I interferon response to Legionella pneumophila. *PLoS Pathog* 5 (11), e1000665 (2009).
150 Li, P. *et al.*, Mice deficient in IL-1 beta-converting enzyme are defective in production of mature IL-1 beta and resistant to endotoxic shock. *Cell* 80 (3), 401-411 (1995).
151 Glomski, I.J., Decatur, A.L., & Portnoy, D.A., Listeria monocytogenes mutants that fail to compartmentalize listerolysin O activity are cytotoxic, avirulent, and unable to evade host extracellular defenses. *Infect Immun* 71 (12), 6754-6765 (2003).
152 Van Rooijen, N. & Sanders, A., Liposome mediated depletion of macrophages: mechanism of action, preparation of liposomes and applications. *J Immunol Methods* 174 (1-2), 83-93 (1994).
153 Sapieha, P. *et al.*, 5-Lipoxygenase metabolite 4-HDHA is a mediator of the antiangiogenic effect of omega-3 polyunsaturated fatty acids. *Sci Transl Med* 3 (69), 69ra12 (2011).
154 Liclican, E.L., Nguyen, V., Sullivan, A.B., & Gronert, K., Selective activation of the prostaglandin E2 circuit in chronic injury-induced pathologic angiogenesis. *Invest Ophthalmol Vis Sci* 51 (12), 6311-6320 (2010).
155 Leedom, A.J., Sullivan, A.B., Dong, B., Lau, D., & Gronert, K., Endogenous LXA4 circuits are determinants of pathological angiogenesis in response to chronic injury. *Am J Pathol* 176 (1), 74-84 (2010).
156 Hassan, I.R. & Gronert, K., Acute changes in dietary omega-3 and omega-6 polyunsaturated fatty acids have a pronounced impact on survival following ischemic renal injury and formation of renoprotective docosahexaenoic acid-derived protectin D1. *J Immunol* 182 (5), 3223-3232 (2009).
157 Annacker, O. *et al.*, Essential role for CD103 in the T cell-mediated regulation of experimental colitis. *J Exp Med* 202 (8), 1051-1061 (2005).

Appendix A – Screening Protocol

OPTIMIZED CONDITIONS

Seeding: 1.8x10^3 cells/well in 40 µl
Transfection Reagent: 0.100 µl RNAiMAX/well in 10 µl Optimem
Oligo: 50 nM (5 µl 500 nM/well)
Incubation: 72 hours
Toxin Treatment: 1,000 ng/ml PA; 500 ng/ml LF; 4.0 hours @ 37C; 40 µl/well

IN ADVANCE

1. Resuspend Flex plate to 500 nM (100 picomoles in 200µl)
2. Rearray into intermediate plates, if necessary
3. Check that all necessary reagents are in sufficient supply
4. Split cells the day before assay
5. Transfer 5µl of oligo from stock plates to assay plates (Bravo)
6. Spot 5µl of control oligos in appropriate wells on assay plates (Columns 2 & 23)

DAY 1

1. Harvest cells in IMM+ and put on ice
    a. Prepare media at 4.5x10^4 cells/mL
    b. Dead volume = 7.5 mL
    c. Volume/plate = 16 mL
2. Prepare RNAiMAX/Optimem solution. (PRE-WARM OPTIMEM TO ROOM TEMP!!)
    a. 10 µl RNAiMAX per 1 mL Optimem
    b. Dead volume = 7.5 mL
    c. Volume/plate = 4.1 mL
3. Plate 10 µl/well of RNAiMAX/Optimem on top of oligo in assay plates (CombiDrop)
4. Incubate 18 min @ RT
5. Plate 40 µl/well of cells into assay plates
6. Incubate 1 hour @ RT
7. Incubate 72 hours @ 37C

DAY 4

1. Prepare lethal toxin (1000 ng/ml PA, 750 ng/ml LF) in IMM+
    a. 1 µl PA/3.2 mL; 1µl LF/11.6 mL
    b. Dead volume = 10 mL
    c. Volume/plate = 14 mL
2. Aspirate treated wells in assay plate (Bravo – remove tips from column 1, 23 & 24 for untreated wells)
3. Transfer 40 µl of lethal toxin to assay plates (Combi)
4. Incubate 3.5 hours @ 37C
5. Prepare fix/stain solution

    a. 10 ml dead volume + 21 ml/plate
    b. 4% PFA; 1:1000 Hoechst
6. Aspirate all wells in assay plate (Bravo)
7. Add 50 µl of fix/stain to each well (Bravo)
8. Incubate 20 min @ RT
9. Wash each well 2x with PBS (Plate washer)
10. Read GFP channel on plate reader

REAGENTS

1. Immortalized and cloned GFP+ bone marrow macrophages from 129 mice (i129 Clone 22.3)
2. IMM+ media (RPMI 1640 + 10% FBS + 1% Glutamine + 1% Pen/Strep)
3. Lipofectamine RNAiMAX (Invitrogen #13778)
4. 16% PFA diluted to 4% in PBS (Electron Microscopy Sciences #15710)
5. Purified protective antigen (3.24 mg/ml) and lethal factor (7.73 mg/ml) from Krantz lab
6. siRNA oligos from Qiagen
7. Optimem (Invitrogen #31985)
8. Hoechst 33342 - 20mM in water (Fisher #83218)

EQUIPMENT

V11 Bravo
Thermo CombiDrop
EnVision Plate Reader

Appendix B – Inflammasome Pilot Screen Oligos

Entrez Gene Id	NCBI gene symbol	Gene Description	siRNA Target Sequence
224630	Bnip1	BCL2/adenovirus E1B interacting protein 1	CACGTCCGGATCTGTAACCAA
224630	Bnip1	BCL2/adenovirus E1B interacting protein 1	CAGGAAGTGGAGAACCACAAA
224630	Bnip1	BCL2/adenovirus E1B interacting protein 1	CCGGAAGCTCATCACAAAGTA
224630	Bnip1	BCL2/adenovirus E1B interacting protein 1	ACAGTCCTTTATATTGTGAAA
12175	Bnip2	BCL2/adenovirus E1B interacting protein 2	ATGGACAATCTCTTTAAATAT
12175	Bnip2	BCL2/adenovirus E1B interacting protein 2	AAATATGTTATTGGCACTTTA
12175	Bnip2	BCL2/adenovirus E1B interacting protein 2	CAGGGTGGACATGAAGGCGAT
12175	Bnip2	BCL2/adenovirus E1B interacting protein 2	GCCTGGCTCCTTAGAAGTTAA
12176	Bnip3	BCL2/adenovirus E1B interacting protein 3	AAGGAATATTGTGGCCTTATA
12176	Bnip3	BCL2/adenovirus E1B interacting protein 3	AAGATTATATTGAGAGAAGAA
12176	Bnip3	BCL2/adenovirus E1B interacting protein 3	CACCTTTATCACTCTGCTGAA
12176	Bnip3	BCL2/adenovirus E1B interacting protein 3	TAGATATAAATAGTATAAATA
12177	Bnip3l	BCL2/adenovirus E1B interacting protein 3-like	CTGGGTGGAGCTACCCATGAA
12177	Bnip3l	BCL2/adenovirus E1B interacting protein 3-like	AAGCTTGAATTTATAGTTATA
12177	Bnip3l	BCL2/adenovirus E1B interacting protein 3-like	TTGGCTGTTTATCTTTAAGAA
12177	Bnip3l	BCL2/adenovirus E1B interacting protein 3-like	TCCTATGGAAATGGAAAGAAA
171388	Bnipl	BCL2/adenovirus E1B 19kD interacting protein like	CAGCTGACACAGGAAAGTAAA
171388	Bnipl	BCL2/adenovirus E1B 19kD interacting protein like	CGGGATCTGCATGGCTCGAAA
171388	Bnipl	BCL2/adenovirus E1B 19kD interacting protein like	TGCCTTCAAGCTGGGATTTAA
171388	Bnipl	BCL2/adenovirus E1B 19kD interacting protein like	CTGTGTGGCATTGGAAGTGTA
105844	Card10	caspase recruitment domain family, member 10	TAGAGTTCTCACACCGTTCAA
105844	Card10	caspase recruitment domain family, member 10	CACAGGGAGTGTGACCCTTAA
105844	Card10	caspase recruitment domain family, member 10	CTGCACACAATGAGTCATTAA
105844	Card10	caspase recruitment domain family, member 10	CAGGAGTGGTTCTGTACTCGA

108723	Card11	caspase recruitment domain family, member 11	CCGGCAGGAACTGGTCAACAA
108723	Card11	caspase recruitment domain family, member 11	AAGGACGACAACTACAACTTA
108723	Card11	caspase recruitment domain family, member 11	CAGCAAGTACTTTCTGCCTTA
108723	Card11	caspase recruitment domain family, member 11	ATGGGATAACGTGGAATGCAA
170720	Card14	caspase recruitment domain family, member 14	CCAGATCATGATGGTGGACTA
170720	Card14	caspase recruitment domain family, member 14	CTACTTGTCTGTGAAGATCAA
170720	Card14	caspase recruitment domain family, member 14	CCACGAGGTCCTGAAACTGAA
170720	Card14	caspase recruitment domain family, member 14	CCGGCTGTGGTGGGACCTGAA
239319	Card6	caspase recruitment domain family, member 6	CAGGATCTAAGGATACATGAA
239319	Card6	caspase recruitment domain family, member 6	CAGGGAGACGTTAAAGAACAT
239319	Card6	caspase recruitment domain family, member 6	AAGCAGCTGGAAAGTCTATAA
239319	Card6	caspase recruitment domain family, member 6	CAAGACTTTGAAGTTATTCAA
332579	Card9	caspase recruitment domain family, member 9	CTGGAGGAGGACTGGCGTCAA
332579	Card9	caspase recruitment domain family, member 9	CACCATCTTCTCCCTACGGAA
332579	Card9	caspase recruitment domain family, member 9	CAGGAATAGTCCATACATTCA
332579	Card9	caspase recruitment domain family, member 9	CAGGACAAAGATAAGCTTCGA
12362	Casp1	caspase 1	CCCAGGCAAGCCAAATCTTTA
12362	Casp1	caspase 1	TACCTCTTCCCGGGACATTAA
12362	Casp1	caspase 1	AAAGGTTGACACAATCTTTCA
12362	Casp1	caspase 1	ACAAGGAGTGGTGTTGTTAAA
12364	Casp12	caspase 12	CTGGAACTTCTTCTTTGTAAA
12364	Casp12	caspase 12	ATGGAATAATAGTATAACAAA
12364	Casp12	caspase 12	TAGGATATAATTGACAAATTT
12364	Casp12	caspase 12	CTAGATAATTTCCATAGGTTA
12365	Casp14	caspase 14	ACGGATGTGTTCATTCATAAA
12365	Casp14	caspase 14	CACAATGAAATGCTATAATTA
12365	Casp14	caspase 14	AAGGAAGAAGACGCCATGTTA
12365	Casp14	caspase 14	CACAAAGAGCACTATTATTTA
12366	Casp2	caspase 2	TTGGAAGATGTCCCAATTTAA
12366	Casp2	caspase 2	TAGGATGTTTCTTGCCACTTA
12366	Casp2	caspase 2	CAGGGTCACTTGGAAGACTTA
12366	Casp2	caspase 2	ATCGGGCATAACTACATGAAA
12367	Casp3	caspase 3	AACAATAATGTCAAATGATAA
12367	Casp3	caspase 3	TTGAAATGAAATTTAATTTAA
12367	Casp3	caspase 3	ATGGATAGTGTTTCTAAGGAA
12367	Casp3	caspase 3	GGGCATATGCATAATAATTAA
12363	Casp4	caspase 4, apoptosis-related cysteine	CACAAGAAATTTACCCAATAA

		peptidase	
12363	Casp4	caspase 4, apoptosis-related cysteine peptidase	CAGATGTGCTACAGTATGATA
12363	Casp4	caspase 4, apoptosis-related cysteine peptidase	CAGGAGGCTCTTACTTCATCA
12363	Casp4	caspase 4, apoptosis-related cysteine peptidase	TCGGGCAACCTTGACGAGATA
12368	Casp6	caspase 6	CAGGAAATTACTATGCATCAA
12368	Casp6	caspase 6	AAGCTGCATTTCTGTCCCAAA
12368	Casp6	caspase 6	ACCCAAGATATTTATCATCCA
12368	Casp6	caspase 6	TCGCGGGCAGGTGAAAGTAAA
12369	Casp7	caspase 7	ATGCATCATCATAAACAACAA
12369	Casp7	caspase 7	CTGAGAGAAGACGACAGTTAA
12369	Casp7	caspase 7	CCAGCTCTTGATGAAAGAATA
12369	Casp7	caspase 7	ATGTTCCTATTTATTGATTAA
12370	Casp8	caspase 8	CACACACATTTCTAAATATAA
12370	Casp8	caspase 8	ATCGAGGATTATGAAAGATCA
12370	Casp8	caspase 8	AACTATGACGTGAGCAATAAA
12370	Casp8	caspase 8	TTGGATGAGATGAGCCTCAAA
26885	Casp8ap2	caspase 8 associated protein 2	CAGTTAGTCATGTATAATAAA
26885	Casp8ap2	caspase 8 associated protein 2	AAGCATTTGTCTTTAGATGAA
26885	Casp8ap2	caspase 8 associated protein 2	AAGAGTAAACTAACTCATGAA
26885	Casp8ap2	caspase 8 associated protein 2	AAGGTGGTTCATTGTGATCAA
12371	Casp9	caspase 9	CCAGCTGAGTTCATTAAACAA
12371	Casp9	caspase 9	AAGGATGTGATTCTTAAATTA
12371	Casp9	caspase 9	AACGACCTGACTGCCAAGAAA
12371	Casp9	caspase 9	CAGGATCCAGAGGCTGTTAAA
244202	Nlrp10	NLR family, pyrin domain containing 10	ACCACAGATATTGGAAGTTTA
244202	Nlrp10	NLR family, pyrin domain containing 10	CAGGAGCTTGCTGGCCATGAA
244202	Nlrp10	NLR family, pyrin domain containing 10	TAGACTTTAATTCTAACATTA
244202	Nlrp10	NLR family, pyrin domain containing 10	CAGGGAGAGGCCACACACAAA
378425	Nlrp12	NLR family, pyrin domain containing 12	CAGCAGAAATTTGTAGATGTA
378425	Nlrp12	NLR family, pyrin domain containing 12	CAGAAGATTCTATTTGATGAA
378425	Nlrp12	NLR family, pyrin domain containing 12	AAGGGTATCAAATGTGAGAAA
378425	Nlrp12	NLR family, pyrin domain containing 12	TCCGAAGGAAATTCCAGCTAA
76858	Nlrp14	NLR family, pyrin domain containing 14	CAGGATCTCTTAGGTATCTTA
76858	Nlrp14	NLR family, pyrin domain containing 14	ATGGAGAATTTGCAACTTTAA
76858	Nlrp14	NLR family, pyrin domain containing 14	CACGTGGAGGTTGAGAAAGTA
76858	Nlrp14	NLR family, pyrin domain containing 14	CAGGGCTGTCTAAGAATGCAA
195046	Nlrp1a	NLR family, pyrin domain containing 1A	CACGTGATGCATGATCTGCAA
195046	Nlrp1a	NLR family, pyrin domain containing 1A	AAAGAAGACAATGTAAAGAAA
195046	Nlrp1a	NLR family, pyrin domain containing 1A	AAGCCTCAATTAGTCATAATA
195046	Nlrp1a	NLR family, pyrin domain containing 1A	TACGATGAACATGGATAAAGA
637515	Nlrp1b	NLR family, pyrin domain containing 1B	ATGTGATGGTATGGAATTCAA
637515	Nlrp1b	NLR family, pyrin domain containing 1B	ACGGGAGGTCTATTTCCGCAA
637515	Nlrp1b	NLR family, pyrin domain containing 1B	ATGGGTCCACTAACAATAGAA
627984	Nlrp1c	NLR family, pyrin domain containing 1C	AACATGGGATTATTCCTAGAA
627984	Nlrp1c	NLR family, pyrin domain containing 1C	AACTGTGAGAATACTGGTAAA
627984	Nlrp1c	NLR family, pyrin domain containing 1C	CACATCCTACAGAAATTGCAA
627984	Nlrp1c	NLR family, pyrin domain containing 1C	AAGGCTCAATTGGTCGTAATA
232827	Nlrp2	NLR family, pyrin domain containing 2	AGGGAAGTAAATAATACTAAA
232827	Nlrp2	NLR family, pyrin domain containing 2	CACATTTAATTCAAATAAGAA

232827	Nlrp2	NLR family, pyrin domain containing 2	CTGAATGAGACTCGTATTCAA
232827	Nlrp2	NLR family, pyrin domain containing 2	CCGGATGAACAACGCATGTTA
216799	Nlrp3	NLR family, pyrin domain containing 3	AACCTCTTATTTGGAGAAGAA
216799	Nlrp3	NLR family, pyrin domain containing 3	ATGGATGGCTTTGATGAGCTA
216799	Nlrp3	NLR family, pyrin domain containing 3	AAGGAGTATTTCTTTAAGTAT
216799	Nlrp3	NLR family, pyrin domain containing 3	CTCCACAATTCTGACCCACAA
243880	Nlrp4a	NLR family, pyrin domain containing 4A	ACAAATCTTATAGATAAATAA
243880	Nlrp4a	NLR family, pyrin domain containing 4A	ATGGGTGTATTGGACCTCAAA
243880	Nlrp4a	NLR family, pyrin domain containing 4A	AAGATGAGTTTCCACAGATTA
243880	Nlrp4a	NLR family, pyrin domain containing 4A	CAGGCATTTCTGGTTGCTGAA
210045	Nlrp4b	NLR family, pyrin domain containing 4B	CAGGGTGTTTACTTTATAGAA
210045	Nlrp4b	NLR family, pyrin domain containing 4B	CAGGATGAATATGATCATCTT
210045	Nlrp4b	NLR family, pyrin domain containing 4B	AAGGAATTACTCATACATGAA
210045	Nlrp4b	NLR family, pyrin domain containing 4B	TACCACTTATCTAAAGAATTA
83564	Nlrp4c	NLR family, pyrin domain containing 4C	CACACTTGTATTCTAAGCATA
83564	Nlrp4c	NLR family, pyrin domain containing 4C	AACAGCCTCTTTGGTGTTATA
83564	Nlrp4c	NLR family, pyrin domain containing 4C	AAGGACATCTACATACTCCAA
83564	Nlrp4c	NLR family, pyrin domain containing 4C	AAGGTGGATGTTCTGCTGCAA
384752	Nlrp4d	NLR family, pyrin domain containing 4D	AAGGAATTTATAAAGTTTAAA
384752	Nlrp4d	NLR family, pyrin domain containing 4D	ATGATCCGTGATAATAACAAA
384752	Nlrp4d	NLR family, pyrin domain containing 4D	ATGGTGATTACTTGTCTTAAA
384752	Nlrp4d	NLR family, pyrin domain containing 4D	CACAAGGAGTAAAGACATCAA
446099	Nlrp4e	NLR family, pyrin domain containing 4E	AACCCATACTTGAGCATCTAA
446099	Nlrp4e	NLR family, pyrin domain containing 4E	CAACAGTGTACCGTGAATTTA
446099	Nlrp4e	NLR family, pyrin domain containing 4E	CTCCCAGACAGTGTCCTCATA
446099	Nlrp4e	NLR family, pyrin domain containing 4E	ACCGTCGACGAAGGAGATAGA
97895	Nlrp4f	NLR family, pyrin domain containing 4F	TACAAGTTTCTTAACACTCAA
97895	Nlrp4f	NLR family, pyrin domain containing 4F	TACAATGTTAAGTATCTTTAA
97895	Nlrp4f	NLR family, pyrin domain containing 4F	CAGGAGATTCTGGAATTGAAA
97895	Nlrp4f	NLR family, pyrin domain containing 4F	CAGAGTTATATGGAAGAGCTA
235779	Nlrp4g	NLR family, pyrin domain containing 4G	AAGCAATAATAGAAACAAATA
235779	Nlrp4g	NLR family, pyrin domain containing 4G	AAGACTTACCTTCTCAGTTAA
235779	Nlrp4g	NLR family, pyrin domain containing 4G	CTCAGGAAACCCAAAGTTATA
235779	Nlrp4g	NLR family, pyrin domain containing 4G	CAAGATAAGATCAGAGCCCAA
23968	Nlrp5	NLR family, pyrin domain containing 5	CAGGAAGAACAGATTACTCTA
23968	Nlrp5	NLR family, pyrin domain containing 5	CAGGATTTCTTTGCTGCCTTA
23968	Nlrp5	NLR family, pyrin domain containing 5	TCCAATGAGTCTGATAGAATA
23968	Nlrp5	NLR family, pyrin domain containing 5	CAGCCTAAACCTGGTGAAGAA
101613	Nlrp6	NLR family, pyrin domain containing 6	CTGGATCATCATAAAGCACAA
101613	Nlrp6	NLR family, pyrin domain containing 6	CAGGAGATAGGTGGATCACTA
101613	Nlrp6	NLR family, pyrin domain containing 6	TCAGACAATATTTCTCAACAA
101613	Nlrp6	NLR family, pyrin domain containing 6	CACCATCGCACCATTGCAATA
233001	Nlrp9a	NLR family, pyrin domain containing 9A	AAGAATTTAAAGAGCATTAAA
233001	Nlrp9a	NLR family, pyrin domain containing 9A	CACGGATATTATTGTTTGGAA
233001	Nlrp9a	NLR family, pyrin domain containing 9A	CAGGATTCTCTGAACAAACTA
233001	Nlrp9a	NLR family, pyrin domain containing 9A	ATGCAAGTCTTTCAAACATTA
243874	Nlrp9b	NLR family, pyrin domain containing 9B	CTGGGCAACAATAACATACAA
243874	Nlrp9b	NLR family, pyrin domain containing 9B	CTGATAGAAACTACCATTTAA
243874	Nlrp9b	NLR family, pyrin domain containing 9B	CAGGAATTGATCTGTGACAAA
243874	Nlrp9b	NLR family, pyrin domain containing 9B	TAGAAGTAGCTGAGAATTTAA
330490	Nlrp9c	NLR family, pyrin domain containing 9C	CAGGATTATCTGAACAGTCTA

330490	Nlrp9c	NLR family, pyrin domain containing 9C	CCCGAATATGGTAGCTTAGAA
330490	Nlrp9c	NLR family, pyrin domain containing 9C	AGGAGTGATGTTTCTGTGTAA
330490	Nlrp9c	NLR family, pyrin domain containing 9C	ATGAAATTTCTGCAAATTCAA
66824	Pycard	PYD and CARD domain containing	CAGCTACTATCTGGAGTCGTA
66824	Pycard	PYD and CARD domain containing	TGGGAACCAGGTAATGGTTAA
66824	Pycard	PYD and CARD domain containing	CAGCTGCAAACGACTAAAGAA
66824	Pycard	PYD and CARD domain containing	TACCTTTGAGAACACATGTAA

Appendix C – Oligo Sequences for shRNA Cloning

Gene ID	Symbol	Description	Oligo ID	Sequence_F	Sequence_R
216188	Aldh1l2	aldehyde dehydrogenase 1 family, member L2	Mm_D330038I09Rik_2	CACGCATACATTGGCCAATAA	TTATTGGCCAATGTATGCGTG
71914	Antxr2	anthrax toxin receptor 2	Mm_Antxr2_2	CACATCGATGATGTAATGATA	TATCATTACATCATCGATGTG
12362	Casp1	caspase 1	Mm_Casp1_4	ACAAGGAGTGGTGTTGTTAAA	TTTAACAACACCACTCCTTGT
230579	Fam151a	family with sequence simliarity 151, member A	Mm_BC026682_1	CAGCGATGTCATGGTCTTAGA	TCTAAGACCATGACATCGCTG
233908	Fus	fusion, derived from t(12;16) malignant liposarcon	Mm_Fus_4	GGCGAGAATGTTACAATTGAA	TTCAATTGTAACATTCTCGCC
246133	Kcne2	potassium voltage-gated channel, Isk-related subf	Mm_Kcne2_2	CACCATGTTGTGTGTGTAATA	TTCAATTGTAACATTCTCGCC
195046	Nlrp1a	NLR family, pyrin domain containing 1A	Mm_Nalp1_3*	GAGCCTCAATTAGTCATAATA	TATTATGACTAATTGAGGCTC
52850	Sgsm1	small G protein signaling modulator 1	Mm_Rutbc2_3	CAGCAGTAAATACTACGAGAA	TTCTCGTAGTATTTACTGCTG
320632	Snrnp200	small nuclear ribonucleoprotein 200 (U5)	Mm_Ascc3l1_2	AAGCCACTTCATGGCCAATAA	TTATTGGCCATGAAGTGGCTT
22051	Trip6	thyroid hormone receptor interactor 6	Mm_Trip6_2	ACCCTTAGTGTTTGCCATCAA	TTGATGGCAAACACTAAGGGT
216188	Aldh1l2	aldehyde dehydrogenase 1 family, member L2	RNAi Consortium	GACACTAATCATGGGAGATAA	TTATCTCCCATGATTAGTGTC
			RNAi Consortium	CGGCCCTAAATTGATGAGATT	AATCTCATCAATTTAGGGCCG
246133	Kcne2	potassium voltage-gated channel, Isk-related subf	RNAi Consortium	TCGTGGAAGATTGGCAGGAAA	TTTCCTGCCAATCTTCCACGA
22051	Trip6	thyroid hormone receptor interactor 6	RNAi Consortium	GTCTGGATGCTGAGATAGATT	AATCTATCTCAGCATCCAGAC
52850	Sgsm1	small G protein signaling modulator 1	RNAi Consortium	GCCTCCTATTTATTCCATTTA	TAAATGGAATAAATAGGAGGC
117167	Steap4	STEAP family member 4	Mm_Tnfaip9_1	CAGGCTGATAATAGCCTTGTA	TACAAGGCTATTATCAGCCTG
66181	Nop10	NOP10 ribonucleoprotein homolog (yeast)	Mm_Nola3_1	TGCCAGGTTATTAAAGATATA	TATATCTTTAATAACCTGGCA
67282	Ccdc53	coiled-coil domain containing 53	Mm_Ccdc53_3	AAGAACCGTGGCCTTTCTAAA	TTTAGAAAGGCCACGGTTCTT
56296	Dmrtb1	DMRT-like family B with proline-rich C-terminal, 1	Mm_Dmrtb1_12	AAGGGCACAGGTGGTTTCCAA	TTGGAAACCACCTGTGCCCTT

Appendix D – qPCR Primers for shRNA Knockdown Confirmation

Gene ID	Symbol	Description	Primer_F	Melt_F	Primer_R	Melt_R	Length
216188	Aldh1l2	aldehyde dehydrogenase 1 family, member L2	CCAAGGAGGTGAACGGGATGAC	59.8	GCTACTGCTCTGTCAACATCCGC	60.1	168
71914	Antxr2	anthrax toxin receptor 2	TCACGTCGATCAGTCACGATGG	58.8	CTTTGTTCAGGACAGGTGCAGG	58.3	128
12362	Casp1	caspase 1	ACAACCACTCGTACACGTCTT	56.2	GGCAGCAAATTCTTTCACCTCTT	56.1	189
230579	Fam151a	family with sequence simliarity 151, member A	TGGTCTTAGAAGCCGATGTCACC	58.7	ACAGCCTTGAGACTCTTGAAGTCC	58.5	177
			GCTGTGAGAACGATGCAATTTG	55.1	TTGAACCCTTCTACGGTGACA	55.9	193
233908	Fus	fusion, derived from t(12;16) malignant liposarc	CTCAGGGTTATGGACAACAGAACC	57.3	ACCACTCTGGTCCTGATTGC	57.1	142
			GCTTCAAACGACTATACCCAACA	55.1	GGCCATAACCACTGTAACTCTGT	56.7	124
637515	Nlrp1b	NLR family, pyrin domain containing 1B	GGTGAACATGAAAGGACAGCAGG	58.3	GGCATCACAGAGATATTGCACTGC	58.3	189
			CAACAAGACTTGAACACAACGAG	54.5	CTCTCAATGACTGTGCTGGGTA	56.5	144
52850	Sgsm1	small G protein signaling modulator 1	GGCTCAACCAATGGCTGTAACC	58.7	CACGATCATGTGATTGACCAGGG	57.9	164
			CTGCCGAAGCTGCCTAACC	58.8	GGGTCCATCAAGAGTGCCT	57	149
320632	Snrnp200	small nuclear ribonucleoprotein 200 (U5)	GAGACTGATGAGAACCTGCTGC	57.6	GGACCGCATGGGAGCTATG	58.2	158
22051	Trip6	thyroid hormone receptor interactor 6	CGGGCATATTGTGAGAGCTGC	58.6	GGCATACCACACAGGTGAAGC	58.5	132
246133	Kcne2	potassium voltage-gated channel, Isk-related su	CACATTAGCCAATTTGACCCAGA	60.8	GAACATGCCGATCATCACCAT	60.5	175
117167	Steap4	STEAP family member 4	GGGAAGTCACTGGGATTGAAAA	60.2	CCGAATAGCTCAGGACCTCTG	61.4	115
66181	Nop10	NOP10 ribonucleoprotein homolog (yeast)	TCGCGTTTATACGCTGAAGAAA	60.4	TGATGGTGATTCGGTGTCTTG	60	110
67282	Ccdc53	coiled-coil domain containing 53	TGTCACAAACGGATCACATTCTG	61	TGGACAGGAACACTTGAACCAT	61.5	167
56296	Dmrtb1	DMRT-like family B with proline-rich C-terminal,	AAGCGGCTTGGTGTCAGAG	62.3	TAGGTCAGCGAGAAAGATGGT	60.3	210

Appendix E - Retroviral constructs used in chapter 3

Name	Description
Empty vector	pMSCV2.2-IRES-GFP
Caspase-1 WT	pMSCV2.2-Caspase-1-IRES-GFP (Caspase-1 from C57/BL6 mice, NM_009807)
Caspase-1 C47	pMSCV2.2-Caspase-1-IRES-GFP D296N, D313N, D314N
Caspase-1 C51	pMSCV2.2-Caspase-1-IRES-GFP D296N, D304N, D313N, D314N
Caspase-1 C52	pMSCV2.2-Caspase-1-IRES-GFP D300N, D304N, D313N, D314N
Caspase-1 C53	pMSCV2.2-Caspase-1-IRES-GFP D296N, D308N, D313N, D314N
Caspase-1 C59	pMSCV2.2-Caspase-1-IRES-GFP D296N, D300N, D308N, D313N, D314N
Caspase-1 C60	pMSCV2.2-Caspase-1-IRES-GFP D296N, D300N, D304N, D308N, D313N, D314N
Caspase-1 C39	pMSCV2.2-Caspase-1-IRES-GFP D122N
Caspase-1 C45	pMSCV2.2-Caspase-1-IRES-GFP D103N
Caspase-1 C67	pMSCV2.2-Caspase-1-IRES-GFP D103N, D122N
Caspase-1 C71	pMSCV2.2-Caspase-1-IRES-GFP D103N, D122N, D296N, D308N, D313N, D314N
Caspase-1 DEAD	pMSCV2.2-Caspase-1-IRES-GFP C284A
Caspase-1 C53-DEAD	pMSCV2.2-Caspase-1-IRES-GFP C284A, D296N, D308N, D313N, D314N
Flag-Nlrp1b	pMSCV2.2-FLAG-Nlrp1b-IRES-GFP (Nlrp1b from 129S1 mice, GenBank: DQ117584.1)
Aim2 WT	pMSCV2.2-Aim2-IRES-GFP (Aim2 from C57/BL6 mice, NM_001013779.2)
CARD-Aim2	pMSCV2.2-CARD-Aim2-IRES-GFP (Nlrc4 bp 1-286 fused to full-length Aim2)

Appendix F – Karyotyping and Chimera Summary

Date: 12/19/2011

Blastocyst Microinjection Results

Project: pRosa26-STOP-Casp1-195

Clone ID: pROSA26_Stop_Casp1_E01 (BL2623) 60% Euploid					
Pedigree	Sex	Birth Date	Age (Days)	Coat Color	Chimera %
BL2623-6-Russell Vance	Male	12/6/11	13	chimera	90%
BL2623-7-Russell Vance	Male	12/6/11	13	chimera	75%
BL2623-16-Russell Vance	Male	12/7/11	12	chimera	85%
BL2623-17-Russell Vance	Male	12/7/11	12	chimera	75%
BL2623-18-Russell Vance	Male	12/7/11	12	chimera	70%
BL2623-19-Russell Vance	Male	12/7/11	12	chimera	70%
BL2623-20-Russell Vance	Male	12/7/11	12	chimera	90%
BL2623-21-Russell Vance	Male	12/7/11	12	chimera	55%
BL2623-22-Russell Vance	Male	12/7/11	12	chimera	45%

Clone ID: pROSA26_Stop_Casp1_D03 (BL2624) 55% Euploid					
Pedigree	Sex	Birth Date	Age (Days)	Coat Color	Chimera %
BL2624-4-Russell Vance	Male	12/7/11	12	chimera	90%
BL2624-5-Russell Vance	Male	12/7/11	12	chimera	75%
BL2624-6-Russell Vance	Male	12/7/11	12	chimera	70%
BL2624-7-Russell Vance	Male	12/7/11	12	chimera	60%
BL2624-11-Russell Vance	Male	12/7/11	12	chimera	65%
BL2624-12-Russell Vance	Male	12/7/11	12	chimera	50%
BL2624-13-Russell Vance	Male	12/7/11	12	chimera	50%

Clone ID: pROSA26_Stop_Casp1_F06 (BL2636) 59% Euploid					
Pedigree	Sex	Birth Date	Age (Days)	Coat Color	Chimera %
BL2636-19-Russell Vance	Male	12/23/11	13	chimera	40%
BL2636-18-Russell Vance	Male	12/23/11	13	chimera	40%
BL2636-17-Russell Vance	Male	12/23/11	13	chimera	40%
BL2636-16-Russell Vance	Male	12/23/11	13	chimera	50%
BL2636-5-Russell Vance	Male	12/23/11	13	chimera	75%
BL2636-4-Russell Vance	Male	12/23/11	13	chimera	45%

Date: 01/05/2012

Blastocyst Microinjection Results

Project: pRosa26-STOP-Nlrc4-196

Clone ID: pRosa26_Stop_Nlrc4_D03 (BL2637) 55% Euploid					
Pedigree	**Sex**	**Birth Date**	**Age (Days)**	**Coat Color**	**Chimera %**
BL2637-11-Russell Vance	Male	12/23/11	13	chimera	40%
BL2637-10-Russell Vance	Male	12/23/11	13	chimera	55%
BL2637-9-Russell Vance	Male	12/23/11	13	chimera	70%

Clone ID: pROSA26_Stop_Nlrc4_A05 (BL2638) 57% Euploid					
Pedigree	**Sex**	**Birth Date**	**Age (Days)**	**Coat Color**	**Chimera %**
BL2638-31-Russell Vance	Male	12/23/11	13	chimera	55%
BL2638-30-Russell Vance	Male	12/23/11	13	chimera	55%
BL2638-29-Russell Vance	Male	12/23/11	13	chimera	65%
BL2638-28-Russell Vance	Male	12/23/11	13	chimera	75%
BL2638-13-Russell Vance	Male	12/23/11	13	chimera	50%
BL2638-12-Russell Vance	Male	12/23/11	13	chimera	80%
BL2638-11-Russell Vance	Male	12/23/11	13	chimera	80%
BL2638-10-Russell Vance	Male	12/23/11	13	chimera	60%
BL2638-9-Russell Vance	Male	12/23/11	13	chimera	60%

Clone ID: pROSA26_Stop_Nlrc4_A04 (BL2649) 70% Euploid					
Pedigree	**Sex**	**Birth Date**	**Age (Days)**	**Coat Color**	**Chimera %**
BL2649-6-Russell Vance	Male	12/30/11	13	chimera	70%
BL2649-12-Russell Vance	Male	12/30/11	13	chimera	75%
BL2649-13-Russell Vance	Male	12/30/11	13	chimera	75%
BL2649-14-Russell Vance	Male	12/30/11	13	chimera	75%
BL2649-15-Russell Vance	Male	12/30/11	13	chimera	70%
BL2649-16-Russell Vance	Male	12/30/11	13	chimera	60%
BL2649-17-Russell Vance	Male	12/30/11	13	chimera	80%